Towards Automated Additive Manufacturing of Bio-Tubes

by

Kali L. Manning

B.S. Worcester Polytechnic Institute, Worcester, MA 2013

Sc.M. Brown University, Providence, RI 2015

Submitted in partial fulfillment of the requirements for the degree of Doctor of Philosophy in Biomedical Engineering, a joint program in the Division of Biology and Medicine and the School of Engineering at Brown University

Molecular Pharmacology, Physiology, and Biotechnology

and

Center for Biomedical Engineering

PROVIDENCE, RHODE ISLAND

MAY, 2020

This dissertation by Kali L. Manning is accepted in its present form by the Biomedical Engineering program, a joint program in the Division of Biology and Medicine and the School of Engineering as satisfying the dissertation requirements for the degree of Doctor of Philosophy

Date	Jeffrey R. Morgan, Ph.D., Advisor

Recommended to the Graduate Council

Date	Diane Hoffman-Kim, Ph.D., Reader
Date	Jacquelyn Schell, Ph.D., Reader
Date	Anubhav Tripathi, Ph.D., Reader
Date	Kimberly Waller, Ph.D., External Reader

Approved by the Graduate Council

Date	Andrew Campbell, Dean of the Graduate School

Curriculum Vitae

NAME

Kali L. Manning

EDUCATION

Brown University, Providence, RI
Ph.D., Biomedical Engineering
Advisor: Jeffrey R. Morgan
Title of Dissertation: Towards Automated Additive Manufacturing of Bio-Tubes
Expected: February, 2020

Brown University, Providence, RI
Sc.M., Biomedical Engineering, 2015
Advisor: Jeffrey R. Morgan
Title of Dissertation: Microtissues are Building Blocks for Macrotissue Formation

Worcester Polytechnic Institute, Worcester, MA
B.S., Biomedical Engineering with Distinction, 2013

PUBLICATIONS

Manning KL, Feder JS, Kanellias M, Murphy J, Morgan JR. Towards Automated Additive Manufacturing of Living Bio-Tubes Using Ring-Shaped Building Units. SLAS Technology. Under Review.

Manning KL, Thomson AH, Morgan JR 2018. Funnel-Guided Positioning of Multi-Cellular Microtissues to Build Macrotissues. Tissue Engineering Part C: Methods 24 (10). doi: 10.1089/ten.tec.2018.0137.

Leary E, Curran S, Susienka M, **Manning KL**, Blakely AM and Morgan JR 2017. Micro-moulded nonadhesive hydrogels to form multi-cellular microtissues – The 3D Petri Dish in Technology Platforms for 3D Cell Culture: A User's Guide (ed S. Przyborski), John Wiley & Sons, Ltd, Chichester, UK. doi: 10.1002/9781118851647.ch5

Blakely AM, **Manning KL**, Tripathi A and Morgan JR 2015. Bio-Pick, Place, and Perfuse: A New Instrument for 3D Tissue Engineering. Tissue Engineering Part C: Methods 21 (7). doi: 10.1089/ten.tec.2014.0439.

PATENTS

Morgan JR, **Manning KL**, Ip B, 2019, Funnel-Guided Microtissue Stacking and Manipulation, International Application Number PCT/US2019/016683, Filed February 5,

2019.

Hiller JA, Hingston JA, He DS, Winsor-Hines D, Harlan R, Corcoran K, Roye GD, Ryder B, Vithiananthan S, Snyder PJ, Storbeck GT, **Manning KL**, Merkling SM, Rockweiler HE, 2017, Systems and methods for obesity diagnosis and/or treatment, US Patent 20180110979, Filed October 20, 2017. Publication April 26, 2018.

Storbeck GT, Hingston JA, Merkling SM, Hiller JA, Corcoran K, **Manning KL,** Roye GD, Vithiananthan S, Ryder B, 2016, Devices and methods for modulating intestinal flow, US Patent 20180110641, Filed October 23, 2017. Publication April 26, 2018.

Hingston JA, Storbeck GT, Hiller JA, Corcoran K, **Manning KL,** Merkling SM, Roye GD, Vithiananthan S, Ryder B, 2017, Devices and methods for reducing absorption, US Patent 20170135836 A1, Filed November 16, 2016. Publication May 18, 2017.

Hingston JA, Storbeck GT, Hiller JA, Corcoran K, Merkling SM, **Manning KL,** Roye GD, Vithiananthan S, Ryder B, 2017, Magnetic devices and related methods for gastrointestinal restriction, US Patent 20170112650 A1, Filed October 25, 2016. Publication April 27, 2017.

CONFERENCE ABSTRACTS

Manning KL, Thomson AH, Morgan JR. 2018. Funnel-Guided Positioning of Multi-Cellular Microtissues to Build Macrotissues. 3D Cell Culture. Freiburg, Germany.

Manning KL, Morgan JR. 2017. Microtissue Sliding Technique for Biofabrication. TERMIS-AM. Charlotte, NC.

Ip BC, Cui F, Murphy J, Wilks BT, **Manning KL**, Susienka MJ, Bull C, Patterson WR. 2016. Bio-pick, Place, and Perfuse Instrument for Building Perfusable Large Proto-organs. TERMIS-AM. San Diego, CA.

Ip BC, Cui F, Murphy J, Wilks BT, **Manning KL**, Susienka MJ, Bull C, Patterson WR. 2016. Bio-pick, Place, and Perfuse Instrument for Building Perfusable Large Proto-organs. Biofabrication. Winston-Salem, NC.

ADDITIONAL RESEARCH EXPERIENCE

Brown University, Providence, RI
Graduate Research Assistant, September 2015 – Present

Boston Scientific, Marlborough, MA
Corporate Research Co-op, 2014

Virginia Polytechnic Institute and State University, Blacksburg, Virginia
Undergraduate Researcher, 2012

LEADERSHIP AND SERVICE

President, Graduate Biomedical Engineering Society, 2015 – 2016

Treasurer, Graduate Biomedical Engineering Society, 2014 – 2015

Masters Student Rep., Graduate Biomedical Engineering Society, 2013 – 2014

WPI Trustee Mentor Program, 2012 – 2013

Director of Sisterhood/Charter Member, Alpha Phi International Fraternity, 2011 – 2013

President, Engineers Without Borders, 2011 – 2012

Biomedical Engineering Society, WPI, 2010 – 2013

TEACHING EXPERIENCE

Teaching Assistant, BIOL 2110: Drug and Gene Delivery, 2016

Teaching Assistant, Summer@Brown Engineering Biomedical Systems, July 2016

Teaching Assistant, BIOL 2230/2240 Biomedical Engineering Seminar, 2015 – 2016

AWARDS AND AFFILIATIONS

American Association for the Advancement of Science, 2017 – Present

Alpha Eta Mu Beta (Biomedical Engineering Honor Society), WPI Chapter, 2012 – 2013

Omicron Delta Kappa (National Leadership Honor Society), WPI Circle, 2012 – Present

WPI Dean's List, Fall 2012

WPI Dean's List, Fall 2011

WPI Dean's List, Spring 2011

WPI Scholarship, 2009 – 2013

WPI University Award, 2009 – 2013

Friends of NYS USBC WBA Inc. Scholarship, 2009

TRAINING

Laboratory: Mammalian cell culture, 3D cell culture, maintenance of cell lines and primary human cells, agarose hydrogel molding, Live/Dead staining, cryostat histology of hydrogels, light and fluorescence microscopy, 3D printing

Software: ZEN, ImageJ, SolidWorks, SigmaPlot, JMP, Mendeley, literature search

Acknowledgements

There are many people who have supported me on my PhD journey, friends, family, and colleagues. First, I would like to thank all of the people at Brown University. My advisor, Jeff Morgan, who gave me this opportunity and the space to grow into an independent scientist and researcher. My committee members who provided guidance and an open door throughout the years. Jackie Schell, who has been a science and life confidant since I started my masters' work at Brown. Kim Waller, who sponsored me and am only just beginning to learn from.

I have been fortunate to work with incredible peers who have been mentors and team members. Team HOMER, your creativity, innovation and dedication was inspiring and I feel honored to have worked on such an exciting project with you. Thank you to Marianne for whole-heartedly jumping on board with my project, and being such an amazing scientist and mentee. Thank you Jacob for your ingenuity and curiosity. Thank you John for your continuous hard work and tenacity, I learned so much from you. Thank you Andrew Thomson for being as excited about falling tissue rings as I was. I truly enjoyed working with all of you. To all the Morgan Lab members who have made our lab such a great place to work over the past 7 years, I am very grateful. To Beth and Mike, for being excellent mentors, trainers and all around good people. To Ben, for always being an ear to talk to, and being a brilliant scientist willing to share ideas. To Blanche, for your continuous support and willingness to help address any questions (especially statistic based ones!). To Andrew, for always being inspired and excited to learn and work, I will always

be your cheerleader. Last, but not least, The Girlz, who have become lifelong friends and have guided me through the craziness of getting a PhD.

To all of my friends who have supported me throughout graduate school, and helped me celebrate all the little victories along the way. Tara, Julie, Kellie and Hillary – you are my sisters and I am so grateful to be able to share this journey with you. To Sessa, Andrea and Paul – I am so happy to have you in my life. Stasia, you are my best friend and I couldn't have done this without your unending confidence in me. You always know how to put life into perspective and keep me grounded, for that I am especially grateful.

To my family, your unwavering support and encouragement to follow my dreams through these 10 years of engineering education are invaluable. Josh, I feel so privileged to have the opportunity to share science with you. It has been so enjoyable working with you and mentoring you. Your excitement and curiosity continues to inspire me and I look forward to continuing our journey as biomedical engineers. Last, but not least, to Evan. You have had my back since the beginning and have endured many sleepless nights and stressful days. Thank you for always being there to remind me of the bigger picture and sharing in my accomplishments, I am so happy to share them with you.

Table of Contents

List of Figures

List of Videos

Chapter 1

Introduction

1.1 Chapter Overview

The work presented herein develops a novel method for the biofabrication of bio-tubes using automated additive manufacturing techniques. The thesis is presented in three sections which aim to (1) develop a new microtissue manipulation platform for the fabrication of bio-tubes, (2) automate the new method and develop a real-time quality control step using vision recognition, and (3) discuss the theory behind fabricating a vascular unit containing a blood vessel-like tube that branches into a perfusable capillary tissue bed.

Chapter 2 discusses the development of the novel funnel-guide method for fabrication of bio-tubes using ring-shaped microtissue building parts. We show the funnel-guide is a technique that harnesses the horizontal self-righting ability of lumen containing microtissues and guides them into a stacking chamber where they vertically stack and fuse to create a tube. The funnel-guide method is modular and customizable to rings composed of various cell types and of differing diameters, making it applicable for use in creating bio-tubes of any composition.

Chapter 3 assesses automating the funnel-guide method using a commercially available liquid handling robot. We show ring throughput can be increased by fabricating

one ring per well of a standard 96-well plate. We developed metrics to inform how dynamic tissue rings can be utilized to build bio-tubes. We automated ring retrieval and placement in the funnel-guide by modifying a commercially available liquid handling robot. Finally, we developed a custom quality control algorithm to evaluate ring parameters in real-time and control the quality of rings placed in the funnel-guide. With the automated system we fabricated an endothelial cell bio-tube with luminal alignment.

Chapter 4 expands on the theory behind fabricating a perfusable capillary tissue bed. Previous work is evaluated and discussed, and hypothetical metrics for fabricating, perfusing, and evaluating a hepatic tissue bed containing a capillary-like network is presented. We developed an assay to assess the fusion of spheroids into a tissue bed, and evaluated agarose as a potential perfusion material. Finally, we created a perfusion platform for bio-tubes and postulate how it could be used to perfuse a vascular-like structure containing a tube that branches into a capillary tissue bed.

The goal of this thesis was to develop and automate a new simple, non-contact, quick microtissue manipulation platform for the construction of bio-tubes. Chapter 5 summarizes the main conclusions from the work discussed in this thesis and expands upon future directions and additional experiments.

1.2 Background and Significance

1.2.1 Tissue Engineering and its Medical Need

Tissue engineering was founded about forty years ago as "*an interdisciplinary field that applies the principles of engineering and life sciences toward the development of biological substitutes that restore, maintain, or improve tissue function or a whole organ*"

[1]. While many strides have been made in the field since its inception, the need for a physiologically relevant biological substitute remains unmet. There are two areas where a physiologically relevant tissue construct fabricated *in vitro* could have a direct impact. First is in drug discovery and the pharmaceutical industry. Currently seven out of eight drugs that enter clinical testing fail, and if a drug does successfully enter the market the process takes more than ten years and costs over $1 billion USD [2]. One reason for this high failure rate is the inability to predict which drugs will fail prior to entering clinical trials. Currently, a majority of preclinical testing is performed using animal models, however, it has been shown that animal models are not predictive of human biology [3]–[5]. Three dimensional *in vitro* models have the potential to replace animal models, however, more work needs to be done to replicate human physiology. The second area is tissue and organ transplantation. As of February 2020, there are over 112,000 people on the waiting list to receive an organ transplant. However, between January and December of 2019, only 39,718 organ transplants were performed [6]. This discrepancy in organs available for transplant results in, on average, seventeen people dying daily while waiting for an organ [6]. If organs and tissues that replicate human physiology could be fabricated *in vitro*, they could be used as an alternative to donor organs, and reduce the number of people waiting for a transplant.

However, the grand challenge of tissue engineering is the fabrication of thick, high cell density, perfusable tissue constructs. Large, high cell density tissue constructs can be fabricated, but without access to nutrients and removal of waste via a perfusion network, the tissue will rapidly develop a necrotic core [7]. The human body overcomes this via the cardiovascular system, which has a capillary within an average of 200 μm of every cell in

the body [8]. Thus vascularization of fabricated tissue constructs with a capillary network that can be perfused is essential to the viability of any fabricated tissue construct.

One structure that is physiologically relevant to several organ systems is the tube. Tubes can be found all throughout the body. The cardiovascular and lymphatic systems are composed of branching networks of blood vessels and lymph ducts respectively. Air is transported through the trachea into bronchi and then bronchioles. The gastrointestinal tract is one long tube, starting with the esophagus and transitioning through the stomach, small intestine and into the large intestine. The kidneys perform filtration through a serious of tubes in the nephrons, and then transport urine into ureters and eventually the urethra. [8], [9] All of these tubes work in symbiosis to maintain homeostasis. Thus, if we could develop a technique to fabricate tubular structures *in vitro*, we could use them as an *in vitro* drug testing platform, and as a component of an organ for transplant. For example, a tube constructed with smooth muscle cells on the exterior and endothelial cells on the lumen could be used as a blood vessel model for *in vitro* drug testing. This blood vessel-like tube could also be used to create a vascular unit containing a blood vessel that branches into a capillary network. A novel structure that could contribute to fabricating thick, organ cell density tissues for transplant.

1.2.2 Microtissue Fabrication

Microtissues are clusters of cells that aggregate and adhere to one another in the process of self-assembly. They can be formed using methods such as hanging drop, micromolding or bioprinting [10]. One commercially available micromolding method is the 3D Petri Dish ® [11]. Flexible molds containing an array of the desired microtissue shape (spheroid, toroid, honeycomb or rod, for example) are filled with molten agarose.

Once solidified, the agarose hydrogel is removed from the mold and the molded array of recesses are filled with a cell suspension. The cells settle by gravity into the recesses, and since cells cannot adhere to the agarose, they adhere to one another, forming microtissues via the process of self-assembly [12]. Cells self-assemble on the order of hours and in the absence of scaffold material, the cells produce endogenous extracellular matrix and establish cell-cell interactions [13]. Additionally, their cell density is akin to that of organs, making them an ideal building block for use in biofabrication techniques [14], [15]. Once self-assembled, microtissues can be removed from the agarose gel and manipulated to be precisely placed to form more complex macrotissue structures.

1.2.3 Microtissue Fusion

The fundamental principal of using microtissues as building blocks to create more complex macrotissue structures, is the fusion of microtissues into a contiguous unit upon contact with one another [16], [17]. Fusion occurs between simple and complex microtissues in both the vertical and horizontal plane [16]. Fusion maintains the cell produced extracellular matrix, cell-cell interactions and high cell density of individual microtissue parts [10], [17]. Fusion can be quantified and evaluated using morphological parameters including tissue length, contact length, and inter-tissue angle. For example, as spheroids fuse the tissue length would decrease, the contact length would increase, and the inter-tissue angle would approach 180°. Microtissue fusion occurs within 5h of initial contact. [18]

1.2.4 Additive Manufacturing – a Biofabrication Strategy

One approach to creating macrotissues is applying the principals of additive manufacturing to biological materials. Additive manufacturing is a process that builds

constructs by adding material layer-by-layer. Biofabrication additive manufacturing techniques can be categorized into two approaches; bioprinting and microtissue manipulation. Bioprinting uses a print head to deposit polymer support structures and cell material simultaneously. Deposition occurs in air and polymerization of support materials can use chemicals. [19] In contrast, microtissue manipulation builds with high cell density microtissues that fuse together while submerged in cell culture medium. Two techniques apply the principals of microtissue manipulation to fabricate tissue constructs, the Kenzan method and the Bio-Pick, Place and Perfuse (Bio-P3).

The Kenzan method uses a custom robotic arm to pick-up, move and puncture individual spheroids onto a microneedle array, where the spheroids fuse into a tubular structure and are then removed from the microneedle array [20]–[22]. The microneedle array consists of needles 180 μm in diameter, which sits in air while the spheroids are impaled onto the array. The spheroids used contain approximately 20K cells and are on average 700 μm in diameter [23]. The needle diameter dictates the size of the spheroids, and limits the use of smaller diameter building parts which would be within the 200 μm diffusion limit.

The Bio-P3 is an innovative instrument that applies the principals of pick-and-place machines used in high-speed assembly of electronics to multicellular microtissue building parts [24]. A bio-gripper, uses a peristaltic pump and fluid pressure, to pick-up honeycomb-shaped microtissue building blocks, move them through culture medium and precisely place them onto a build head [25]. The process is repeated to create a stack of honeycomb microtissues with aligned lumens, which are constantly being held in place and perfused by the build head while undergoing fusion [26]. The Bio-P3 can be used to build with eight

orbital honeycomb microtissues 21.9 mm in length, approximately 200 μm in thickness, and containing 1.41 x 10^6 cells. One honeycomb part used by the Bio-P3 is the equivalent of 71 spheroid parts used in the Kenzan method, drastically reducing the number of build steps required.

The Kenzan method and Bio-Pick, Place and Perfuse are platform technologies that can be applied to numerous tissue types. For example, microtissue manipulation platforms could be used to build vasculature and a capillary tissue bed. Tubular structures have been fabricated and implanted *in vivo* using microtissue manipulation techniques [20]. Previous work has shown spheroid fusion will occur between spheroids containing capillary networks [27]–[31]; HUVEC and parenchymal cells have fused to form a ring [30], [31], and a round patch-like shaped structure [27]. Thus, it is possible for a blood-vessel like tube to be constructed and fused to a tissue bed using microtissue maipulation.

1.2.5 Advanced Regenerative Manufacturing Institute

In 2016 the Advanced Regenerative Manufacturing Institute (ARMI) was awarded $80 million in federal funding to work towards its mission "*to make practical the large-scale manufacturing of engineered tissues and tissue-related technologies, to benefit existing industries and grow new ones*" [32]. The institutes' efforts are divided into three focus areas, education and workforce development, technology, and the Tissue Foundry. The focus on education and workforce development stems from the need to advance the tissue manufacturing industry as a whole, including the future workforce. The Tissue Foundry would be a "*single manufacturing line that includes the use of multiple bioreactors that can be used for any tissue and include basic non-invasive sensors for real-time monitoring of samples*" [32]. The Tissue Foundry could incorporate multiple

automated sequences to take a vial of cells and grow it into a tissue product. ARMI's technical scope has five thrust areas, (1) cell selection, culture and scale-up, (2) biomaterial selection and scale-up; (3) tissue process automation and monitoring; (4) tissue maturing technologies and (5) tissue preservation and transport [32]. Advances in these five areas could create a tissue manufacturing scheme to translate advances in tissue engineering and regenerative medicine into the commercial sector.

1.2.6 Automated Biofabrication Techniques

While there has been advances in automation for two-dimensional cell culture techniques, there has been limited exploration of automated biofabrication methods. Platforms have been developed for automating cell culture processes such as feeding, washing, passing and seeding [33], [34]. Automated primary tissue processing platforms have been developed to harvest adipose-derived regenerative cells [35]. Liquid handling robots exist throughout the field to perform standard assays, and have the capability to move, heat and shake well plates and conical tubes. However, all of these methods yield cell suspensions or solutions, not macrotissue structures. Bioprinting can be considered an automated technique that uses a print head to fabricate constructs with scaffolding and cellular material [36], [37]. But, the deposition of a polymer support structure occurs in air, which deprives cells of media, and limits the overall size of the construct. Additionally, bioprinted constructs do not achieve organ cell density. Recently, an increased throughput Kenzan method was developed that moves a 4 x 4 array of spheroids, and impales them onto a microneedle array [38]. Another recently developed technique uses prongs to punch an agarose gel, containing a single tissue ring, up and out of a 96-well plate. The ring is then placed onto a mandrel, and the process repeated to form a stack of rings [39]. Both

the increased throughput Kenzan method and the agarose punch method involve microtissue manipulation steps that occur outside the culture medium. Additionally, both methods require precise placement of microtissue building parts which makes automation challenging. There is a need for a simple self-aligning automated technique using standard components readily available and easily translatable into existing automated schemes. Advancing automated biofabrication methods is one facet of the field of tissue engineering that will progress ideas and encourage clinical translation.

1.3 Closing Remarks

There is a need for a simple, quick, self-aligning modular method to fabricate custom bio-tubes. Prior to this work, there did not exist an automated microtissue manipulation method using an off-the-shelf liquid handling robot with a real-time quality control step using vision recognition. The development of a new automated microtissue manipulation technique is a step towards manufacturing tissue products. With any manufacturing scheme, it produces products faster, more reproducibly, and more uniformly of a higher quality than if manually constructed. This is an essential step in the effort to translate tissue engineered innovations into the clinical setting, and work towards having physiologically relevant constructs for use as *in vitro* models and for eventual transplantation.

1.4 References

[1] R. Langer and J. P. Vacanti, "Tissue engineering," *Science (80-.).*, vol. 260, no. 5110, pp. 920–926, May 1993.

[2] J. A. DiMasi, H. G. Grabowski, and R. W. Hansen, "Innovation in the pharmaceutical industry: New estimates of R&D costs," *J. Health Econ.*, vol. 47, pp. 20–33, May 2016.

[3] G. Mazzoleni, D. Di Lorenzo, and N. Steimberg, "Modelling tissues in 3D: The next future of pharmaco-toxicology and food research?," *Genes and Nutrition*, vol. 4, no. 1. BioMed Central, pp. 13–22, Mar-2009.

[4] F. Pampaloni, E. G. Reynaud, and E. H. K. Stelzer, "The third dimension bridges the gap between cell culture and live tissue," *Nat. Rev. Mol. Cell Biol.*, vol. 8, no. 10, pp. 839–845, Oct. 2007.

[5] N. T. Elliott and F. Yuan, "A review of three-dimensional in vitro tissue models for drug discovery and transport studies," *Journal of Pharmaceutical Sciences*, vol. 100, no. 1. John Wiley and Sons Inc., pp. 59–74, 01-Jan-2011.

[6] "Data - OPTN." [Online]. Available: https://optn.transplant.hrsa.gov/data/. [Accessed: 08-Feb-2020].

[7] S. Bersini, I. K. Yazdi, G. Talò, S. R. Shin, M. Moretti, and A. Khademhosseini, "Cell-microenvironment interactions and architectures in microvascular systems," *Biotechnol. Adv.*, 2016.

[8] M. Kutz, *Standard Handbook of Biomedical Engineering & Design*. McGraw-Hil, 2003.

[9] J. D. Bronzino, *Biomedical Engineering Handbook*, Second. CRC Press LLC, 2000.

[10] D. M. Dean, A. P. Napolitano, J. Youssef, and J. R. Morgan, "Rods, tori, and honeycombs: the directed self-assembly of microtissues with prescribed microscale geometries.," *FASEB J.*, vol. 21, no. 14, pp. 4005–12, Dec. 2007.

[11] "3D Cell Culture | 3D Petri Dish | Microtissues." [Online]. Available: http://www.microtissues.com/.

[12] E. Leary, S. Curran, M. Susienka, K. L. Manning, A. M. Blakely, and J. R. Morgan, "Micro-moulded non-adhesive hydrogels to form multicellular microtissues - the 3D Petri Dish®," in *Technology Platforms for 3D Cell Culture*, Chichester, UK: John Wiley & Sons, Ltd, 2017, pp. 97–122.

[13] A. Napolitano *et al.*, "Scaffold-free three-dimensional cell culture utilizing micromolded nonadhesive hydrogels," *Biotechniques*, vol. 43, no. 4, pp. 494–500, Oct. 2007.

[14] D. K. Molina and V. J. M. DiMaio, "Normal Organ Weights in Women," *Am. J. Forensic Med. Pathol.*, vol. 33, no. 4, p. 1, 2011.

[15] D. K. Molina and V. J. M. DiMaio, "Normal Organ Weights in Men," *Am. J. Forensic Med. Pathol.*, vol. 33, no. 4, p. 1, 2011.

[16] C. M. Livoti and J. R. Morgan, "Self-Assembly and Tissue Fusion of Toroid-Minimal Building Units," *Tissue Eng. Part A*, vol. 16, no. 6, pp. 2051–2061, 2010.

[17] A. P. Rago, D. M. Dean, and J. R. Morgan, "Controlling cell position in complex heterotypic 3D microtissues by tissue fusion.," *Biotechnol. Bioeng.*, vol. 102, no. 4, pp. 1231–41, Mar. 2008.

[18] M. J. Susienka, B. T. Wilks, and J. R. Morgan, "Quantifying the kinetics and morphological changes of the fusion of spheroid building blocks," *Biofabrication*,

vol. 8, p. 045003, 2017.

[19] F. Marga *et al.*, “Toward engineering functional organ modules by additive manufacturing.,” *Biofabrication*, vol. 4, no. 2, p. 022001, Jun. 2012.

[20] Y. Takeoka *et al.*, “Regeneration of esophagus using a scaffold-free biomimetic structure created with bio-three-dimensional printing,” *PLoS One*, vol. 14, no. 3, p. e0211339, 2019.

[21] M. Itoh, K. Nakayama, R. Noguchi, K. Kamohara, and K. Furukawa, “Scaffold-Free Tubular Tissues Created by a Bio-3D Printer Undergo Remodeling and Endothelialization when Implanted in Rat Aortae,” *PLoS One*, vol. 10, no. 9, p. e0145971, 2015.

[22] K. Arai *et al.*, “Fabrication of scaffold-free tubular cardiac constructs using a Bio-3D printer,” *PLoS One*, vol. 13, no. 12, p. e0209162, Dec. 2018.

[23] N. I. Moldovan, N. Hibino, and K. Nakayama, “Principles of the Kenzan Method for Robotic Cell Spheroid-Based Three-Dimensional Bioprinting,” *Tissue Eng. Part B. Rev.*, vol. 23, no. 3, pp. 237–244, 2017.

[24] A. M. Blakely, K. L. Manning, A. Tripathi, and J. R. Morgan, “Bio-Pick, Place, and Perfuse: A New Instrument for Three-Dimensional Tissue Engineering,” *Tissue Eng. Part C Methods*, vol. 21, no. 7, pp. 737–746, Jul. 2015.

[25] B. C. Ip, F. Cui, A. Tripathi, and J. R. Morgan, “The bio-gripper: a fluid-driven micro-manipulator of living tissue constructs for additive bio-manufacturing,” *Biofabrication*, vol. 8, no. 2, p. 025015, 2016.

[26] B. C. Ip, F. Cui, B. T. Wilks, J. Murphy, A. Tripathi, and J. R. Morgan, “Perfused Organ Cell-Dense Macrotissues Assembled from Prefabricated Living

Microtissues," *Adv. Biosyst.*, vol. 2, p. 1800076, Aug. 2018.

[27] R. Noguchi *et al.*, "Development of a three-dimensional pre-vascularized scaffold-free contractile cardiac patch for treating heart disease," *J. Hear. Lung Transplant.*, vol. 35, no. 1, pp. 137–145, 2016.

[28] P. A. Fleming, W. S. Argraves, C. Gentile, A. Neagu, G. Forgacs, and C. J. Drake, "Fusion of uniluminal vascular spheroids: a model for assembly of blood vessels.," *Dev. Dyn.*, vol. 239, no. 2, pp. 398–406, Feb. 2010.

[29] C. Gentile, P. a. Fleming, V. Mironov, K. M. Argraves, W. S. Argraves, and C. J. Drake, "VEGF-mediated fusion in the generation of uniluminal vascular spheroids," *Dev. Dyn.*, vol. 237, no. 10, pp. 2918–2925, 2008.

[30] J. M. Kelm *et al.*, "Tissue-transplant fusion and vascularization of myocardial microtissues and macrotissues implanted into chicken embryos and rats.," *Tissue Eng.*, vol. 12, no. 9, pp. 2541–53, Sep. 2006.

[31] J. M. Kelm *et al.*, "Design of custom-shaped vascularized tissues using microtissue spheroids as minimal building units.," *Tissue Eng.*, vol. 12, no. 8, pp. 2151–60, Aug. 2006.

[32] "Advanced Regenerative Manufacturing Institute." [Online]. Available: https://www.armiusa.org/. [Accessed: 26-Nov-2019].

[33] R. Kato *et al.*, "A Compact, Automated Cell Culture System for Clinical Scale Cell Expansion from Primary Tissues," *Tissue Eng. Part C Methods*, vol. 16, no. 5, pp. 947–956, Oct. 2010.

[34] R. J. Thomas, A. Chandra, Y. Liu, P. C. Hourd, P. P. Conway, and D. J. Williams, "Manufacture of a human mesenchymal stem cell population using an automated

cell culture platform," *Cytotechnology*, vol. 55, no. 1, pp. 31–39, Sep. 2007.

[35] J. K. Fraser, K. C. Hicok, R. Shanahan, M. Zhu, S. Miller, and D. M. Arm, " The Celution ® System: Automated Processing of Adipose-Derived Regenerative Cells in a Functionally Closed System ," *Adv. Wound Care*, vol. 3, no. 1, pp. 38–45, Jan. 2014.

[36] N. V. Mekhileri *et al.*, "Automated 3D bioassembly of micro-tissues for biofabrication of hybrid tissue engineered constructs," *Biofabrication*, vol. 10, no. 2, p. 024103, Jan. 2018.

[37] P. Bartolo, M. Domingos, A. Gloria, and J. Ciurana, "BioCell Printing: Integrated automated assembly system for tissue engineering constructs," *CIRP Ann. - Manuf. Technol.*, vol. 60, no. 1, pp. 271–274, 2011.

[38] W. LaBarge, A. Morales, D. Pretorius, A. Kahn-Krell, R. Kannappan, and J. Zhang, "Scaffold-Free Bioprinter Utilizing Layer-By-Layer Printing of Cellular Spheroids," *Micromachines*, vol. 10, no. 9, p. 570, Aug. 2019.

[39] C. J. Nycz, H. A. Strobel, K. Suqui, J. Grosha, G. S. Fischer, and M. W. Rolle, "A Method for High-Throughput Robotic Assembly of Three-Dimensional Vascular Tissue," *Tissue Eng. Part A*, vol. 25, no. 17 and 18, pp. 1251–60, 2019.

Chapter 2

Funnel-Guided Positioning of Multi-cellular Microtissues to Build Macrotissues

Tissue Engineering: Part C. 24(10) doi: 10.1089/ten.tec.2018.0137

Kali L. Manning, Sc.M.[1, 2], Andrew H. Thomson[1], Jeffrey R. Morgan, Ph.D. [1, 2]

[1] Department of Molecular Pharmacology, Physiology and Biotechnology

[2] Center for Biomedical Engineering

Brown University, Providence, RI, USA

2.1 Abstract

The field of tissue engineering is developing new additive manufacturing technologies to fabricate 3D living constructs for use as in vitro platforms for the testing of drugs and chemicals, or to restore lost function in vivo. In this paper, we describe the funnel-guide, a new additive manufacturing strategy for the non-contact manipulation and positioning of multi-cellular microtissues and we show that the funnel-guide can be used to build macrotissues layer-by-layer. We used agarose micro-molds to self-assemble cells into toroid-shaped and honeycomb-shaped microtissues, and observed that when falling in cell culture medium, the microtissues spontaneously righted themselves to a horizontal orientation. We fabricated a funnel to guide these falling toroids and honeycombs into precise positions and stack them wherein they fused to form tubular structures. We tested multiple cell-types and toroid sizes, and ultimately used the funnel-guide to create a stack of 45 toroids that fused into a tube 5 mm long with an inner diameter of 600 μm. The funnel-guide is a new principle for the manipulation of microtissues and is a platform for the layer-by-layer positioning of microtissue building blocks to form macrotissues.

2.2 Introduction

The primary goal of tissue engineering is to construct large solid tissues with *in vivo* cell density that can be used to restore lost function *in vivo*. In addition, these living constructs can be used as *in vitro* platforms for the testing of drugs and chemicals. Additive manufacturing (layer-by-layer) is one of several strategies being deployed for tissue engineering. [1] Extrusion based methods, such as 3D bio-printing, use a computer guided nozzle to precisely deposit a biocompatible polymer containing cells and/or spheroids to build tissues layer-by-layer [2]. Bio-printing has been used to construct tissues such as skin and cartilage, as well as tubes such as blood vessels and valves. [1], [3], [4] The polymer provides the majority of the structural integrity of the printed tissue and often the conditions necessary for polymerization limit its use. For example, most 3D printed tissues are deposited layer-by-layer on a surface in air to allow for polymerization. Thus, a limitation of 3D printing is its inability to print tissues submerged in cell culture medium or in the actively perfused environment necessary to replenish the nutrients needed to sustain the viability of large constructs with organ cell density.

The manipulation and placement of scaffold-free spheroids or microtissues as building blocks is an alternative additive manufacturing method. Scaffold-free microtissues produced by hanging drops and agarose micro-molds, rely on the innate ability of cells to aggregate and self-assemble a multi-cellular microtissue [5]. When the surfaces of these microtissues are brought into contact, they undergo fusion to form a larger tissue and, like self-assembly, this fusion occurs submerged in cell culture medium [6], [7]. The Kenzan method builds a macrotissue by precisely placing spheroids and piercing them onto an array of microneedles. Adjacent spheroids fuse to form a larger tissue which can

be removed from the microneedles for further processing which can include culture in a bioreactor with perfusion for tubular structures. [8], [9]

The Bio-Pick, Place and Perfuse (Bio-P3) is another microtissue manipulation method. Agarose micro-molds are used to direct cells to self-assemble microtissues into the shape of a large honeycomb (~8 x 10^6 cells/honeycomb). After removal from the mold, the planar honeycomb shaped microtissues are gripped by fluid suction across a transparent membrane. Layer-by-layer, the gripped honeycombs are moved through culture medium where they are stacked on a build head. The lumens of each layer are aligned and the build head continuously draws culture medium through the stack as the layers fuse into a macrotissue. [10], [11]

Scaffold-free tissue engineering creates tissue building parts with different shapes (e.g., spheroid, toroid, honeycomb). These building parts have organ cell density and fuse to one another.[12], [13] However, there are a limited number of technologies that can manipulate these building parts to create more complex macrotissues. We hypothesize that the shape of a building part and how it settles in liquid medium is a property that can be harnessed. Here we describe the funnel-guide (FG) a new microtissue manipulation method for the easy positioning and stacking of multi-cellular microtissues. We used agarose micro-molds to self-assemble cells into toroid-shaped microtissues and when these toroids were transferred by pipette to a chamber, we observed that when falling in cell culture medium the toroids spontaneously righted themselves to a horizontal orientation. We designed the mouth and stem of a funnel to guide these falling toroids into precise positions and stack them, wherein they fused to form a tubular structure. Using the same principles, we designed a funnel-guide to position and stack honeycomb shaped microtissues. The

funnel-guide is a new principle for the manipulation of microtissues and is a platform for the easy layer-by-layer positioning of microtissue building blocks to form macrotissues.

2.3 Materials and Methods

2.3.1 Cell Culture, Micro-Mold Fabrication and Formation of Microtissues

Human hepatocellular carcinoma (HepG2) cells were expanded in Eagle's Minimum Essential Medium (EMEM) (Corning Incorporated, Corning, NY) supplemented with 10% fetal bovine serum (FBS) (Thermo Fisher Scientific, Waltham, MA) and 1% penicillin/streptomycin (MP Biomedicals, LLC, Santa Ana, CA). Human umbilical vein endothelial cells (HUVEC) were expanded in Endothelial Growth Medium (EGM) with Supplement Kit (PromoCell, Heidelberg, Germany) and 1% penicillin/streptomycin (MP Biomedicals, LLC). Cultures were maintained in a 37°C, 5% CO_2 atmosphere. Cells were trypsinized, counted, and re-suspended to the desired cell density for each experiment.

Agarose gels were cast from 3D Petri Dish ® micro-molds (Microtissues, Inc., Providence, RI) as previously described [10]. Agarose gels were made with powdered agarose (Low-EEO/Multi-Purpose/Molecular Biology Grade, Fisher BioReagents) (Thermo Fisher Scientific) sterilized by autoclaving and then dissolved in sterile water to 2% (weight/volume). Micro-molds with different recess geometries were used to create spheroid, toroid or honeycomb microtissues. Round recesses for spheroids were 800 µm in diameter and contained 35 recesses per gel. Toroid recesses were 1400 µm in diameter with a central agarose peg of 600 µm and surrounding 400 µm trough, and contained 36 recesses per gel. Large toroid recesses were 2.2 mm in diameter with a central agarose peg of 1 mm and surrounding 600 µm troughs, and contained 25 recesses. The large toroid mold was a

thermowax mold produced with a rapid prototyping machine (3D Systems Corporation, Andover, MA). The wax molds were used to cast 13% polyacrylamide (Dow Corning Corporation, Midland, MI) gels. Agarose gels were cast from the polyacrylamide gels. Honeycomb recesses had a maximum diameter of 3.4 mm with a central peg and single orbital of six pegs 600 μm in diameter and a surrounding trough of 400 μm. Each gel contained a single honeycomb recess. Gels were seeded at a density of 2,000 cells per spheroid feature, 50,000 cells per toroid feature, 120,000 cells per large toroid feature, and 375,000 cells per honeycomb feature. Cells aggregated in the micro-molds and self-assembled microtissues were used 24 hours after cell seeding.

2.3.2 Fabrication and Use of the Tissue Sliding Ramp

The tissue sliding set-up consisted of a 30 mL beaker sitting in a circular recess of an acrylic platform attached to a goniometer used to set the angle of the ramp (Thorlabs, Newton, NJ). Beneath the beaker were grid lines for measuring distance. The sliding surface was created by pipetting 3 mL of 2% (weight/volume) molten agarose into a 30 mL beaker, allowing it to solidify and then equilibrating it with 12 mL of room temperature EMEM supplemented with 1% penicillin/streptomycin. The beaker was then placed in the acrylic platform at an angle set by the goniometer. HepG2 toroid and honeycomb microtissues were carefully placed into the beaker using 200 μl or 1000 μl pipette tips (VWR, Radnor, PA), made to have wider bores by cutting with a sterile razor blade (McMaster Carr, Elmhurst, IL). Once on the ramp, the time to travel 10 mm was measured for angles of 15°, 20°, and 30° and velocities calculated for toroids and honeycombs.

2.3.3 Fabrication and Use of the Funnel-Guide

A negative replica of the funnel-guide (FG) was designed in SolidWorks (Dassault Systemes SolidWorks Corporation, Waltham, MA) and consisted of three chambers; a free-fall chamber, a funnel chamber and a stacking chamber. The free-fall chamber was 8 mm x 8 mm and10 mm in height, the funnel was 77°and 13 mm in height and the stacking chamber was square in shape, 10 mm in height and either 1.5 mm, 800 µm or 2.3 mm in diameter for the regular, small and large toroids, respectively. The FG for honeycombs had a 14 mm free-fall, 77° funnel and a 3.5 mm honeycomb shaped stacking chamber. The negative replicas of the FGs (FG molds) were fabricated using a Form 1+ SLA 3D printer (Formlabs, Somerville, MA), and were UV cured for 15 minutes using a photochemical reactor (Rayonet, Branford, CT).

The FG was formed in agarose by using the negative FG as a mold. Molten 2% agarose (weight/volume) was added to either a cuvette, or 1 cm inner diameter polycarbonate square plastic tubing (McMaster Carr, Elmhurst, IL), and the FG mold inserted. After agarose solidification, the FG mold was removed, leaving behind a void in the agarose in the shape of the desired FG. FGs used for velocity measurements were filled with serum-free medium and immediately used. FGs used for toroid fusion and tube creation were removed from the tubing and equilibrated in 10 mL serum-free medium overnight at 37°C. Toroids and honeycombs were added to the FG using a wide-bore pipette tip.

2.3.4 Measuring the Settling Velocity of Microtissues

A cuvette (Dynalon Corporation, Rochester, NY) filled with serum-free medium was used to measure the free-fall velocity of HUVEC and HepG2 spheroids, toroids, and

HepG2 honeycombs. EGM supplemented with 1% penicillin/streptomycin was used for the HUVEC microtissues, and EMEM supplemented with 1% penicillin/streptomycin was used for the HepG2 microtissues. Microtissues were placed into the cuvette using wide-bore 200 µl or 1000 µl pipette tips. The addition of the microtissue and its fall to the bottom of the cuvette was recorded using a DinoLite digital microscope (BigC Dino-Lite, Torrance, CA) and the ImageJ (National Institutes of Health, Bethesda, MD) Webcam Capture plugin that captured images every 250 msec. Time lapse images were used to calculate the velocities of falling microtissues in all three chambers.

2.3.5 Evaluation of Funnel-Guides and Tube Extraction

Microtissue alignment within the stacking chamber was assessed by visual inspection and documented with the DinoLite digital microscope. Images of the side of the stack and the bottom of the stack looking into the lumen were taken at 0h and 24h. Microtissue fusion was evaluated via extraction of the tissue tube from the FG. FGs used for tube extraction were cut with a razor blade vertically into two pieces after equilibration. The two halves were then placed into the square polycarbonate tubing, filled with the appropriate culture medium and toroids added to create a stack. Stacks were allowed to fuse overnight at 37°C and 5% CO_2. At 24h, the tubes created by the fused toroids were extracted by removing the FG and placing it into a 100 mm culture dish (Corning Incorporated, Corning, NY) filled with 40 mL of serum-free medium. Spatulas were then used to gently lift one half of the FG away from the other, releasing the tube from the stacking chamber.

2.3.6 LIVE/DEAD® Staining

For LIVE/DEAD® staining HepG2 toroid microtissues were washed for ten minutes in EMEM supplemented with 1% penicillin/streptomycin three times. Toroids were then incubated in a mixture of EMEM supplemented with 1% penicillin/streptomycin with 1 µm calcein-AM and 4 µm ethidium homodimer-1 (Invitrogen, Carlsbad, CA) for one hour at 37ºC. 24h toroids were removed from gels and pipetted into the mixture. Microtissue viability was assessed with fluorescent imaging using a Zeiss Axio Observer Z1 equipped with an AxioCam MRm camera with ZEN software (Carl Zeiss Microscopy, LLC, Thornwood, NY) and an X-Cite 120 fluorescence illumination system (EXFO Photonic Solutions, Mississauga, Ontario, Canada).

2.3.7 Statistical Analysis

Statistical analysis of velocities was done using a Kruskal-Wallis one-way analysis of variance (ANOVA) on ranks, and a post hoc analysis using Dunn's Method, with significant values having a $p<0.05$.

2.4 Results

2.4.1 Velocity of Microtissue Sliding Depends on Angle

To determine if toroids and honeycombs would slide along a non-adherent surface in a liquid environment, we designed a sliding ramp using a goniometer (**Figure 2.1**). HepG2 cells were seeded in either toroid (~5 x10^4 per tissue) or honeycomb (~3.75 x 10^5) shaped micro-molds. Twenty four hours after self-assembly, toroids and honeycombs were removed from the micro-molds and placed at inclines of 15°, 20° or 30° (**Supplemental Video 2.1.**) Toroids and honeycombs slid at all three angles tested and the velocities of all

inclines were significantly different, with microtissues sliding the fastest at 30°. Additionally, velocities of toroids and honeycombs were significantly different, with honeycombs sliding at a faster velocity.

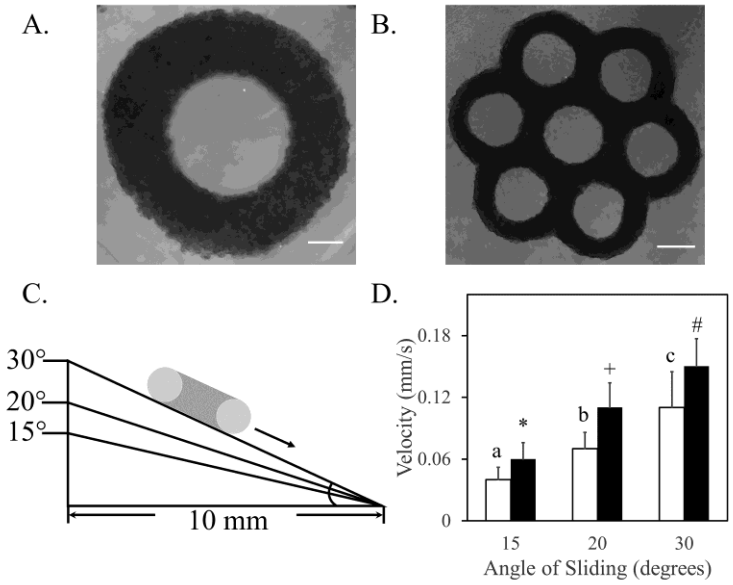

Figure 2.1 *Velocity of microtissue sliding depends on angle.* Images of microtissues self-assembled by seeding HepG2 cells in either toroid (5.0 x 10^4) (A) or honeycomb (3.75 x 10^5) (B) shaped agarose micro-molds. Toroid and honeycomb microtissues removed from the micro-molds were slid down a 10 mm incline of 15°, 20° and 30° and the velocity of sliding measured (C). Velocities with a letter are significantly different from velocities with a symbol (toroid vs. honeycomb). Velocities with different symbols are significantly different from one another (angles tested). Velocities with different letters are significant from one another (angles tested) ($p<0.05$). White bars represent toroids and black bars represent honeycombs (D). Error bars represent standard deviation (n =30). Scale bars are 200 µm and 500 µm.

2.4.2 Toroids Spontaneously Right Themselves During Free-Fall

To determine if a stack of toroids could be built via sliding, we designed a device molded in agarose with two components, a funnel chamber (30°, 10 mm tall, 12 mm mouth) and a stacking chamber (1.5 mm diameter, 20 mm tall) (**Figure 2.2.2**). To test the

device, we filled it with cell culture medium, dropped in toroids and observed their sliding and settling behavior using real time video. Toroids settled onto the wall of the device, and slid into the stacking chamber with a vertical orientation, preventing lumen alignment. However, when dropping toroids, we noticed an interesting behavior. Independent of its initial orientation, a free falling toroid righted itself and assumed a horizontal orientation for the rest of the free-fall (**Supplemental Video 2.2)**. To understand this phenomenon, we dropped toroids into a cuvette to observe their free-fall and measure their velocity. On average, the toroids required 10mm of free-fall to right themselves and assume a horizontal orientation. To ensure this was not cell type specific or dependent on individual cell diameter, we tested toroids of HUVEC and MCF-7 cells (data not shown), which have a cell diameter of 14 μm and 24 μm, respectively. Similar to HepG2 toroids, toroids of HUVEC and MCF-7 cells also righted themselves within 10 mm of free-fall. There was no visible difference in toroid falling or orientation when we tested the funnel-guide in serum-free EMEM, DMEM and EGM, EGM with ~2% serum and EMEM with 10% serum (data not shown).

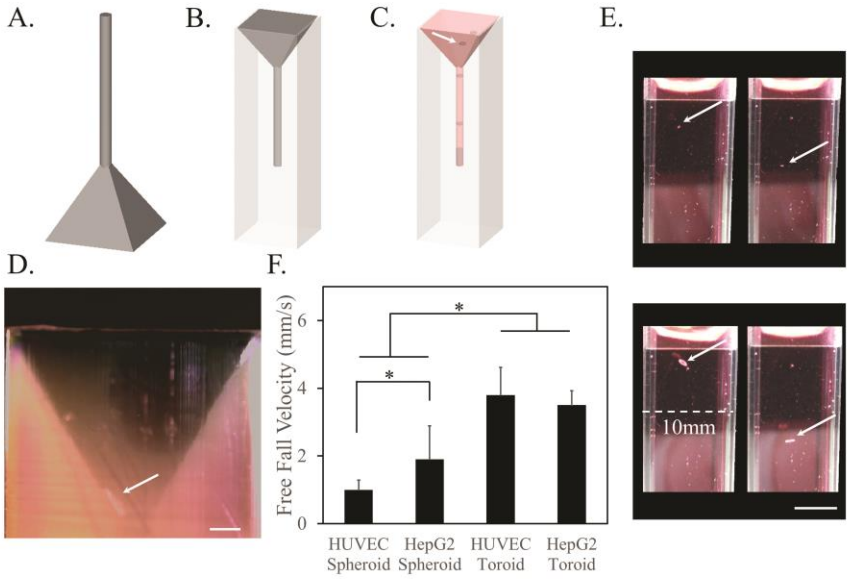

Figure 2.2 *Toroids right themselves to a horizontal orientation when in free-fall.* Schematics of a device with a funnel chamber and a stacking chamber designed to determine if sliding could be used to create a stack of toroids (A, B, C). To form the device, a mold was inserted into a cuvette filled with molten agarose and then removed upon solidification. The molded agarose gel was filled with culture medium, and HepG2 toroids dropped into the funnel. Images of dropped toroids that have settled onto the funnel wall, and slid down into the stacking chamber in a vertical orientation (D). Scale bar is 1.5 mm. Falling toroids righted themselves to a horizontal orientation in free-fall. Images of spheroids (top) and toroids (bottom) falling in a cuvette filled with culture medium, indicated by arrows (E). Toroids righted themselves to a horizontal orientation within 10 mm of free-fall, as shown in the bottom right image. Scale bar is 6 mm. Quantification of free-fall velocities of HepG2 and HUVEC spheroids and toroids (F). HUVEC spheroid and HepG2 spheroid velocities were significantly different, and spheroid and toroid velocity values were statistically significant with a p-value <0.05 calculated by Kruskal-Wallis ANOVA on ranks, and a post hoc analysis using Dunn's Method. Error bars represent the standard deviation (n = 31, 48, 37, 30 for HUVEC spheroid, HepG2 spheroid, HUVEC toroid and HepG2 toroid respectively).

2.4.3 Defining the Critical Components of the Funnel-Guide

To determine if the ability of toroids to right themselves could be harnessed, we designed a funnel-guide (FG) (**Figure 2.3**). The FG had three chambers, a free-fall chamber (10 mm in height), a funnel chamber (13 mm in height), and a stacking chamber (10 mm

in height). The angle of the funnel was increased from 30° to 77°. To test the performance of the guide, we dropped in toroids and observed their settling behavior and measured their velocity. Surprisingly, unlike our first mold with a 30° funnel chamber, toroids did not settle onto the wall, instead they righted themselves and remained horizontal as they were guided by the funnel down to the stacking chamber (**Supplemental Video 2.3**). Velocities in the free-fall, funnel and stacking chambers were all progressively slower and significantly different. However, the toroids were misaligned when they settled into the stacking chamber with a circular cross section (50 μm gap between the toroid and the walls). To improve settling and alignment, we changed the funnel and stacking chambers to have a square cross section, in order to decrease resistance between the microtissue and the wall. Velocities in the free-fall and stacking chamber, and funnel and stacking chamber were statistically different. The design of the cross section of the stacking chamber of the funnel-guide is important for alignment of the stack of toroids. The chamber with the square cross section resulted in alignment of the stack of toroids, whereas the stack of toroids in the chamber with a circular cross section were unacceptable. The stacking chamber with a square cross section had a 300 μm space on the four corners and a 50 μm gap along the sides, and using the FG with this stacking chamber, we created a stack of 45 aligned toroids.

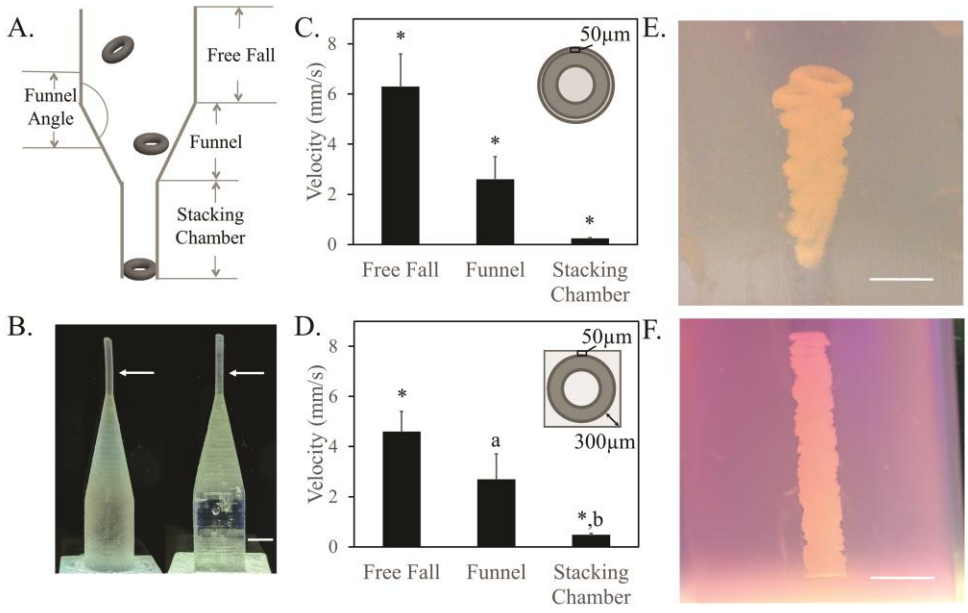

Figure 2.3 *Design and testing of the funnel-guide (FG).* Schematic of key elements of the FG: a 10 mm free-fall space for the toroid to right itself, a funnel with an angle between $30< \measuredangle < 77$, and a stacking chamber with a diameter slightly larger than the toroid diameter (A). Images of the 3D printed molds used to mold the FG. Molds that form a circular (left) or square (right) stacking chamber (arrows) (B). Scale bar is 5 mm. Velocities of toroids in the free-fall chamber, the funnel chamber and the stacking chamber for FGs with either a circular stacking chamber (C) or a square stacking chamber (D). For the circular stacking chamber, each value was statistically significant. For the square stacking chamber, free-fall and funnel chambers were significantly different from the stacking chamber velocity, with a p-value <0.05 calculated by Kruskal-Wallis ANOVA on ranks, and a post hoc analysis using Dunn's Method (n = 10, circular, n = 10 square). Images of a stack of toroids in the circular stacking chamber (10 HepG2 toroids)(E) and the square stacking chamber (45 HepG2 toroids)(F). Scale bars are 1 mm and 2 mm, respectively.

2.4.4 Stacking of Toroids Occurs Independent of Size and Cell Type

To determine if the FG could be used with toroids of different sizes and cell types, we tested large HepG2 toroids (diameter of 2.2 mm, ~1.2 x10^5 cells) and small HUVEC toroids (diameter of 700 µm, ~5.0 x 10^4 cells) (**Figure 2.4**). When dropped into the FG, large HepG2 toroids righted themselves to a horizontal orientation and were guided by the funnel into the stacking chamber (square cross section 2.3 mm by 2.3 mm) to form a stack

of 20 toroids. Likewise, smaller HUVEC toroids were guided into the stacking chamber (square cross section 800 µm by 800 µm) and formed a stack of 20 toroids. Stacks were incubated for twenty four hours at 37ºC and images taken before and after incubation showed that the toroids had fused into a tube, which was confirmed by which was confirmed by gently taking apart two halves of the FG to harvest the tube (**Supplemental Video 2.4**). To determine the viability of microtissues after they have been picked up with a pipette, HepG2 toroids (5.0×10^4 and 1.2×10^5) were pipetted and stained for viability. Error! Reference source not found. shows that the majority of the cells are alive, with some ead cells.

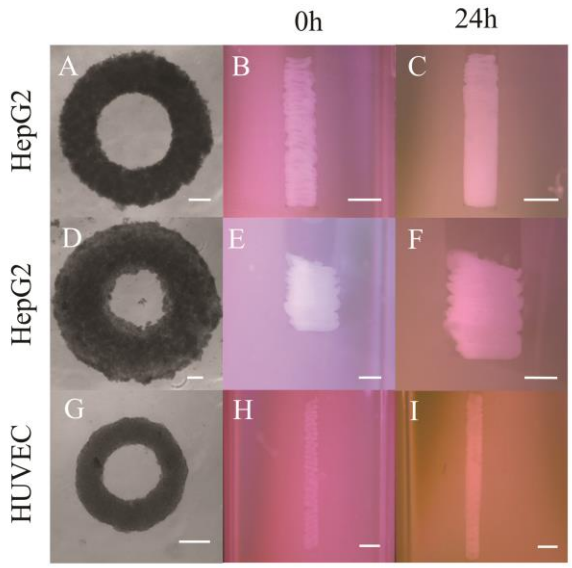

Figure 2.4 *FGs can stack larger toroids and toroids of different cell types.* Images of a small HepG2 toroid (5.0×10^4 cells)(A), a large HepG2 toroid (1.2×10^5 cells)(D) and a small HUVEC toroid (5.0×10^4 cells)(G). Scale bars are 200 µm. Images immediately after stack formation (B, E, H) and twenty four hours after incubation at 37ºC (C, F, I). Stack of forty small HepG2 toroids (B, C). Scale bars are 1.5 mm. Stack of twenty large HepG2 toroids (E, F). Scale bars are 1.0 mm. Stack of twenty five small HUVEC toroids (H, I). Scale bars are 1.0 mm.

2.4.5 Honeycombs Can Be Stacked

To determine if honeycombs (3.4 mm longest diameter, ~3.75 x 10^5 HepG2 cells) could be stacked, we measured their velocity in free-fall and observed that they also righted themselves (Error! Reference source not found.) (**Supplemental Video 2.5**). A FG for honeycombs was fabricated and tested by dropping in 10 honeycombs. Honeycombs righted themselves, were guided down to the stacking chamber (3.5 mm in diameter, honeycomb shaped) and formed an aligned stack of 10 honeycombs (**Supplemental Video 2.6**). Velocities in each chamber were significantly different and imaging from the bottom of the stack revealed that all 7 lumens were aligned.

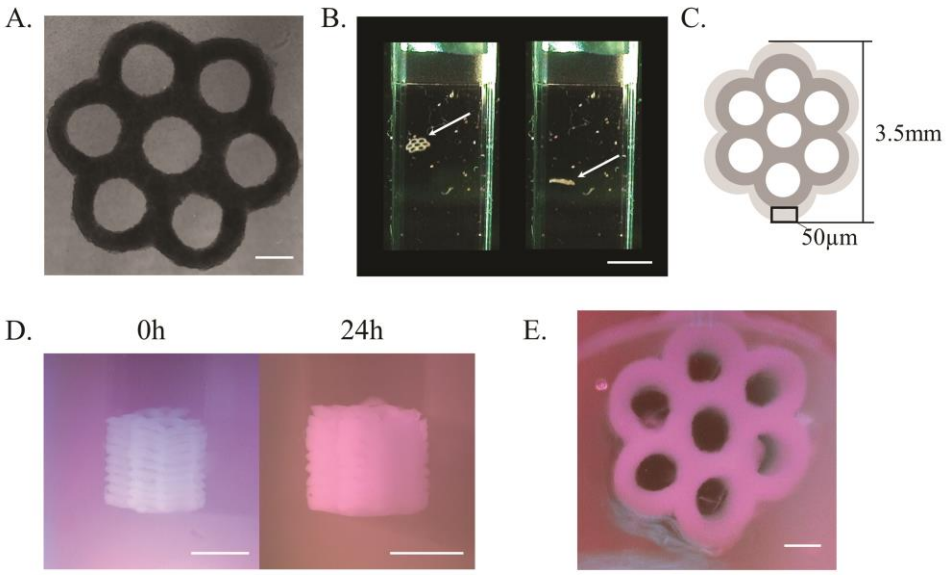

Figure 2.5 *Honeycombs can be stacked by a FG.* Image of a honeycomb microtissue formed by seeding HepG2 cells (3.75 x 10^5 cells) into an agarose micro-mold. Scale bar is 500 µm (A). Images of honeycombs (arrows) in free-fall in a cuvette righting themselves to a horizontal orientation (B). Scale bar is 6 mm. Cross section diagram of FG with a honeycomb shaped stacking chamber 3.5 mm in maximum diameter (C). Side view images of a stack of ten HepG2 honeycombs formed by a FG designed for honeycombs. Images immediately after stack formation and twenty four hours after incubation at 37°C (D). Scale bars are 2 mm. Velocities for honeycombs (± standard deviation) in the free-fall chamber (6.9±1.9 mm/s), the funnel chamber (3.0±0.4 mm/s) and the stacking chamber (0.44±0.08

mm/s) were statistically significant with a p-value <0.05 calculated by Kruskal-Wallis ANOVA on ranks, and a post hoc analysis using Dunn's Method (n = 20). Image from below of a stack of five HepG2 honeycombs showing alignment of lumens. Scale bar is 500 µm. (E)

2.5 Discussion

The field of tissue engineering is developing new additive manufacturing technologies to fabricate 3D living constructs. In this paper, we describe the funnel-guide, a new additive manufacturing strategy for the non-contact manipulation and positioning of multi-cellular microtissues and show that the funnel-guide can be used to build macrotissues layer-by-layer. When transferred to the funnel-guide by a pipette, toroid and honeycomb shaped microtissues right themselves and assume a horizontal orientation as they fall through the culture medium. The funnel-guide harnesses this phenomenon and guides the settling microtissues into prescribed positions. By carefully designing the critical features of the funnel-guide (falling chamber, funnel angle and stacking chamber) we were able to create a stack of 45 toroids, and a stack of 10 honeycombs with aligned lumens that fused to form macrotissues.

The building blocks positioned by the funnel-guide were produced by seeding cells into agarose micro-molds that directed the cells to aggregate and self-assemble toroid and honeycomb shaped microtissues of prescribed geometries. Both microtissues are planar (~200 µm in thickness) radially symmetrical structures with holes or lumens (toroid 1, honeycomb 7) made of cells that form tissue rings. When we tested different sizes (toroid outer diameters 700 µm, 1.4 mm and 2.2 mm, honeycomb diameter 3.4 mm), we observed that all structures righted themselves as they settled and this occurred within a distance of 10mm regardless of size or shape. The only exception were toroids or honeycombs that

were not intact. They failed to assume a horizontal orientation suggesting that microtissue shape influences settling behavior.

To position the free-falling microtissues, the funnel-guide has three chambers, the free-fall chamber, the funnel chamber and the stacking chamber. The free-fall chamber has a vertical dimension (>10 mm) that provides enough distance for a microtissue to right itself during free-fall. The free-fall chamber also has a large square opening (8 mm x 8 mm) to easily accommodate the delivery of microtissues from a wide bore pipette tip (diameter ~3 mm) that is carefully brought into contact with the surface of the culture medium. The free-fall chamber connects to the funnel chamber whose design focuses the falling microtissue without disrupting its horizontal orientation. We found that shallow angles, such as 30°, disrupted the horizontal orientation and caused the falling microtissue to settle onto the surface of the funnel and begin sliding. Whereas a steep angle, such as 77°, did not disrupt the horizontal orientation, but instead guided the falling microtissue down towards the opening of the stacking chamber.

There are three important design features of the stacking chamber; its length, its size and the shape of its cross sectional area (mouth). The length of the stacking chamber dictates the maximum height of the stack of microtissues. The size and shape of the stacking chamber's mouth controls the precision of the entry of falling microtissues as well as the orientation and alignment of the microtissues as they settle in the stacking chamber. The size and shape of the mouth and stacking chamber must be large enough to accommodate the size of the falling microtissue, but not too large that it fails to provide the constraint needed to align falling microtissues into a stack. There is a 50 μm gap between the tissue and the wall of the stacking chamber. This gap allows the tissue to settle

freely, while restricting *x-y* motion in order to guide it towards the stack of existing tissues. Size and shape should also accommodate some variation in the size of the microtissues. Throughout our experiments, we observed that HepG2 toroids settle and align more consistently than HUVEC toroids. This could be because the size of HepG2 toroids were more consistent in size than HUVEC toroids, which are more contractile and were more variable in size after harvesting from the agarose micro-molds. The lumens of individual toroids contract over time and contraction varies with cell type. Contraction does proceed at a predictable rate and this shrinkage can be anticipated in the design of the part [6].

The shape of the mouth and cross sectional area of the stacking chamber controls the entry and alignment of the falling microtissues. In our first designs with a circular mouth and tubular stacking chamber, the horizontal orientation of falling toroids was not adequately maintained resulting in unacceptable alignment. When the mouth and chamber were changed to a square shape, the horizontal orientation of falling toroids was maintained and alignment of the stack was achieved. The square shape likely decreases the resistance on the falling microtissue from the wall of the stacking chamber, by providing openings for fluid flow in the corners. This decreased resistance allows for the toroids to gently settle to the bottom of the stacking chamber without disruption of the horizontal orientation. Shape is also important for guiding honeycombs into proper alignment. The honeycomb shape of the stacking chamber orients the honeycomb petals when entering the stacking chamber, resulting in alignment of the 7 lumens. To facilitate extraction of tubes, the FG was split into two halves using a razor blade prior to use. This split did not alter the functions of the FG. After settling and fusion of toroids, the two halves of the FG were gently taken apart to harvest the tube (**Supplemental Video 2.4**).

Measurements of velocity provided valuable insights into design as well as operating principles. In free-fall, velocity increased as microtissue size was increased (spheroid < toroid < honeycomb). The falling trajectory of an object through liquid is dictated by the Reynolds number, the moment of initial inertia and the ratio of object thickness to diameter, and can be calculated using Stoke's Law. The equation for a spheroid is $v = \frac{2}{9}\frac{\rho_p - \rho_f}{\mu} g r^2$, and for a torus $v = \frac{P}{2\mu} r + u$ where *v* is velocity, ρ_p is the part density, ρ_f is the fluid density, μ is the dynamic viscosity, *g* is gravity, *r* is the radius of the part, *P* is pressure, and u is a harmonic function. [14], [15] Radius is directly proportional to velocity, thus an increase in radius, (400 μm spheroid versus a 1.4 mm toroid), should result in an increase in velocity. It is unclear why HepG2 spheroids fell at a faster velocity than HUVEC spheroids. Two possible explanations are a difference in size (HepG2 spheroids were larger) and or a difference in density. We also observed that large toroids and honeycombs had a more erratic motion upon placement in liquid free-fall. This could be explained by an increase in the ratio of object thickness to diameter causing more chaotic falling trajectories for larger microtissues [16]. The ratio of thickness to diameter increases from ~1:7 for regular toroids to ~1:12 for large toroids, and ~1:17 for honeycombs. However, the above principles assume laminar flow, and during our experimentation we observed eddies, as seen in **Supplemental Video 2.2**. These eddies suggest turbulent flow, meaning a more complex model than Stoke's Law is needed for microtissue settling velocity.

When the gravity-driven motion of microtissues was constrained, velocity also varied in some interesting ways. In a simple incline, the velocity of sliding microtissues increased when incline angle was increased from 10^o to 30^o. Sliding velocity also increased

for larger microtissues (toroid versus honeycomb). However, to accurately model this motion, more details are needed such the influence of frictional and drag forces. Likewise changes in the velocities in the different compartments of the funnel-guide are not easy to explain. Velocities were significantly slower in the stacking chamber versus the funnel chamber and both were significantly slower than the free-fall chamber. Accurate models of these motions will also require more details such as the influence of funnel and stacking chamber geometries on frictional and drag forces.

When compared to other microtissue manipulation methods (Kenzan and Bio-P3), the funnel-guide has similarities and differences. All three methods use scaffold-free microtissue building blocks that are made by the aggregation and self-assembly of cells. These building blocks have cell densities comparable to that of *in vivo* organs. For the Kenzan method the building blocks are spheroids produced by ultra-low attachment plates, whereas the funnel-guide and the Bio-P3 use microtissues with more complex shapes (toroid, honeycomb) produced in micro-molds of agarose. All three methods use their building blocks to construct macrotissues submerged under cell culture medium, are compatible with perfusion and rely on the building blocks to spontaneously fuse to form the macrotissue. The funnel-guide and the Bio-P3 use larger building blocks with significantly more cells than spheroids and these building blocks have a more complex preformed architecture. Both reduce the number of building steps and fusion events to make the macrotissue. The Kenzan method and the Bio-P3 have direct contact with the building part. The Kenzan method uses a mobile arm to pick up and impale spheroids onto microneedle arrays [8]. The Bio-P3 uses fluid suction across a membrane to grip a microtissue and place it on a build head or drop it over a guide post. In contrast, the funnel-

guide uses the fluid suction of a standard pipette to pick up a free moving building part and deliver it to the funnel-guide with the building part constantly under culture medium.

Compared to some bioprinting methods that extrude alginate containing a low density of cells under culture medium, the FG creates tubular macrotissues with organ cell density by using lumen containing building parts with high cell density and without the use of scaffold material [17]–[19]. The tubular format is conducive to perfusion for further tissue maturation and use of the FG may be scalable using standard automated liquid handling devices. This new method enables the easy positioning of toroids into a stack that fuses. It works with toroids of different diameters as well as toroids of different cell types. However, a major disadvantage of all tissues made with scaffold-free methods are biomechanical properties. Therefore, tubes made in this way will require active perfusion and significantly longer maturation times to achieve suitable levels of ECM production and acceptable biomechanical properties depending on the cell type(s) selected. Future work will include perfusion and extended maturation of the tubes in culture as well as detailed biomechanical characterization of the tubes.

2.6 Conclusion

We have successfully designed the funnel-guide, a new microtissue manipulation platform and used it to build stacks of toroid shaped microtissues (45) and honeycomb shaped microtissues (10) that fused to form tubular macrotissues. The funnel-guide is a simple, quick, noncontact, additive manufacturing method that uses a specially designed device to position microtissues into precise locations in order to build macrotissues layer-by-layer. The fundamental principles of the funnel-guide (guiding the gravity-driven motion of microtissue building parts) can be used to design funnel-guides for the placement

of building parts of other sizes and shapes and to use these guides to build even more complex macrotissues. Funnel-guide mediated construction is amenable to automation and occurs in cell culture medium as well as in an environment conducive to the perfusion needed sustain the viability of large macrotissues with high cell density.

2.7 Acknowledgements

Brown University has filed a patent on this work. This work was funded by the NSF grant CBET-1428092.

2.8 Conflict of Interest

JR Morgan has an equity interest in Microtissues Inc. This relationship has been reviewed and is managed by Brown University in accordance with its conflict of interest policies.

2.9 References

[1] F. Marga *et al.*, "Toward engineering functional organ modules by additive manufacturing.," *Biofabrication*, vol. 4, no. 2, p. 022001, Jun. 2012.

[2] C. Norotte, F. S. Marga, L. E. Niklason, and G. Forgacs, "Scaffold-free vascular tissue engineering using bioprinting.," *Biomaterials*, vol. 30, no. 30, pp. 5910–7, Oct. 2009.

[3] S. V Murphy and A. Atala, "3D bioprinting of tissues and organs," *Nat. Biotechnol.*, vol. 32, no. 8, p. 773, 2014.

[4] V. Mironov, V. Kasyanov, and R. R. Markwald, "Organ printing: from bioprinter to organ biofabrication line.," *Curr. Opin. Biotechnol.*, vol. 22, no. 5, pp. 667–73, Oct. 2011.

[5] A. M. Blakely, J. Y. Schell, A. P. Rago, P. R. Chai, A. P. Napolitano, and J. R. Morgan, "Formation of Multicellular Microtissues and Applications in Biofabrication," in *Biofabrication: Micro- and Nano-fabrication, Printing, Patterning and Assemblies*, F. Gabor and W. Sun, Eds. Elsevier, 2013, pp. 149–166.

[6] C. M. Livoti and J. R. Morgan, "Self-Assembly and Tissue Fusion of Toroid-Minimal Building Units," *Tissue Eng. Part A*, vol. 16, no. 6, p. 2051, 2010.

[7] A. P. Rago, D. M. Dean, and J. R. Morgan, "Controlling cell position in complex heterotypic 3D microtissues by tissue fusion.," *Biotechnol. Bioeng.*, vol. 102, no. 4, pp. 1231–41, Mar. 2008.

[8] N. I. Moldovan, N. Hibino, and K. Nakayama, "Principles of the Kenzan Method for Robotic Cell Spheroid-Based Three-Dimensional Bioprinting," *Tissue Eng. Part B. Rev.*, vol. 23, no. 3, pp. 237–244, 2017.

[9] M. Itoh, K. Nakayama, R. Noguchi, K. Kamohara, and K. Furukawa, “Scaffold-Free Tubular Tissues Created by a Bio-3D Printer Undergo Remodeling and Endothelialization when Implanted in Rat Aortae,” *PLoS One*, vol. 10, no. 9, p. e0145971, 2015.

[10] A. M. Blakely, K. L. Manning, A. Tripathi, and J. R. Morgan, “Bio-Pick, Place, and Perfuse: A New Instrument for 3D Tissue Engineering,” *Tissue Eng. Part C Methods*, vol. 21, no. 7, pp. 737–746, 2015.

[11] B. C. Ip, F. Cui, A. Tripathi, and J. R. Morgan, “The bio-gripper: a fluid-driven micro-manipulator of living tissue constructs for additive bio-manufacturing,” *Biofabrication*, vol. 8, no. 2, p. 025015, 2016.

[12] A. Heinemann, F. Wischhusen, K. Püschel, and X. Rogiers, “Standard liver volume in the caucasian population,” *Liver Transplant. Surg.*, vol. 5, no. 5, pp. 366–368, Sep. 1999.

[13] E. Bianconi *et al.*, “An estimation of the number of cells in the human body,” *Ann. Hum. Biol.*, vol. 40, no. 6, pp. 463–471, Nov. 2013.

[14] S. Wakiya, “On the Exact Solution of the Stokes Equations for a Torus,” *J. Phys. Soc. Japan*, vol. 37, no. 3, pp. 780–783, 1974.

[15] H. Zhong, C. Lee, Z. Su, S. Chen, M. Zhou, and J. Wu, “Experimental investigation of freely falling thin disks. Part 1. The flow structures and Reynolds number effects on the zigzag motion,” *J. Fluid Mech.*, vol. 716, pp. 228–250, 2013.

[16] S. B. Field, M. Klaus, M. G. Moore, and F. Nori, “Chaotic dynamics of falling disks,” *Nature*, vol. 388, no. 6639, pp. 252–254, Jul. 1997.

[17] T. J. Hinton *et al.*, “Three-dimensional printing of complex biological structures by

freeform reversible embedding of suspended hydrogels," *Sci. Adv.*, vol. 1, no. 9, p. e1500758, Oct. 2015.

[18] A. G. Tabriz, M. A. Hermida, N. R. Leslie, and W. Shu, "Three-dimensional bioprinting of complex cell laden alginate hydrogel structures," *Biofabrication*, vol. 7, no. 4, p. 045012, Dec. 2015.

[19] T. Billiet, M. Vandenhaute, J. Schelfhout, S. Van Vlierberghe, and P. Dubruel, "A review of trends and limitations in hydrogel-rapid prototyping for tissue engineering," *Biomaterials*, vol. 33, no. 26, pp. 6020–6041, Sep. 2012.

2.10 Supplemental Information

2.10.1 Supplemental Figures

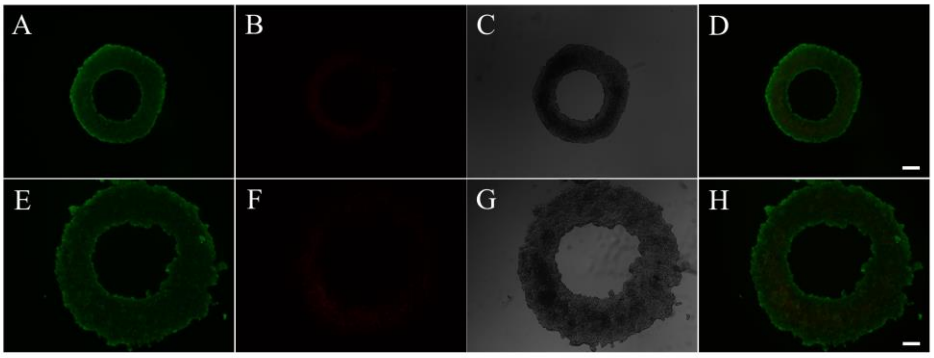

Supplemental Figure 2.1 *Toroid building part LIVE/DEAD®.* HepG2 toroid building parts seeded at 5.0 x 10^4 cells per toroid (A-D) and 1.2 x 10^5 cells per toroid (E-H). Twenty four hour toroids removed from the micromolds were incubated in a 1 µm calcein-AM and 4 µm ethidium homodimer-1 solution at 37ºC for one hour before imaging. Calcein-AM can be seen as green (A, E), ethidium homodimer-1 as red (B, F), bright field images are shown in (C, G) and an overlay of red and green channels in (D, H). Scale bars are 200 µm.

2.10.2 Supplemental Videos

Supplemental videos can be found here:

https://www.liebertpub.com/doi/full/10.1089/ten.tec.2018.0137

Supplemental Video 2.1 *Honeycomb sliding*. HepG2 honeycomb (3.75 x 10^5 cells) sliding at a 30° angle.

Supplemental Video 2.2 *Toroid free-fall.* HepG2 toroid (5.0 x 10^4 cells) free-falling in a cuvette.

Supplemental Video 2.3 *Toroid funnel-guide.* HepG2 toroid (5.0 x 10^4 cells) being guided by the funnel-guide.

Supplemental Video 2.4 *Tube extraction.* Stack of 20 HepG2 toroids (5.0×10^4) fused for twenty four hours at 37ºC, are extracted by gently separating two halves of the FG with spatulas.

Supplemental Video 2.5 *Honeycomb free-fall.* HepG2 honeycomb (3.75×10^5 cells) free-falling in a cuvette.

Supplemental Video 2.6 *Honeycomb funnel-guide.* HepG2 honeycomb (3.75×10^5 cells) being guided by a funnel-guide with a honeycomb shaped stacking chamber.

Chapter 3

Towards Automated Additive Manufacturing of Living Bio-Tubes Using Ring-Shaped Building Units

Submitted to *SLAS Technology*. Under Review.

Kali L. Manning, Sc.M.[1, 2], Jacob Feder[1], Marianne Kanellias, Sc.M.[1,2] John Murphy III[1], Jeffrey R. Morgan, Ph.D. [1, 2*]

1 Department of Molecular Pharmacology, Physiology and Biotechnology

2 Center for Biomedical Engineering

Brown University, Providence, RI, USA

3.1 Abstract

Tissue engineering has been largely confined to academic research institutions with limited success in commercial settings. To help address this issue, more work is needed to develop new automated manufacturing processes for tissue-related technologies. In this article, we describe the automation of the funnel-guide, an additive manufacturing method that uses living tissue rings as building units to form bio-tubes. We developed a method based on 96-well plates and a modified off-the-shelf liquid handling robot to retrieve, perform real-time quality control, and transfer tissue rings to the funnel-guide. Cells seeded into 96-well plates containing specially designed agarose micro-molds self-assembled and formed ring-shaped microtissues that could be retrieved using a liquid handling robot. We characterized the effects of time, cell type and mold geometry on the morphology of the ring-shaped microtissues to inform optimal use of the building parts. We programmed and modified an off-the-shelf liquid handling robot to retrieve ring-shaped microtissues from the 96-well plates and we fabricated a custom illuminated pipette to visualize each ring-shaped microtissue prior to deposit in the funnel-guide. Imaging at the liquid-air interface presented challenges that were overcome by controlling lighting conditions and liquid curvature. Based on these images, we incorporated into our workflow a real-time quality control step based on visual inspection and morphological criteria to assess each ring prior to use. We used this system to fabricate bio-tubes of endothelial cells with luminal alignment.

3.2 Introduction

Living tissue engineered products have the potential to serve as platforms for drug discovery and toxicity testing, as well as implants to replace damaged or diseased tissues and organs grafts. However, successful commercialization of tissue engineered products has been limited due to a number of factors including challenges in manufacturing. Most tissue engineered products are fabricated one-at-a-time using labor intensive methods. As outlined by the Advanced Regenerative Manufacturing Institute (ARMI), automation and monitoring (quality control) of tissue production is essential to commercial translation [1]. Automation can decrease cost, increase throughput and output while decreasing human error and increasing product fidelity due to the addition of quality control metrics. Although automation methods exist for the culture of cells in two dimensions, there has been limited development in the automation and scale-up of three-dimensional (3D) tissue engineered products [2].

Bio-printing is a common additive manufacturing approach to fabricating tissue engineered products. 3D macro-structures such as valves and tubes have been built drop-by-drop using liquid polymer scaffolds containing cells [3]–[5]. However, bio-printing has several limitations yet to be overcome. The density of cells in the polymer scaffold is low and doesn't equal that of most tissues and organs. Polymerization of the scaffold occurs in air and so the ultimate size of the printed construct is limited because cells cannot be maintained in the liquid nutrient culture medium they absolutely require [6]. Lastly, bio-printing requires the delivery of tens of thousands of small drops (manufacturing steps) and strategies to quality control those steps have yet to be developed.

An alternative additive manufacturing approach is the manipulation and placement of 3D microtissue building units comprised of cells that have aggregated and self-assembled. These microtissues are formed without the use of a scaffold, have a high cell density comparable to normal tissue and organs and will fuse with one another while submerged under cell culture medium. [7], [8] [9]–[11] Microtissue building units are easily fabricated using hanging drop or micro-molding techniques and have been formed in a variety of shapes including spheroids, rods, rings and honeycombs with cell numbers ranging from of as few as about 500 cells per spheroid to over eleven million cells per honeycomb. Moreover, as discrete building units of hundreds to thousands of cells they significantly decrease the number of building steps and lend themselves to new strategies and metrics for quality control. [12]–[14]

Currently available methods to manipulate microtissues include the Kenzan method, the Bio-Pick, Place and Perfuse (Bio-P3), and the Funnel-Guide. The Kenzan method uses a robotic arm to aspirate up and then precisely pierce spheroids onto a microneedle array where they fuse with one another [15]–[18]. The Bio-P3 utilizes fluid suction through a membrane to grip and move honeycomb building parts through culture medium and stack them onto a build head where the microtissue layers fuse and their lumens are perfused with culture medium during the build [19]–[21]. The funnel-guide utilizes a funnel-shaped vessel to stack ring-shaped microtissues that have been added one-at-a-time using a standard liquid handling pipette. As the ring-shaped microtissues fall through the culture medium, the funnel-guide guides them to form a stack of living rings that fuse into a single bio-tube [22].

In this study, we describe the automation of the work flow around the funnel-guide. We've developed a method based on 96-well plates that can be used to automate and scale-up the production of 3D ring-shaped microtissues. Cells seeded into 96-well plates containing specially designed agarose micro-molds self-assembled and formed ring-shaped microtissues that could be retrieved using a liquid handling robot. We characterized the effects of time, cell type and mold geometry on the morphology of the ring-shaped microtissues to inform optimal use of the building parts. We modified an off-the-shelf liquid handling robot to retrieve ring-shaped microtissues from the 96-well plates and we fabricated a custom internally backlit pipette to visualize each ring-shaped microtissue prior to deposit in the funnel-guide. Based on these images, we incorporated into our workflow a real-time quality control step based on visual inspection and morphological criteria to assess each ring prior to use. We used this system to fabricate bio-tubes of endothelial cells with luminal alignment. The overall goal was to create a fully automated funnel-guide work flow with a quality control step for use in the fabrication of complex 3D tissue engineered products that can be used with a variety of cell-types.

3.3 Materials and Methods

3.3.1 Cell Culture, Micro-Mold Fabrication and Formation of Ring-Shaped Microtissues

Human hepatocellular carcinoma (HepG2) cells were expanded in Eagle's Minimum Essential Medium (EMEM) (Corning Incorporated, Corning, NY) supplemented with 10% fetal bovine serum (FBS) (Thermo Fisher Scientific, Waltham, MA) and 1% penicillin/streptomycin (MP Biomedicals, LLC, Santa Ana, CA). Human umbilical vein endothelial cells (HUVEC) were expanded in Endothelial Growth Medium (EGM) with

Supplement Kit (PromoCell, Heidelberg, Germany) and 1% penicillin/streptomycin (MP Biomedicals, LLC). Cultures were maintained in a 37°C, 5% CO_2 atmosphere. Cells were trypsinized, counted, and re-suspended to the desired cell density for each experiment.

Agarose gels were cast from 3D Petri Dish ® micro-molds (Microtissues, Inc., Providence, RI) as previously described [20]. 96-well agarose gels were cast from either PEEK or stainless steel molds (Proto Labs Inc., Maple Plains, MN). Briefly, 90 µl (PEEK mold) or 80 µl (stainless steel mold) of molten agarose were pipetted into the 96-well plate, and a drop of agarose placed into the recesses in the mold before inverting and placing into the 96-well plate. Once the agarose solidified, the mold was removed. Gels were equilibrated in serum-free EMEM or EGM at 37ºC and 5% CO_2 for 24 hours prior to use. Agarose gels were made with powdered agarose (Low-EEO/Multi-Purpose/Molecular Biology Grade, Fisher BioReagents) (Thermo Fisher Scientific, Waltham, MA) sterilized by autoclaving and then dissolved in sterile water to 2% (weight/volume). 3D Petri Dish ® recesses were 1400 µm in diameter with a central agarose peg of 600 µm and surrounding 400 µm trough, and contained 36 recesses per gel. 96-well recesses were 2200 µm in diameter with a central agarose peg of 1400 µm and a surrounding 400 µm trough. Each well contained an agarose gel with a single ring-shaped recess. Gels were seeded at a density of, 50,000, 75,000 or 100,000 cells per feature, or 100,000, 150,000 or 200,000 cells per 96-well feature. Cells aggregated in the micro-molds and self-assembled microtissues were used 4 hours after cell seeding.

3.3.2 Evaluation of the Morphological Changes of Tissue Rings

Tissue rings were either imaged inside agarose molds, or transferred using a wide-bore pipette tip into 96-well plates with agarose coated wells equilibrated with culture

medium. Snapshot and time lapse imaging was done using a Zeiss Axio Observer Z1 equipped with an AxioCam MRm camera with ZEN software (Carl Zeiss Microscopy, LLC, Thornwood, NY). Side-view imaging was performed by transferring rings into a cuvette (Dynalon Corporation, Rochester, NY) filled with growth medium. Images were captured using a DinoLite digital microscope (BigC Dino-Lite, Torrance, CA). Tissue ring release from the micro-mold was quantified in a Kaplan-Meier curve, where release from the mold was an event. Tissue formation only counted rings with the potential to form; mold defects were excluded from analysis. Measurements of cross-sectional area (A_C) were obtained using a thresholding macro on ImageJ (National Institutes of Health, Bethesda, MD). Measurements of ring outer diameter (D_O) and lumen diameter (D_L) were obtained using Zen software by taking an average of a vertical and horizontal measurement of each parameter. Thickness ($T_{x,y}$) of ring walls was calculated by Eq. (1) $D_O - D_L/2$. Measurements of A_C, D_O, D_L, and $T_{x,y}$ were normalized to the T=0 measurements. Height (H) measurements were taken using ImageJ (National Institutes of Health, Bethesda, MD). Ring volume was calculated using Eq. (2) $V = (\pi hr)(2\pi R)$, where h is the semi-minor axis of the ellipsoid cross-section ($H/2$, where H is the total measured height of the ring), r is the semi-major axis (or radius, calculated as $T/2$), and R is the major radius of the top-down shape (calculated as Eq. (3) $(r + (D_L/2))$.

3.3.3 Fabrication and Use of the Funnel-Guide

Funnel-guide negative replicas were fabricated as previously described [22]. Briefly, SolidWorks (Dassault Systems SolidWorks Corporation, Waltham, MA) was used to design the negative which consisted of three chambers, a free-fall chamber, a funnel-chamber and a stacking-chamber. Free-fall and funnel-chamber dimensions remained the

same at 8 mm x 8 mm and 10 mm in height, and 77º and 13 mm in height. The stacking-chamber dimensions were 1.9 mm in diameter and 10 mm in height, to accommodate the 96-well rings. The negative replicas of the funnel-guide were 3D printed by Proto Labs (Proto Labs Inc., Maple Plains, MN). Funnel-guides were then fabricated by pouring polydimethylsiloxane (PDMS) (SYLGARD 184 Silicone Elastomer Kit, Dow Chemical Company, Midland, MI) into a cuvette (Dynalon Corporation, Rochester, NY). PDMS was cured for 1 hour at 100 ºC, and then overnight at room temperature. The funnel-guide negative replica was removed, leaving behind a void in the PDMS in the shape of the desired funnel-guide, and then the inside was coated with a 3% (weight/volume) Pluronic® F-68 (Sigma-Aldrich, St. Louis, MO) solution overnight.

3.3.4 Automated Fabrication of Bio-Tubes

To automate the fabrication of bio-tubes using the funnel-guide, an OpenTrons OT-One (OpenTrons, Brooklyn, NY) was modified accordingly. The A-axis motor and drive assembly was unplugged and removed. The pipette was relocated to be driven by the B-axis, which has been plugged into the A-axis. The *z*-axis was vertically extended by adding a piece of aluminum stock frame (McMaster Carr, Elmhurst, IL). The A-axis limit switch was repurposed to be the *z*-axis probe limit switch, and was connected to the B-axis limit switch input which was reconfigured to act as the probe. To probe the *z* height, the limit switch and spring steel flexures (McMaster Carr, Elmhurst, IL) were mounted on a custom pipette tip holder designed using SolidWorks (Dassault Systems SolidWorks Corporation, Waltham, MA) and 3D printed using Shapeways 3D Printing Company services (Shapeways HQ, New York, NY).

A LabVIEW (National Instruments, Austin, TX) interface was created to control the OpenTrons OT-One liquid handling robot. At start-up, the user calibrates positions of the pipette-tip, well A1 of the 96-well plates, the camera and the funnel-guides. The user can input the number of 96-well plates and funnel-guides to be used. Located at the bottom of the LabVIEW interface is the Advanced Parameter Area, which contains the parameters that affect ring pick-up from the 96-well plate. These parameters include "well height": the height above the bottom of the well that the robot pipettes from; "feedrate": the rate of aspirating and dispensing; "disp": the baseline position for the pipette/A axis; "asp": the distance the robot moves the pipette plunger up and down to aspirate and dispense; "extra liquid": the additional aspiration distance to allow for reverse pipetting; "meniscus comp": the distance to move the pipette plunger down prior to taking a picture for QC in order to change the curvature of the meniscus; "agitation count": the number of times to pipette while in the well; and "speed": the rate the pipette moves along its axes. Once calibrated and all parameters set, the user presses "Build" which initiates the following sequence; move to pipette tip rack, move to well A1, probe *z* height until limit switch activated, move to well B1, pick-up tissue ring, move to camera, perform QC, place tissue ring in funnel-guide or back in 96-well plate depending on the outcome of QC, move to well C1, repeat loop until all 96-well plates have been used, return home. Throughout the build process, parameters can be changed in real-time by the user if needed.

3.3.5 Real-Time Quality Control of Ring-Shaped Tissue Building Parts

A camera (Blackfly S model) (FLIR Systems, Inc., Wilsonville, OR) and lens (2X, 0.10 NA, Ultra Compact Objective) (Edmund Optics Inc., Barrington, NJ) were mounted in an upward facing orientation to the base of the OT-One. Our custom pipette tip holder

was designed to hold a black pipette tip (TipOne for Tecan Genesis and Freedom EVO) (Tecan, Männedorf, Switzerland), 1/8" diameter acrylic light pipe (McMaster Carr, Elmhurst, IL), and a custom PCB assembly containing a LED and constant-current driver electronics (JLCPCB, Shenzhen, Guangdong, China), in order to back-light the ring-shaped tissue while inside the pipette tip. During the build process, a single image of the ring in the pipette tip was taken. This image was used by our custom QC algorithm to perform real-time analysis of ring metrics. The QC algorithm uses the LabVIEW (National Instruments, Austin, TX) "Find Circular Edges 3 VI" to identify the tissue ring. Briefly, the algorithm finds a circular edge according to the input parameters within a given region of interest (ROI). The search area is the area between two concentric rings; the algorithm generates lines between the inner and outer ring and then calculates the gradient of the image along those lines. For each line, the spot with the largest gradient becomes a hit point, which are then used to create a circle of best fit, the output of the algorithm. This analysis was conducted three times; first using the entire image as the ROI to identify the pipette tip, then using the area of the pipette tip as the ROI to locate the outer edge of the tissue ring, and finally using the outer edge as the ROI to identify the lumen of the tissue ring.

QC values were set through analysis of 5 plates of HUVEC 150K 4h tissue rings. QC measurements were taken using an offline LabVIEW VI, averaged, and the range set to two standard deviations from the mean. For inner and outer diameter measurements, QC LabVIEW values were converted to metric units by fitting a linear trend to a dataset of QC values and measured diameter values taken in ZEN software. The determined equation was

Eq. (4) $y = 2.7351x - 76.485$ where y represents the measured value, and x represents the QC value from LabVIEW.

3.3.6 Evaluation of Automated Funnel-Guided Fabrication

The modified OT-One system was used to build a bio-tube composed of thirty vertically aligned HUVEC 150K 4h tissue rings. Six bio-tubes were fabricated, and success was determined through visual inspection as each tissue ring was placed into the funnel-guide. Images of the bio-tube were taken using a Pixel 3 camera (Alphabet Inc. Mountain View, CA) throughout the building process, at 5 rings high, 15 rings high, and 30 rings high. To evaluate the alignment of the tissue rings, a top-view image was taken using an Olympus SZ-PT dissecting microscope (Olympus Corporation, Shinjuku, Japan) and Pixel camera (Alphabet Inc. Mountain View, CA).

3.3.7 Statistical Analysis

Statistical analysis was done on JMP software (SAS Institute Inc., Cary, NC). Significance for A_C, D_O, D_L, and $T_{x,y}$ was determined using a MANOVA with full factorial analysis for the repeated measurement of time, where significance denotes a $p<0.05$. Data analyzed by MANOVA were first examined using a Shapiro-Wilk test to determine that the data came from a normal distribution. A_C data were Log_{10} transformed to achieve normality. Ring formation as a function of peg angle and cell type were analyzed using a logistic regression where significance denotes $p<0.05$. Data were first examined using Shapiro-Wilk test to determine the data came from a normal distribution. Significance between Kaplan-Meier survival curves were tested via pairwise Log-rank analysis ($p<0.05$) with Cox's proportional hazard regression analysis used for multivariable comparison ($p<0.005$).

3.4 Results

3.4.1 Tissue Rings Undergo Morphological Changes

To determine the morphological changes that occur when tissue rings are self-assembled, we seeded HUVECs in agarose micro-molds containing 36 ring-shaped features composed of a circular trough (400 μm wide, 1400 μm outer diameter) surrounding a central agarose peg (600 μm diameter). Cells were seeded at 5×10^4, 7.5×10^4 or 1×10^5 cells per ring and brightfield images were obtained every 30 minutes for 20 hours (**Figure 3.1**). Within hours, the cells self-assembled a ring-shaped tissue that contracted around the central agarose peg. Over time, these HUVEC rings moved up the agarose peg and released themselves from the micro-mold (**Supplemental Video 3.1**). The percent of tissue rings in the mold that had not yet released themselves (survival) was plotted as a function of time as a Kaplan-Meier survival curve for each cell seeding density and compared. Survival of tissue rings seeded with the lowest cell number (5×10^4 cells/ring) was significantly longer at 13 hours median survival time (determined by parametric model analysis with Weibull probability fit) than the higher cell seeding numbers. This group also showed less variation in the rate of loss (standard deviation from mean) than the higher seeding numbers.

To determine the morphological changes of rings outside of the mold, HUVEC rings formed from 5×10^4 and 1×10^5 cells per ring were removed from the molds after 6 hours of self-assembly, placed in a 96-well plate coated with agarose and imaged over 3 days. By 72 hours, the rings contracted and closed their lumens. To quantify the rate of these morphological changes, we imaged rings every 30 minutes for the first 20 hours. From these images, we measured cross-sectional area of the ring (A_c), outer diameter of

the ring (D_O), diameter of the ring's lumen (D_L), and width of the ring measured in the *x*, *y* dimensions (T_{xy}). All values were normalized to the starting value, and plotted over time. Cross-sectional area, outer diameter and lumen diameter all significantly declined over 20 hours, and this decrease was significantly impacted by seeding density, where 5×10^4 cells per ring had a greater rate of decrease over time than 1×10^5 cells per ring. Ring thickness significantly increased over time, with 1×10^5 rings increasing significantly more than 5×10^4 rings. There was a significant difference between seeding density and time on ring thickness, where the seeding density significantly impacted the rate of change. To examine this more closely, we compared ring width (*x, y*) to ring height (*z*) as measured from side view images (**Supplemental Figure 3.1**). At time 0 and 20 hours, ring width was consistently greater than ring height for both cell numbers per ring. The higher cell seeding did result in an increase in width as well as height. From time 0 to 20 hours, width and height increased for high and low cell numbers, but the effect was only significant for rings with the higher cell number. These measurements allowed us to calculate the volume of the rings over time and both declined in volume with the lower cell number having a significantly greater decrease in ring volume (30% ± 3.6% vs 19% ± 3.9%).

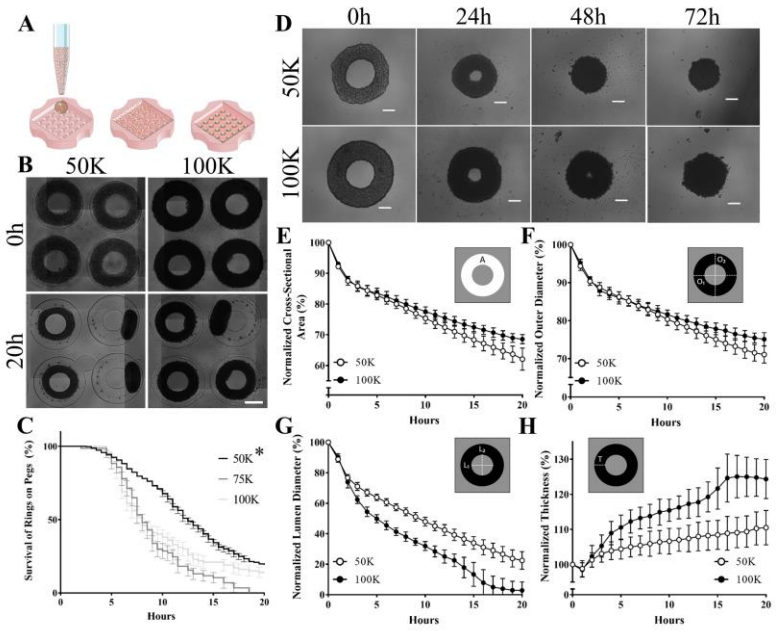

Figure 3.1 *Self-assembled tissue rings undergo morphological changes.* Schematic of process to form self-assembled tissue rings (A). Tissue rings of HUVECs were fabricated by seeding a cell suspension into a non-adherent agarose mold where cells settled by gravity into ring-shaped recesses and self-assembled. Rings were made using 5 $x10^4$ cells/ring and 1 $x10^5$ cells/ring, and were imaged inside the mold at 0 hours and 20 hours using brightfield microscopy (B). Scale bar is 200 µm. Tissue rings that moved up the agarose peg and released themselves over the course of 20 hours are plotted as a survival curve for three seeding numbers, 5 x 10^4, 7.5 x 10^4 and 1 x 10^5 cells/ring with * denoting significance calculated by Log-rank test and Cox's proportional hazard regression analysis for multivariable comparison, $p<0.05$ (n= 534, 78, 108, respectively) (C). HUVEC rings at 50K and 100K were removed from the mold at 6 hours, placed on an agarose surface, and imaged with brightfield microscopy over 72 hours (D). Scale bars are 200 µm. Released HUVEC rings on agarose were imaged every 30 min for 20 hours and the following parameters measured: cross-sectional area (E), outer diameter (F), lumen diameter (G) and thickness *x, y* (H). Insets show measurements taken. Values were normalized to T=0 measurements and plotted over 20 hours. All four parameters saw a significant change over time, with the percent change being significantly impacted by seeding density. Where 50K decreases significantly more in A_c and D_O, 100K decreases significantly more in D_L, and 100K increases significantly more in T_{xy} (n = 27 for 50K and n= 15 for 100K). Measurements for A_C were Log_{10} transformed for statistical analysis, significance calculated by MANOVA, $p<0.05$.

3.4.2 Production of Tissue Rings in a 96-Well Plate

To adapt the agarose molds to an automated work flow, we designed a new molding system for 96-well plates so that each well has one circular feature molded in agarose that, when seeded with cells, forms one ring-shaped tissue per well (**Figure 3.2**). To form these 96-well plates, molten agarose was added to each well and a mold was inserted into the plate. After the agarose gelled, the mold was removed. To facilitate the easy retrieval of tissue rings from the wells, we altered the angle of the central agarose peg and tested angles of 45°, 60°, 75° and 90° (**Supplemental Figure 3.2**). All four angles were successfully molded in a 96-well plate forming circular troughs that were 2200 μm in diameter with a central peg 1400 μm in diameter and a surrounding 400 μm trough.

To test these angles, we seeded plates with HUVEC or HepG2 cells at 1.0, 1.5 or 2.0 x 10^5 cells per well. Time lapse videos showed that HUVEC cells (1.5 x 10^5) formed rings that moved up and off the 60° peg by 24 hours (**Supplemental Video 3.2**). In contrast, HepG2 cells formed rings that stayed on the 60° peg at 24 hours. To evaluate ring formation, we measured the number of intact rings at 24 hours and plotted this as a function of peg angle for both cell types at three seeding densities. The highest percentage of rings formed in wells with 60° and 75° pegs with seeding densities of 1.5 x 10^5 and 2.0 x 10^5. HepG2 ring formation was impacted the most by peg angle, where 60°, 75° and 90° pegs formed significantly more rings than 45° pegs. In contrast, HUVEC ring formation was impacted the most by seeding density, where 1.0 x 10^5 cells formed significantly less rings. 60° and 75° pegs formed significantly more HUVEC rings than 45° pegs. We determined 45° to have a significantly shorter survival time than 60° and 75° pegs at 3 hours, 60° to have a significantly shorter survival time than 75° and a significantly longer survival time

than 45° pegs at 4 hours, and 75° to have a significantly longer survival time than both 60° and 45° pegs at 10 hours. Based on these data, we elected to use HUVEC rings formed from 1.5 x 10^5 cells on a 60° peg and harvested at 4 hours to test our automated work flow.

To determine the morphological changes of HepG2 and HUVEC rings formed using 96-well plates, tissue rings (1.5 x 10^5 cells) were removed from the molds after 24 hours of self-assembly and placed in a 96-well coated with agarose (**Figure 3.3**). Rings were imaged every 24 hours, and parameters of cross-sectional area (A_c), outer diameter (D_O), lumen diameter (D_L), and thickness (T_{xy}) were measured, normalized to the starting value, and plotted over time. As expected, there is a decrease in A_c, D_O and D_L for HUVEC rings. This decrease is significant, with HUVEC rings decreasing significantly more than HepG2 rings over time. Thickness also changes significantly over time, with a statistically significant difference between HUVEC and HepG2 rings. Cell type significantly impacts the rate of change for all four variables.

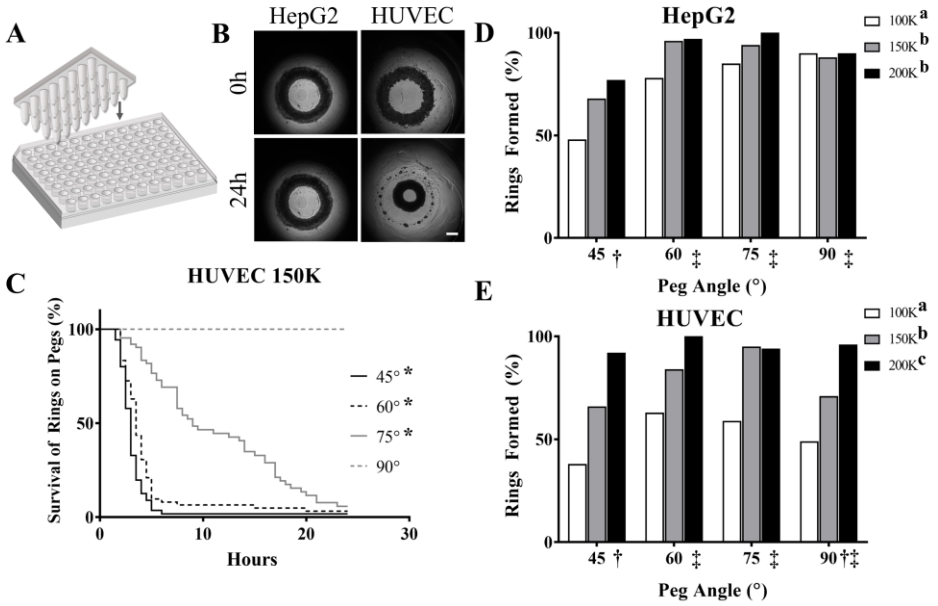

Figure 3.2 *Tissue rings produced in a 96-well plate.* Schematic of mold used to form one ring-shaped agarose recess per well of a 96-well plate (A). Micro-molded 96-well plates were fabricated by pipetting molten agarose into the plate, inserting the mold, and removing the mold after the agarose gelled. The tissue ring surrounds a central peg of agarose and four angles of this peg were tested 45°, 60°, 75° and 90°. Tissue rings (1.5 x 10^5 cells) formed on 60° pegs using HepG2s and HUVECs, imaged at 0 hours and 24 hours (B). Scale bar is 500 μm. Rings self-released from the mold plotted over the course of 20 hours as a survival curve as a function of peg angle (45°, 60°, 75° and 90°) for HUVEC 150K rings with * denoting significance calculated by Log-rank test and Cox's proportional hazard regression analysis for multivariable comparison, $p<0.05$ (n = 219) (C). Ring formation plotted as a function of peg angle for three seeding densities and two cell types, HepG2 (D) and HUVEC (E). For HepG2 rings, 60°, 75° and 90° pegs form significantly more rings than 45° pegs, and 100K seeding forms significantly less rings, with peg angle having the greatest impact on ring formation. For HUVEC rings, 60° pegs form significantly more than 45° pegs and 75° pegs form significantly more than 45° pegs. 150K seeding density forms significantly more than 100K, and 200K forms significantly more than 150K and 100K, with seeding density having the greatest impact on ring formation (n = 239, 253, 254 for HepG2 100K, 150K and 200K, respectively; n = 213, 219, 228 for HUVEC 100K, 150K and 200K, respectively). Significance calculated by logistical regression analysis, $p<0.05$, where values with different letters denotes significance, and values with different symbols denotes significance.

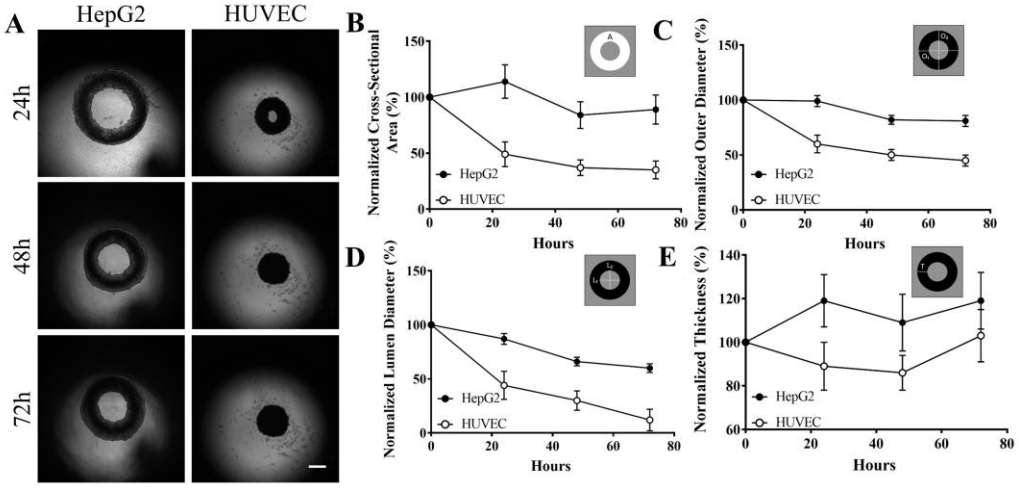

Figure 3.3 *Morphological changes of tissue rings are cell type dependent.* Rings were formed by seeding 1.5 x 10^5 HepG2 cells and HUVECs into 96-well plates with agarose recesses each with a 60° peg, grown for 24 hours, removed and placed on a non-adherent agarose surface. Images were acquired at 24 hours, 48 hours and 72 hours using brightfield microscopy (A). Scale bar is 500 µm. Ring cross-sectional area (B), outer diameter (C), lumen diameter (D) and thickness (E), plotted as a function of time. All four parameters changed significantly over time, with the rate of change being impacted by cell type where HUVEC rings changed significantly more than HepG2 rings (n = 23, 36 for HepG2 and HUVEC respectively). Significance calculated by MANOVA, $p<0.05$.

3.4.3 Automated Work Flow for Tissue Rings

To determine if tissue rings could be retrieved from the 96-well plates and delivered one at a time to the funnel-guide for biofabrication, we created a custom LabVIEW interface to control a liquid handling robot as it executed an automated workflow (**Figure 3.4**) (**Supplemental Figure 3.3**). The main components of the repetitive workflow are as follows: i) liquid suction via a pipette to retrieve one tissue ring from one well of a 96-well plate, ii) movement of pipette containing tissue ring to a location directly over an upward facing camera to image the tissue ring, iii) image-based quality control (QC) of the tissue

ring, iv) delivery of the tissue ring to the funnel-guide, or back into the 96-well plate depending on the QC outcome. To ensure retrieval of the tissue rings, the tip of the pipette was moved to a specified and precise height within each well of the 96-well plate. To remove variability in tip height in each 96-well, we designed a custom pipette tip holder with a mounted flexure and *z*-limit switch, which was triggered by probing the depth of the first well of the 96-well plate with the pipette tip at start-up (**Supplemental Video 3.3**). To evaluate the retrieval of tissue rings, we imaged 96-well plates prior to ring retrieval, and cross-referenced with QC images in order to calculate the percent success of ring retrieval. 4h 150K HUVEC rings have a pick-up percentage of approximately 88%.

To acquire the QC images of the tissue rings while in the pipette, we designed a custom pipette holder and optimized the lighting conditions (**Figure 3.5**). Within seconds of being retrieved from a well, a tissue ring settles by gravity to the bottom of the liquid being held by the pipette tip. The ring, which is horizontal and parallel to the air/liquid interface, can be imaged by an upward facing camera, but we found that lighting was critical for obtaining images suitable for real-time QC. We tested ambient light, side-light, back-light, and combinations of the three and determined that back-lighting via an LED coupled to an acrylic light pipe in the pipette provided reproducible images with a white background and the sharpest contrast between the tissue ring and the pipette tip. We also eliminated the interfering effects of ambient light by using a black pipette tip. In addition to light intensity, we also found that the curvature of the liquid upon which the tissue ring was resting was another factor influencing image quality. Slight downward adjustments of the pipette's plunger that increased the liquid's curvature could also significantly improve image quality. To address this issue, we created in the LabVIEW interface a liquid

curvature compensation parameter that can be adjusted to alter the liquid's curvature in real-time. Using our custom imaging set-up, we imaged over 900 HUVEC rings (1.5 x 10^5 cells) and have an imaging success percentage of 94%.

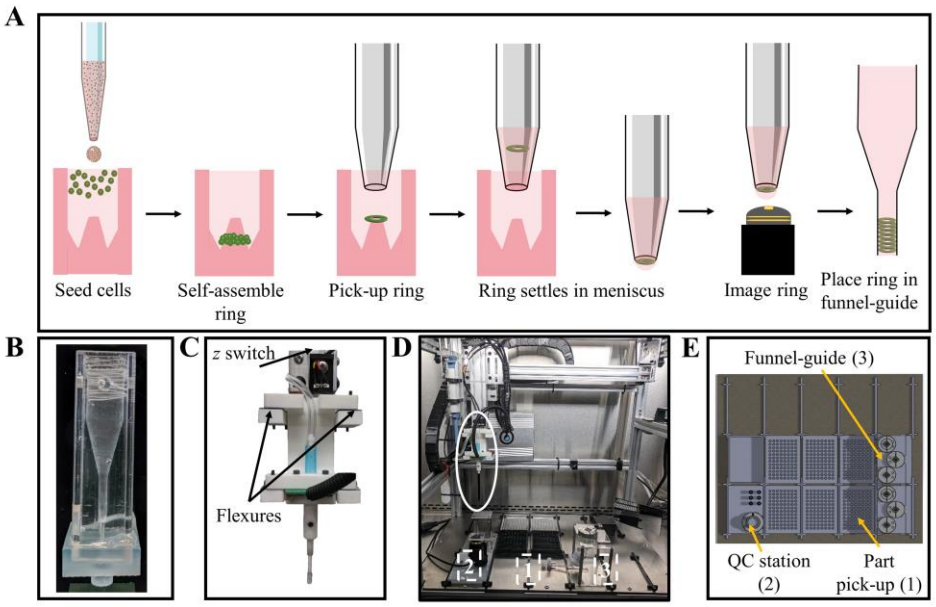

Figure 3.4 *Automated work flow to use tissue rings in biofabrication.* Schematic of the key steps in the workflow of a liquid handling robot (A). Tissue rings were fabricated by seeding cells into a 96-well plate. Tissue rings self-assemble, one per well. A liquid handling robot uses a pipette to retrieve a ring. The ring in the pipette settles to the tip's bottom and the pipette is moved over an upward facing camera to image the ring. Depending on the outcome of the image-based quality control algorithm, rings are either placed in a funnel-guide (3) (B), or put back in the 96-well plate. A custom pipette tip holder with mounted flexures and *z*-limit switch ensures the pipette tip goes to the same height in each well (C) (circled in (D)). Snapshot and schematic of the Opentrons OT-1 liquid handling robot with areas designated for part pick-up (1), image-based quality control (2), and funnel-guide building area (3) (D) (E). The steps of the build workflow run on a loop until all ring building parts have been used.

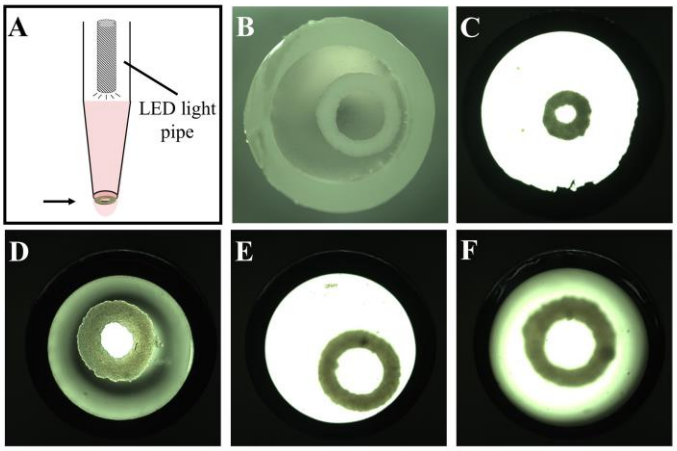

Figure 3.5 *Imaging of retrieved tissue rings.* Schematic of a custom designed pipette tip holder built to house the pipette tip and the back lighting system in order to take images of a tissue ring when it is positioned over the upward facing camera. The light source is an LED mounted to a PCB, with a potentiometer to control intensity. The light is directed to the tissue ring via a light pipe inserted into the pipette tip (A). The method of lighting influences image quality. Image of a tissue ring in a conventional translucent tip with ambient light (B). Image of a tissue ring in a black opaque tip with back lighting (C). Curvature of the liquid at the end of tip influences image quality. Stepwise adjustments of the pipette's plunger that progressively increases the liquid's curvature also alter the quality of the image (D, E, F).

3.4.4 Tissue Rings Can Be Quality Controlled in Real-Time

To determine if rings could be located and analyzed while inside the pipette tip, we developed a LabVIEW algorithm to process and analyze the images (**Figure 3.6**). The algorithm identifies the tissue ring by finding circular edges via a search within a given region of interest (ROI), and the identification of the largest gradient between two concentric rings. First, the algorithm uses the entire image as its ROI to identify the inner edge of the pipette tip. After this inner edge is located, the algorithm uses this new area as the ROI to identify the outer edge of the tissue ring. Finally, it uses the outer edge of the

tissue ring as the ROI to identify the inner edge, or the lumen, of the tissue ring. Once the tissue ring has been identified, it can be evaluated using parameters of center distance, inner diameter, inner roundness, outer diameter and outer roundness (**Supplemental Figure 3.4**). In order to determine the parameter range for HUVEC rings (1.5 x 10^5 cells), we retrieved tissue rings from five 96-well plates, imaged the rings and measured these parameters. Parameters were determined for center distance (108), inner diameter (199-353), inner roundness (0.001-16), outer diameter (603-722) and outer roundness (0.001-30). QC values for inner diameter and outer diameter correspond to lumen diameters of 469 – 890 µm and outer diameters of 1578 – 1900 µm. Using the algorithm, we were able to identify and measure 71% of the HUVEC rings.

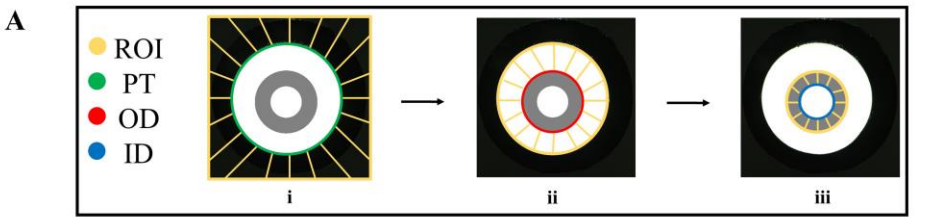

F

QC Parameter	Center Distance	Inner Diameter	Inner Roundness	Outer Diameter	Outer Roundness
Minimum Value	-	100	0.001	500	0.001
Maximum Value	120	300	10	700	10

Figure 3.6 *Image-based quality control of tissue rings.* A custom algorithm for quality control (QC) was developed to locate the outer diameter (red circle) and inner diameter (blue circle) of a tissue ring inside the pipette tip (A), measure given parameters, compare these values to set values, and determine if the ring passes or fails. The algorithm uses an ROI (yellow) to identify the pipette tip (green) (i), the outer diameter of the tissue ring (red) (ii), and the inner diameter of tissue ring (blue) (iii). Images of a HUVEC ring (1.5 x 10^5 cells) (B, C) and a malformed ring (D, E) inside the pipette tip were processed using the algorithm. Output of an acceptable ring that passes QC and would be deposited into the

funnel-guide (C), where the red circle shows the QC identified outer diameter, and the blue circle shows the QC identified inner diameter. Output of an unacceptable malformed ring that fails QC and would be discarded back into the well plate (D), where the red circle shows the QC identified outer diameter, and the blue circle shows the QC identified inner diameter. Tabulated QC parameters and the acceptable value ranges for HUVEC rings (F).

3.4.5 Bio-Tube Fabrication Can Be Automated

To determine if we could automate the funnel-guided fabrication of bio-tubes, we used the developed liquid handling workflow with real-time quality control to fabricate six bio-tubes each containing thirty tissue rings (**Figure 3.7**). The bio-tubes were fabricated with tissue rings that were successfully picked-up, imaged, and passed the QC step. As each ring was placed in the funnel-guide, it self-righted to a horizontal orientation, was guided down to the stacking chamber, and settled to create an aligned stack of tissue rings (**Supplemental Video 3.4**). In order to validate luminal alignment of the tissue rings, a dissecting microscope was used to take a top-down image of the bio-tube while inside the stacking chamber. Light is clearly visible through the center of the lumens, showing ring alignment.

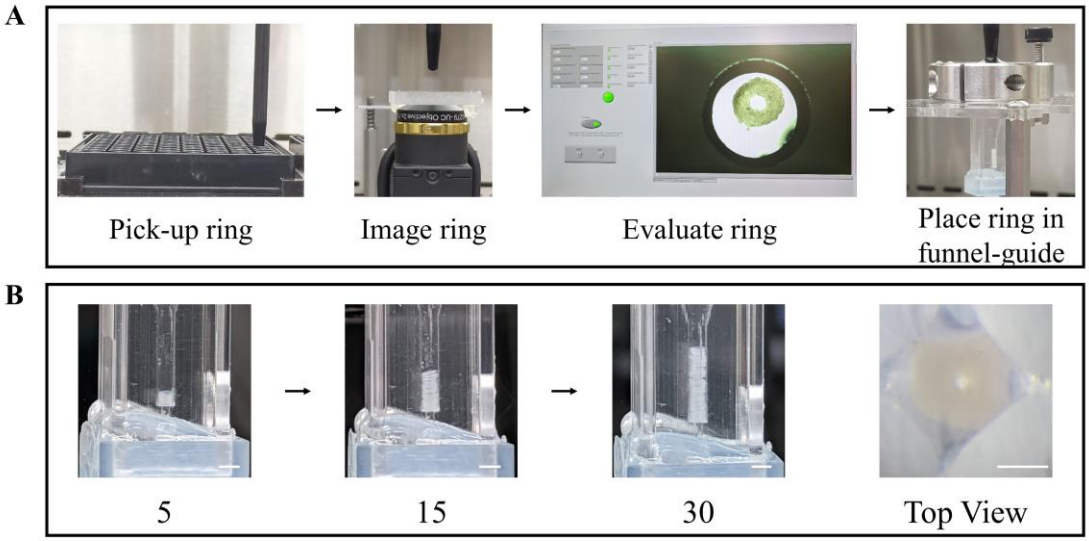

Figure 3.7 *Automated fabrication of bio-tubes.* Images of the key steps of the automated fabrication process (A). Tissue rings are picked-up from the well of a 96-well plate by liquid suction, and imaged while suspended at the air/liquid interface using an upward facing camera. The captured image is used to perform real-time quality control via a custom LabVIEW interface. If the tissue ring falls within the range of the specified quality control parameters, it is then delivered to the funnel-guide. Images of bio-tube fabrication (B). Bio-tubes are constructed via the addition of individual tissue rings, which are guided into the stacking chamber via the funnel chamber of the funnel-guide. As more tissue rings are added, the stack grows in height. Alignment of the tissue rings is shown via a top-down image of the final stack of 30 rings inside the stacking chamber, where light from the bottom of the stack can be seen through the lumens. Scale bars are 2 mm, 2 mm, 2 mm, and 1 mm, respectively.

3.5 Discussion

Since its inception nearly forty years ago, tissue engineering has been largely confined to academic research institutions, and due to numerous challenges as well as a gap in manufacturing technologies, there has been limited success in commercial settings. To help address this issue, more work is needed to develop new automated manufacturing processes for tissue-related technologies [1]. Here we describe the automation of the funnel-guide, an additive manufacturing method that uses tissue rings as building units to

form bio-tubes [22]. All automated manufacturing processes require suitable building materials and a fundamental understanding of their inherent properties. The use of living cells in tissue engineering presents new and exciting challenges to both automation and to manufacturing. Significant advances in laboratory automation has set the stage for developing new manufacturing strategies for the emerging field and industry of 3D tissue engineering. In this paper, we address several of those challenges in the context of using a liquid handling robot to automate the funnel-guide. The fundamental building unit of these bio-tubes is a ring-shaped microtissue comprised of tens of thousands of cells. We show that these building units can be produced via an easily automated process and more importantly that these units can be used to build bio-tubes layer-by-layer via automation of the funnel-guide.

To facilitate the automated production of ring-shaped building units, we designed a new micro-molding system for standard 96-well plates used in laboratory automation. Each well contains a single ring-shaped recess molded in agarose. Since agarose is non-adhesive for cells, cells pipetted into the well settled into the recess, aggregated and self-assembled around a central conical peg (1.1 mm tall) of agarose to form a ring-shaped microtissue, one per well, in less than 20 hours. The resulting ring-shaped building units have an outer diameter of about 1.77 mm, an inner diameter of about 1.2 mm, a *z* thickness of about 275 μm, a volume of about 5.8×10^8 μm^3 and are comprised of between one hundred to two hundred thousand living cells. The processes by which cells aggregate and self-assemble is very complex and involves numerous cellular processes that include, but are not limited to, cell-cell adhesions, cytoskeletal contraction, cell migration/deformation and synthesis of extracellular matrix proteins. These dynamic processes cause these living rings to

undergo morphological changes that can alter their size and shape, thus presenting new challenges to the manufacture of uniform building units. Moreover, although nearly all cell types perform these complex cellular activities there are significant differences between cell types that can further impact the fabrication of building units.

As the rings contracted around the cone, they climbed upwards. The cone shape and upward motion of the rings helped facilitate their removal from the well by the fluid suction of a pipette which is a key aspect of our automated work flow. The formation of rings as well as retrieval of rings in ANSI/SLAS 96-well plates offers numerous advantages in laboratory automation including the use of liquid handling robots to scale-up the production and retrieval of tissue rings as well as the use of existing robotic workflows and integrated equipment for cell culture, imaging and biochemical assessments. If larger rings are needed, a similar strategy can be adapted to 48 or 24-well plates to produce rings with inner diameters of about 2.5 mm and 5 mm, respectively. So long as the ring can fit inside a wide-bore pipette tip, the retrieval can be automated using a liquid handling robot.

The successful formation of rings and their rate of upward movement varied with cell type and was influenced by the angle of the agarose cone as well as the number of cells seeded. Both HepG2s and HUVECs required a minimum number of cells to successfully form rings. HepG2 rings climbed more slowly up the cone and were more influenced by the cone's angle than HUVEC rings. These data are consistent with a previous study that demonstrated cell type differences in the rate of ring movement up a cone. [23]

As the rings moved up the cone, they underwent morphological changes most notably a decrease in the diameter of their lumen. As a building unit, the lumen diameter is an important feature because it dictates the size of the lumen of the bio-tube to be built.

Because the ring contacts and contracts around the cone, the diameter of the ring's lumen is dictated by the cone's shape and the ring's height on the cone, or how high the ring has moved. As with ring formation, this motion is dependent on time, cell type, number of cells seeded and cone geometry. Seeding a well with a specified number of cells and harvesting the resulting ring at a specific time yields a building unit of defined size and shape. However, as our data also demonstrate, mold design and time of harvest are not sufficient, cell type must also be factored in when designing the process for making building units. HepG2 and HUVEC rings varied in their number of cells needed to form rings as well as the rate of ring movement up the cone.

Morphological changes to the ring building unit continued after the ring was harvested from the cone. Both HepG2 and HUVEC rings contracted and slowly decreased the diameter of their lumens over time, but this process was significantly slower (hours) than the rate of contraction while on the peg and provided more than sufficient time (minutes) to retrieve a ring building unit and transfer it to the funnel-guide before the occurrence of a significant morphological change. Interestingly contraction of HepG2 rings was significantly slower than HUVEC rings further demonstrating cell type specific differences.

Together these data demonstrate that the ring building unit is a dynamic 3D structure that undergoes significant changes as it is formed by tens of thousands of living cells. We've shown that it is possible to direct and harness these changes, thereby rendering them predictable and making it possible to produce ring-shaped building units of defined size and shape. The major factors are the mold design (diameter of circular recess and the shape/angle of the central conical peg), the number of cells seeded, and the time at which

the ring is retrieved from the peg. There are differences between cell types, but these differences are easily controlled by adjusting the shape/angle of the central conical peg, the number of cells seeded and/or the time at which the ring is retrieved from the peg. Future studies will continue to evaluate the differences between rings formed from various cell types and combinations of cell types. This information will inform the construction of bio-tubes for organ systems containing multiple relevant cell types, such as a blood vessel composed of endothelial cells and smooth muscle cells. We could also investigate methods of stabilizing the contractile building parts using physical and biological inhibitors [23], [24]. For example, once stacked, the bio-tube could be perfused to apply radial pressure to stagnate continued morphological changes [25], [26].

The ability to retrieve a ring one-at-a-time enabled us to devise a quality control step based on visual inspection. When a ring was retrieved, we observed that the ring quickly settled to the liquid/air interface at the bottom of the pipette tip and could be visualized by an upward facing camera. Acceptable images required optimal lighting as well as careful adjustment of the convex liquid surface which created a lens effect that could distort the image. Ring intactness as well as inner and outer diameter of the ring could be quickly identified to determine if a building part was suitable for transfer to the funnel-guide. The ability to quickly inspect building parts before use is an important addition to a robust automated manufacturing process, especially additive manufacturing. If a single defective ring were incorporated into the build of a bio-tube it would ruin the entire build. In addition to simple morphologic criteria, other optical parameters as well as other imaging modalities could be used to assess in real-time the suitability of a ring building unit.

Once a ring was deemed suitable, it was transferred by the liquid handling robot to the funnel-guide where simple contact between the pipette tip and the surface of the liquid in the funnel-guide released each ring. Within a maximum of 43 seconds, each ring had slowly settled in the funnel-guide by gravity to land on a stack of rings that fused into a bio-tube. The automated work flow for building bio-tubes had three major steps: i) ring pick up, ii) ring imaging/evaluation and iii) ring deposit in funnel-guide. The cycle time between the addition of two rings to the funnel-guide was 28 seconds; taking approximately 45 minutes to build a bio-tube containing 96 rings. Individual ring building units have a *z* height of about 275 µm, so all the rings from a single 96-well plate could produce a stack of rings with a starting height of about 2.64 cm. Each ring is about one hundred to two hundred thousand cells compared to about one thousand cells in a single spheroid which is another building unit used in additive manufacturing. Thus, compared to spheroid building units, ring building units decrease the number of manufacturing steps by a factor of about one hundred.

In this study, we demonstrated a proof-of-concept that we can automate funnel-guided bio-tube fabrication using a modified off-the-shelf liquid handling robot. This provides an advantage over existing systems such as the Kenzan and robotic assembly of vascular tissue where the spheroid and ring tissue parts are removed from the culture medium during the build process [14], [17]. Additionally, our method does not require the tissue to be punctured with needles, or strung through a mandrel for alignment, decreasing tissue part manipulation. Future experiments will include the development of a perfusion system connected to the base of the funnel-guide to ensure appropriate distribution of nutrients and continued improvements to the QC algorithm. Future iterations of the

algorithm could incorporate an object counting function which would exclude images with excess cellular debris, and could incorporate elliptical best fit features to better approximate the variety of luminal shapes.

In summary, we've modified a standard liquid handling robot and ANSI/SLAS 96-well plates to develop an automated process for additive manufacturing of bio-tubes from ring-shaped building units. We provide the means and fundamental knowledge to scale-up the production of ring-shaped building units of prescribed size and shape that are comprised of over a hundred thousand living cells. Our automated process includes the retrieval of rings one-at-a-time from a 96-well plate, and a new quality control step where rings are visually inspected in real-time before they are transferred to the funnel-guide for bio-tube formation. This work helps demonstrate that laboratory automation can help solve the manufacturing bottleneck in the field of tissue engineering.

3.6 Author Contributions

KLM and JRM developed the idea and wrote the paper. KLM conducted experiments and data analysis for Figures 2-7. MK conducted experiments and data analysis for Figure 1. JSF developed the LabVIEW interfaces and the QC algorithm. KLM and JSF worked to modify the liquid handling robot workflow and develop operation parameters. KLM, JSF and JM developed custom pipette tip holder. JM assisted with experiments and developed custom components for the modified liquid handling robot.

3.7 Acknowledgments

This work was funded by a grant from the National Science Foundation NSF PFI-TT-3 12554728. The authors would like to thank Joshua Manning for his assistance

capturing photographs and videos, and Blanche C. Ip, Ph.D. and Benjamin Wilks for their assistance with statistical analysis.

3.8 Conflict of Interest

J.R. Morgan has an equity interest in Microtissues, Inc. This relationship has been reviewed and is managed by Brown University in accordance with its conflict of interest policies.

3.9 References

[1] "Advanced Regenerative Manufacturing Institute." [Online]. Available: https://www.armiusa.org/. [Accessed: 26-Nov-2019].

[2] R. J. Thomas, A. Chandra, Y. Liu, P. C. Hourd, P. P. Conway, and D. J. Williams, "Manufacture of a human mesenchymal stem cell population using an automated cell culture platform," *Cytotechnology*, vol. 55, no. 1, pp. 31–39, Sep. 2007.

[3] F. Marga *et al.*, "Toward engineering functional organ modules by additive manufacturing.," *Biofabrication*, vol. 4, no. 2, p. 022001, Jun. 2012.

[4] C. Norotte, F. S. Marga, L. E. Niklason, and G. Forgacs, "Scaffold-free vascular tissue engineering using bioprinting.," *Biomaterials*, vol. 30, no. 30, pp. 5910–7, Oct. 2009.

[5] S. V Murphy and A. Atala, "3D bioprinting of tissues and organs," *Nat. Biotechnol.*, vol. 32, no. 8, pp. 773–785, 2014.

[6] N. V. Mekhileri *et al.*, "Automated 3D bioassembly of micro-tissues for biofabrication of hybrid tissue engineered constructs," *Biofabrication*, vol. 10, no. 2, p. 024103, Jan. 2018.

[7] A. P. Rago, D. M. Dean, and J. R. Morgan, "Controlling cell position in complex heterotypic 3D microtissues by tissue fusion.," *Biotechnol. Bioeng.*, vol. 102, no. 4, pp. 1231–41, Mar. 2008.

[8] A. Napolitano *et al.*, "Scaffold-free three-dimensional cell culture utilizing micromolded nonadhesive hydrogels," *Biotechniques*, vol. 43, no. 4, pp. 494–500, Oct. 2007.

[9] C. M. Livoti and J. R. Morgan, "Self-Assembly and Tissue Fusion of Toroid-

Minimal Building Units," *Tissue Eng. Part A*, vol. 16, no. 6, pp. 2051–2061, 2010.

[10] H. A. Strobel *et al.*, "Assembly of tissue engineered blood vessels with spatially-controlled heterogeneities," no. 508, pp. 1–42, 2018.

[11] P. A. Fleming, W. S. Argraves, C. Gentile, A. Neagu, G. Forgacs, and C. J. Drake, "Fusion of uniluminal vascular spheroids: a model for assembly of blood vessels.," *Dev. Dyn.*, vol. 239, no. 2, pp. 398–406, Feb. 2010.

[12] E. Leary, C. Rhee, B. T. Wilks, and J. R. Morgan, "Quantitative Live-Cell Confocal Imaging of 3D Spheroids in a High-Throughput Format," *SLAS Technol.*, vol. 23, no. 3, pp. 231–242, Jun. 2018.

[13] J. M. Kelm *et al.*, "Design of custom-shaped vascularized tissues using microtissue spheroids as minimal building units.," *Tissue Eng.*, vol. 12, no. 8, pp. 2151–60, Aug. 2006.

[14] C. J. Nycz, H. A. Strobel, K. Suqui, J. Grosha, G. S. Fischer, and M. W. Rolle, "A Method for High-Throughput Robotic Assembly of Three-Dimensional Vascular Tissue," *Tissue Eng. Part A*, vol. 25, no. 17 and 18, pp. 1251–60, 2019.

[15] N. I. Moldovan, N. Hibino, and K. Nakayama, "Principles of the Kenzan Method for Robotic Cell Spheroid-Based Three-Dimensional Bioprinting," *Tissue Eng. Part B. Rev.*, vol. 23, no. 3, pp. 237–244, 2017.

[16] M. Itoh, K. Nakayama, R. Noguchi, K. Kamohara, and K. Furukawa, "Scaffold-Free Tubular Tissues Created by a Bio-3D Printer Undergo Remodeling and Endothelialization when Implanted in Rat Aortae," *PLoS One*, vol. 10, no. 9, p. e0145971, 2015.

[17] R. Machino *et al.*, "Replacement of Rat Tracheas by Layered, Trachea-Like,

Scaffold-Free Structures of Human Cells Using a Bio-3D Printing System," *Adv. Healthc. Mater.*, p. 1800983, Jan. 2019.

[18] K. Arai *et al.*, "Fabrication of scaffold-free tubular cardiac constructs using a Bio-3D printer," *PLoS One*, vol. 13, no. 12, p. e0209162, Dec. 2018.

[19] B. C. Ip, F. Cui, B. T. Wilks, J. Murphy, A. Tripathi, and J. R. Morgan, "Perfused Organ Cell-Dense Macrotissues Assembled from Prefabricated Living Microtissues," *Adv. Biosyst.*, vol. 2, p. 1800076, Aug. 2018.

[20] A. M. Blakely, K. L. Manning, A. Tripathi, and J. R. Morgan, "Bio-Pick, Place, and Perfuse: A New Instrument for Three-Dimensional Tissue Engineering," *Tissue Eng. Part C Methods*, vol. 21, no. 7, pp. 737–746, Jul. 2015.

[21] B. C. Ip, F. Cui, A. Tripathi, and J. R. Morgan, "The bio-gripper: a fluid-driven micro-manipulator of living tissue constructs for additive bio-manufacturing," *Biofabrication*, vol. 8, no. 2, p. 025015, 2016.

[22] K. L. Manning, A. H. Thomson, and J. R. Morgan, "Funnel-Guided Positioning of Multicellular Microtissues to Build Macrotissues," *Tissue Eng. Part C Methods*, vol. 24, no. 10, pp. 557–565, Oct. 2018.

[23] J. Youssef, A. K. Nurse, L. B. Freund, and J. R. Morgan, "Quantification of the forces driving self-assembly of three-dimensional microtissues.," *Proc. Natl. Acad. Sci. U. S. A.*, vol. 108, no. 17, pp. 6993–8, Apr. 2011.

[24] M. J. Susienka, B. T. Wilks, and J. R. Morgan, "Quantifying the kinetics and morphological changes of the fusion of spheroid building blocks," *Biofabrication*, vol. 8, p. 045003, 2017.

[25] M. L. Moya, Y.-H. Hsu, A. P. Lee, C. C. W. Hughes, and S. C. George, "In vitro

perfused human capillary networks.," *Tissue Eng. Part C. Methods*, vol. 19, no. 9, pp. 730–7, 2013.

[26] D. T. T. Phan *et al.*, "A vascularized and perfused organ-on-a-chip platform for large-scale drug screening applications," *Lab Chip*, vol. 17, no. 3, pp. 511–520, 2017.

3.10 Supplemental Information

3.10.1 Supplemental Figures

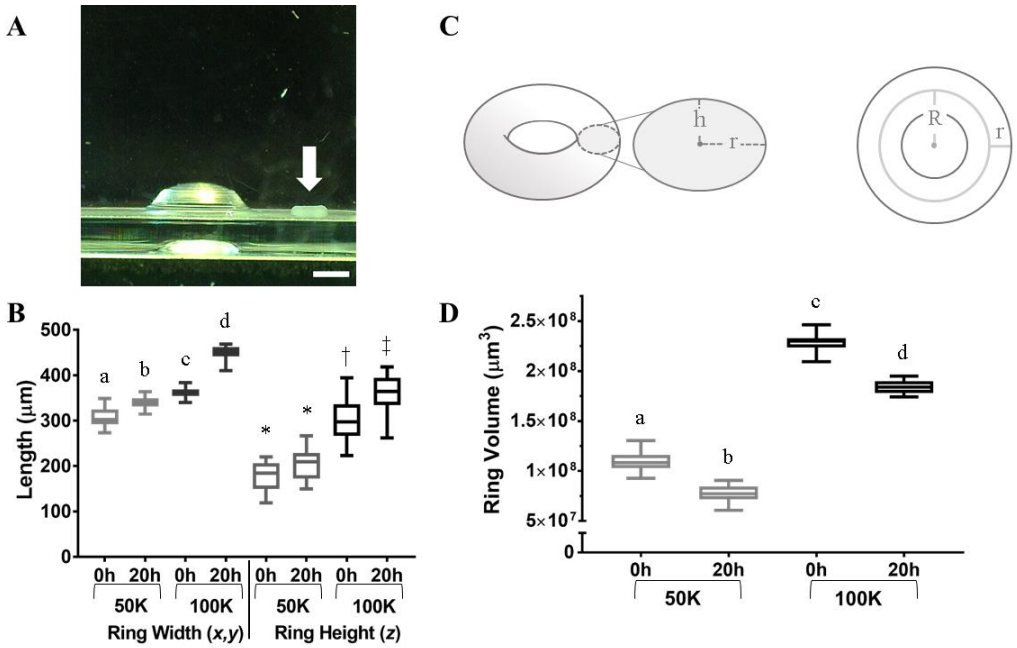

Supplemental Figure 3.1 *Volume of tissue rings changes.* Tissue ring with 5 x 10^4 and 1 x 10^5 cells were transferred into a media-filled cuvette and imaged side-on at T=0 and T=20 hours (A). Ring width (thickness) and height was plotted for the two seeding densities at both time points. Ring thickness significantly increased after 20 hours for both seeding densities (two-way ANOVA with Tukey's correction $p<0.05$). Significant differences in ring height were found between 5 x 10^4 and 1 x 10^5 at both time points, however only the 1 x 10^5 group increased significantly in thickness over time (two-way ANOVA with Tukey's correction, $p<0.05$). Values with different letters are significant from one another, and values with different symbols are significant from one another (B). Schematic of tissue ring volume calculation where volume was calculated using a modified equation that assumes an elliptical wall cross-section with minor height, *h*, and minor radius, *r* (C). Significant differences in ring volume were found between 5 x 10^4 and 1 x 10^5 at both time points as well as a significant decrease within groups (two-way ANOVA with Tukey's correction $p<0.05$), values with different letters denotes significance (D). n = 27 and 15 for HUVEC 5 x 10^4 and 1 x10^5 samples respectively. Scale bar is 1 mm.

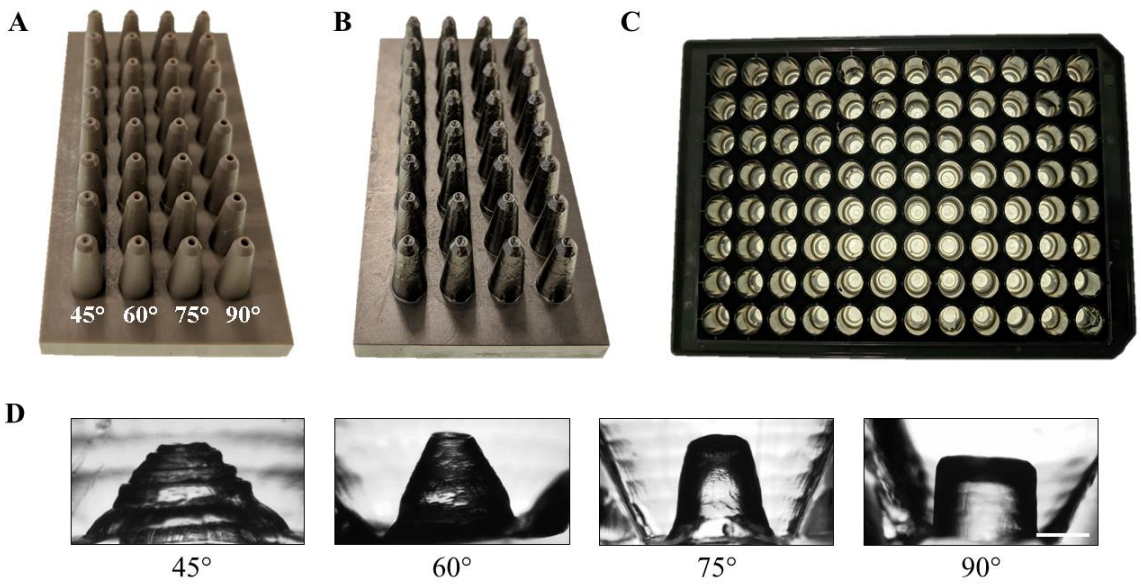

Supplemental Figure 3.2 *96-well molds*. Photo of mold for 96-well plates. A 4 x 8 mold machined in PEEK where each row will form a row of ring-shaped agarose molds whose central peg has a different angel (45°, 60°, 75°, 90°) (A) and a 4 x 8 mold machined in stainless steel that will form ring-shaped agarose molds where all the central pegs have a 60° angle (B). Photo of agarose gels with ring-shaped recesses molded in each well of a 96-well plate (C). Photos of cross sections of ring-shaped agarose molds with central pegs with 4 different angles (D). Scale bar is 1 mm.

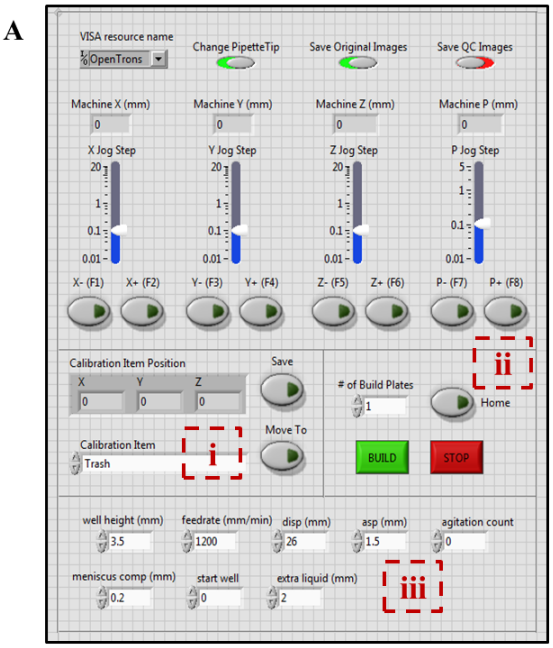

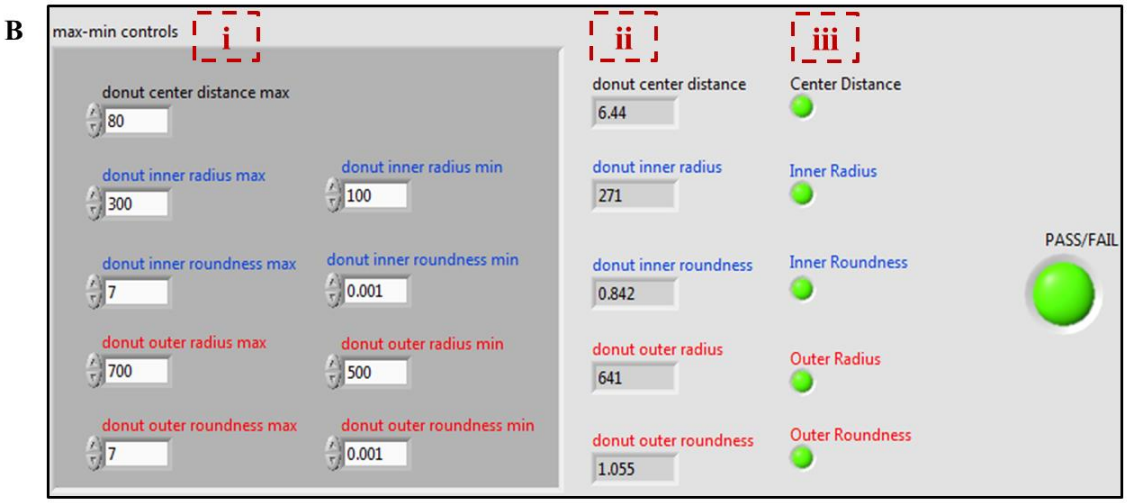

Supplemental Figure 3.3 *LabVIEW user interfaces.* Screenshot of the LabVIEW interface that controls the automated workflow of the Opentrons OT-1 where the user can calibrate item positions (i), input build parameters (ii), and control ring pick-up parameters (iii) (A). Screenshot of LabVIEW quality control interface where the user can input parameter ranges (i), view the measured parameter value (ii), and view if the tissue ring passes or fails (iii) (B).

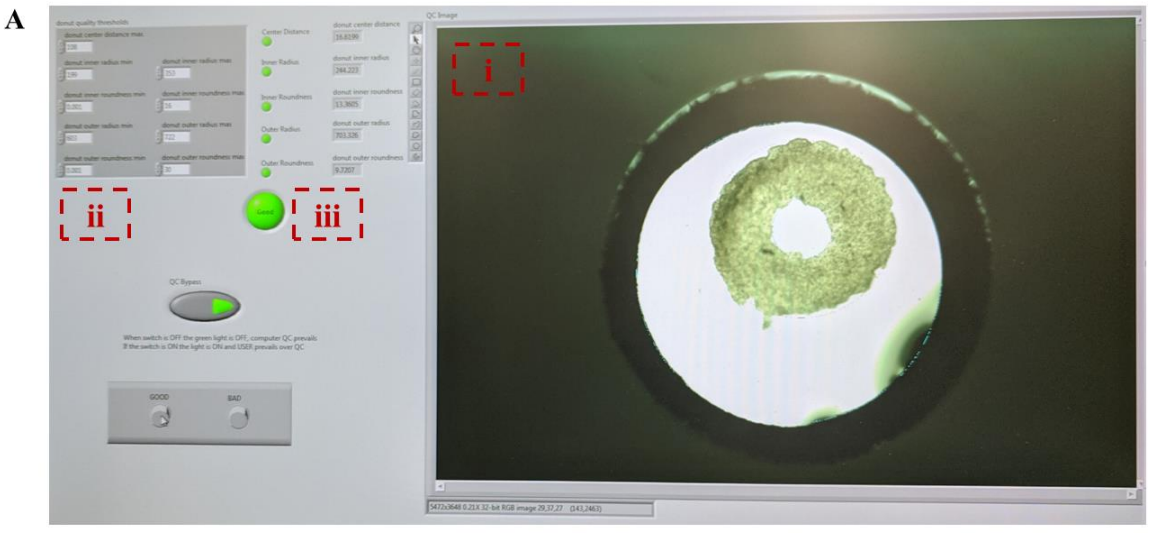

B

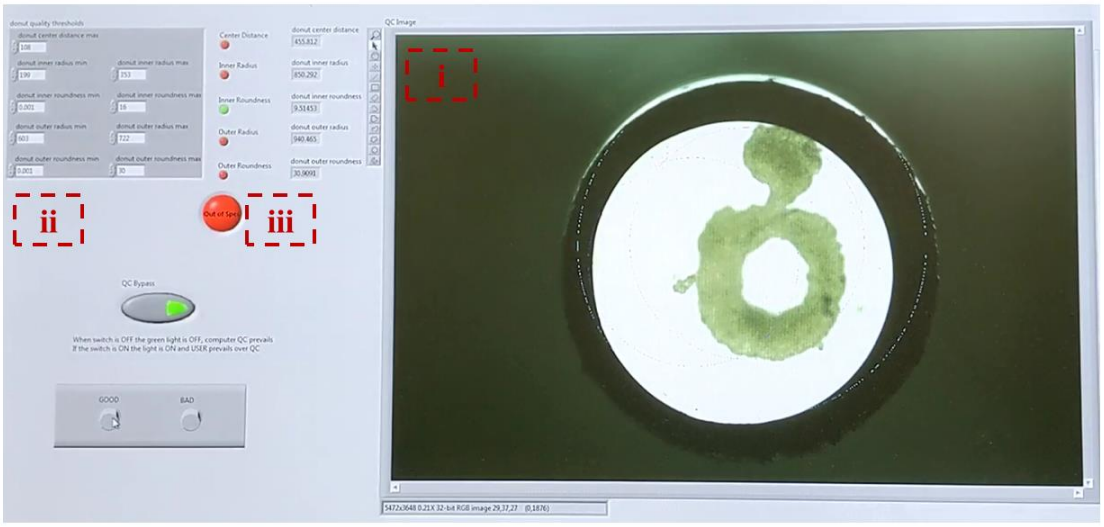

Supplemental Figure 3.4 *Real-time tissue ring quality control.* Screenshots of the custom LabVIEW algorithm performing quality control on two tissue rings. The first panel shows QC of a tissue ring (i) that passes, with the center distance, inner radius, inner roundness, outer radius and outer roundness parameters measured within the given range (ii). The read-out lights for each parameter are green, and the overall read-out light is green (iii) (A). The second panel shows QC of a tissue ring (i) that fails, with center distance, inner radius, outer radius and outer roundness parameters measured outside the given range (ii). The read-out lights for the failed parameters are red, and the overall read-out light is red (iii) (B).

3.10.2 Supplemental Videos

Supplemental Video 3.1 *Tissue rings self-releasing from mold.* Time lapse video of HUVEC rings (5 x 10^4 cells/ring) from T= 0 – 20 hours where each frame represents 30 minutes. Scale bar is 1 mm.

Supplemental Video 3.2 *96-well ring releasing from 60º peg.* Time lapse video of 1.5 x 10^5 HUVEC rings from T= 0 – 24 hours where each frame represents 30 minutes. Scale bar is 500 μm.

Supplemental Video 3.3 *Automated build cycle initiation with Z axis probing.* Video of the OT-One liquid handling robot initiating the build sequence. The robotic arm with the custom pipette tip holder moves through the following sequence: move to pipette tip rack, move to well A1 of plate 1, probe *z* depth, move to well B1, aspirate to retrieve tissue ring, move to camera.

Supplemental Video 3.4 *Automated ring placement in funnel-guide.* Video of a tissue ring that has passed QC and is being placed in the mouth of the funnel-guide. The ring is transferred from the pipette tip into the funnel-guide upon contact of the meniscus with the culture medium inside the funnel-guide. The ring then rights itself to a horizontal orientation and is guided to the stacking chamber where it settles and aligns onto the forming stack.

Chapter 4

Constructing a Scaffold-Free Perfusable Capillary Tissue Bed

Kali L. Manning, Sc.M.[1, 2]

[1] Department of Molecular Pharmacology, Physiology and Biotechnology

[2] Center for Biomedical Engineering

Brown University, Providence, RI, USA

4.1 Abstract

One of the primary challenges facing tissue engineering is the development of thick tissues with high cell densities. Without a vascular network to perfuse nutrient rich media, tissues rapidly develop a necrotic core. One method to address this need is the application of additive manufacturing techniques to fabricate high cell density tissue beds via fusion of prevascularized microtissues. The following chapter outlines the theory behind the fabrication of an *in vitro* capillary tissue bed. This includes pertinent physiological information, relevant prior work, experimental design, preliminary data, and outlines for future work. The defined capillary bed could be connected to a bio-tube fabricated via the funnel-guide method to create a novel structure that can be perfused. It is described, and intended to be evaluated, as a hepatic tissue bed with the stated metrics drawn from human physiological data. Preliminary data shows capillary-like networks can form in spheroids given an appropriate adjacent cell-type. Additionally, spheroids containing liver cells and endothelial cells can fuse together to form a pseudo tissue bed. Finally, a gravity driven perfusion system was developed that integrates with the funnel-guide, and could be used to perfuse a capillary tissue bed.

4.2 Introduction

One of the primary challenges facing tissue engineering is the development of thick tissues with high cell densities. When constructed *in vitro* without a nutrient supply, tissues rapidly develop a necrotic core. Conversely, the body cannot be relied on to vascularize a thick tissue because the average speed of sprouting is 0.25-0.5 mm/day, which is insufficient to sustain the tissue after transplantation. [1] Prevascularization of thick tissues with a vascular tree of larger vessels branching into capillaries would provide nutrient access *in vitro* and allow for immediate connection and perfusion *in vivo.* Current techniques to construct vasculature include creating single tissue engineered blood vessels (TEBV) using scaffold and scaffold-free approaches, such as the funnel-guide (FG), bioprinting single vessels that branch and contain networks of small vessels, spontaneously forming capillary networks in spheroids and scaffolds, and developing microfluidic platforms to study microvasculature flow [2]. However, to the best of our knowledge, a single perfusable scaffold-free vascular unit containing small vessels branching into a capillary bed has not been constructed. **Figure 4.1** is a schematic of the novel structure, constructed in three parts, a single tube, a branching tube and a perfusable capillary network. This novel structure could contribute to the translation of tissue engineered structures as *in vitro* diagnostic tools and eventually into clinical settings.

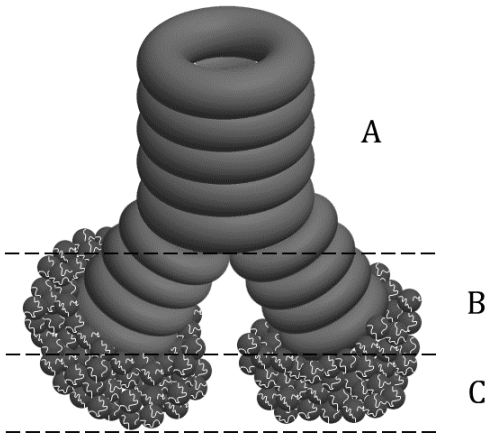

Figure 4.1. *Theoretical capillary tissue bed connected to a branched TEBV.* The capillary tissue bed could be fused to TEBV fabricated using the funnel-guide method. The final theoretical structure will consist of a single tube (A) that branches (B) into a capillary network (C).

Approaches to creating small diameter TEBV (<6 mm) can take several forms such as folding a sheet around a mandrel, bioprinting, or using microtissue building units [3]–[14]. The mandrel technique allows for the control of lumen size and the addition of multiple cell types, however some techniques take weeks to develop the vessel [15]–[17], and require material degradation for removal which poses a challenge as dissolution of the material can impact viability [15], [16], [18]. Bioprinting allows for the creation of branching vessels and the connection to a perfusion system by printing support structures simultaneously, and via sacrificial lattices that can be post-seeded with cells [19]–[21]. However, this does not create a structure with physiologically relevant cell densities. Other techniques combine bioprinting and microtissues, by bioprinting with removable agarose rods [22], or microtissues within a needle array so that it can be removed and manipulated. The Kenzan method manipulates multi-cellular spheroids and pierces them onto a microneedle array [23]. Using the Kenzan method a 1.5 mm diameter vessel was created using 500 multicellular spheroids containing fibroblasts and endothelial cells (ECs), and

subsequently removed after 4 days and perfused [24]. A trachea-like tube was also created using chondrocyte, EC and mesenchymal stem cell spheroids, and evaluated via implantation into a rat trachea [25]. Missing from these studies is a quick and simple method to construct scaffold-free vessels. The funnel-guide is a quick and simple automated method for fabrication of bio-tubes. Bio-tubes fabricated using the FG method could be joined to a capillary tissue bed to create the novel structure shown in **Figure 4.1Error! Reference source not found.**.

While the TEBV provides the connection to the perfusion system, the key component to providing nutrients to the entire tissue is the capillary network. Approaches to creating capillary networks *in vitro* rely on the innate ability of ECs to undergo angiogenesis in scaffold and scaffold-free environments. *In vivo* conditions of angiogenesis including hypoxia and the presence of growth factors including vascular endothelial growth factor (VEGF), can also be incorporated *in vitro* to encourage and direct vessel formation [26]–[28]. Several types of ECs will undergo *in vitro* angiogenesis including human umbilical vein endothelial cells (HUVECs), human dermal microvascular endothelial cells (HDMECs), and human aortic endothelial cells (HAECs) to name a few [29]. Scaffold systems proven amenable to vascularization include fibrin gels [30], 50/50 PLLA/PLGA scaffolds [31], collagen [32] and Matrigel [33]–[35]. However, the scaffold-free environment is advantageous because cells will have cell-cell interactions, produce their own ECM, and have a higher cell density compared to scaffold systems, more closely approximating the *in vivo* environment [36]. In a scaffold-free environment, ECs need to be co-cultured with other cell types to form capillary networks [37]–[39]. A variety of cell types have been successfully cultured with HUVECs including hepatocytes [40],

fibroblasts [41]–[45], human mesenchymal stem cells (hMSCs) [46], cardiomyocytes [47], islet cells [48], human indiced pluripotent stem cells (iPSCs) [49], and smooth muscle cells (SMCs) [50]. In addition, these capillary networks have proved to be patent [51]. Patency can be determined using a variety of methods including immunohistochemistry (IHC) for CD31 and von Willebrand factor (vWF) [52], [53], fluorescent microscopy [54], [55], and transplantation into a mouse/rat with subsequent tail vein injection of lectin or FITC dextran [40], [46].

Certain techniques can be employed to influence capillary formation in scaffold-free systems, including spheroid size and culture time. HUVEC and NHF spheroids cultured in a 1:2 ratio saw network formation in the 300 μm and 500 μm diameter spheroids, but not the 100 μm spheroids. These same spheroids saw the formation of a more complex and developed network at 7 days of culture time compared to 4 and 1 day of culture time. [56], [57] Another technique that influences the capillary network formation in spheroids is the co-culturing ratio (**Figure 4.2**). A lower number of ECs encourages capillary network formation. Low amounts of ECs created networks that did not cover the entirety of the spheroid, and too much ECs resulted in clumps that did not elongate. [46] While the co-culturing ratio controls the robustness of the network formed, microtissue shape controls the capillary network directional orientation. The EC networks align along the edges of a 1:4 HUVEC NHF rod tissue, curving at the two ends, elongating parallel to the sides on the edges, and perpendicular to the sides in the middle of the tissue. [42]

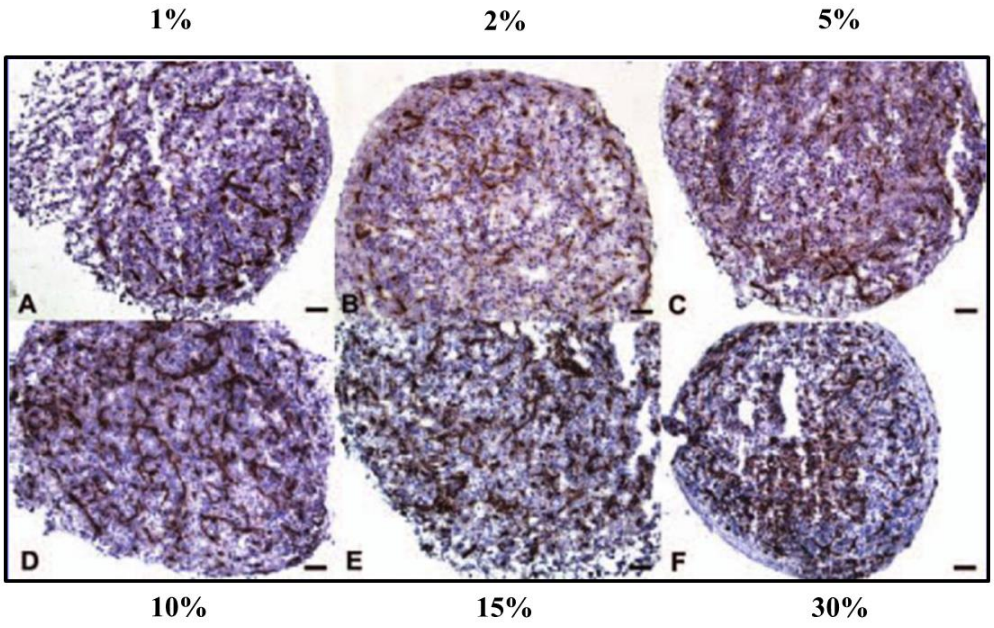

Figure 4.2. *Amount of endothelial cells influences network formation in spheroids.* Cross-sectional images of CD31 stained sections of HUVEC and hMSC spheroids cultured for 10 days with varying ratios of HUVECs; 1% (A), 2% (B), 5% (C), 10% (D), 15% (E), 30% (F). Scale bars are 100 µm. [46]

Mecahnical forces such as fluid flow and shear stress will also influence the formation of capillary networks. Current work on evaluating the effects of flow on the formation of capillary networks are conducted using microfluidic devices or bio-printed scaffold constructs, with ECs seeded in a hydrogel scaffold. In both set-ups, ECs spontaneously form capillary networks within a scaffold, and are perfused using either a peristaltic or syringe pump, or a hydrostatic pressure head difference. The perfusion is initially interstitial flow across the scaffold, eventually flowing through the capillaries as they form [58]–[62]. Flow rates are either set with a pump, or dependent on the pressure head or desired shear stress. Flow rates dictated by pumps range from 5-100 µl/min [21], [63], [64]. Pressure head differences range from 5-10 mmH_2O, or 10 µl volume difference [58], [59], [65], [66]. Microfluidic devices that use shear stress rates to dictate flow use

shears around 10 dyne/cm^2 [32], [67]. The influence of shear stress is contested, with studies reporting both sprouting attenuation and triggering [32], [65]. Interstitial flow directs capillary sprout formation, with sprouts forming in the direction opposite of flow [65], [66]. However, the presence of fluid flow contributes to the development of a robustly organized network, regardless of flow direction [65]. Mechanical engagement of the newly formed capillaries was necessary to maintain sprouting and prevent retraction [32]. Engaging forming capillaries with flow encourages interconnected network formation throughout the entire tissue bed. [32], [33], [66], [68], [69] An interesting approach to engaging prevascularized scaffold-free spheroids placed them within a microfluidic chamber, between channels containing vascularized hydrogels. The networks in the hydrogels connected to the networks in the spheroids, and were perfusable. [70], [71] Missing from these studies is a scaffold-free perfusable capillary network, constructed through fusion of prevascularized microtissue building parts.

4.3 Methods

4.3.1 Overall Experimental Approach

In order to build a perfusable capillary bed, a platform could be designed that provides direct flow to the capillaries using gravity and a porous substrate or mesh. The capillary bed could be composed of a parenchymal cell and ECs, and either be formed by fusing spheroids containing capillary networks together, or by seeding the mixed cells into a quadrangle mold. The monodispersed cell approach could allow for engagement with fluid flow earlier than the spheroid fusion method. Flow rates through multiple porous substrates and non-adherent meshes could be tested concurrently to determine ones that have physiologically relevant flow rates. The capillary bed could sit on the selected

material, and media could be flowed through using a pressure head. Assessment techniques could include visualization of flow using fluorescent dye and network visualization via IHC for EC specific markers.

4.3.2 Capillary Tissue Bed Metrics

Capillaries have a diameter in the range of 3.5-10 µm, and an average length of 750 µm [72], [73]. The hypothesized perfusable capillary bed could cover an area of 1 cm^2, and contain 3,000 capillaries/mm^3 with average diameters of 8 µm, and average lengths of 750 µm. Capillaries could be formed in spheroids by co-culturing HUVECs with a parenchymal cells, such as HepG2 cells, in a 1:2 ratio. The capillary bed could be built by fusing these spheroids together in a 1 cm^2 square gel. The presence of a connected capillary network can be evaluated by engaging the capillary bed with media perfusion at a physiologically relevant flow rate, between 13.5-102.6 µl/min per mm^2, for 5 days, and through microscopy. Capillary network presence throughout the bed could be evaluated via tissue sectioning and staining for CD31. Flow through the tissue bed could be assessed using 70 kDa FITC dextran.

4.3.3 Cell Culture, Micro-Mold Fabrication and Formation of Microtissues

HepG2 and HUVECs were be maintained as previously described in Chapter 2 [2]. Prior to passage and seeding, HUVECs were stained with 5 µM CellTracker™ Red for 30min (Thermo Fisher Scientific, Waltham, MA). Non-adhesive agarose hydrogels were fabricated by pipetting molten agarose into molds containing 35 circular microwells 800 µm x 800 µm, and 1 square microwell (quadrangle mold) 1 cm x 1 cm (Microtissues Inc., Providence, RI). Agarose gels were made with powdered agarose (Low-EEO/Multi-Purpose/Molecular Biology Grade, Fisher BioReagents) (Thermo Fisher Scientific)

sterilized by autoclaving and then dissolved in sterile water to 2% (weight/volume). A positive replica of the quadrangle mold was designed in SolidWorks (Dassault Systemes SolidWorks Corporation, Waltham, MA) and 3D printed on a Form1+ SLA 3D printer (FormLabs, Somerville, MA). There was a rectangular recess 10 mm x 10 mm x 5 mm in the center of the mold. 3D printed parts were replicated using OOMOO 30® Silicone Rubber (Smooth-On, East Texas, PA). Casts were vacuumed to remove air bubbles, and cured at room temperature overnight. Prior to use, the elastomer molds were autoclave sterilized. Large spheroids were seeded with both HUVEC and HepG2 cells in a ratio of 1:2 HUVEC:HepG2, for a total seeding density of 2K cells per microwell (667 HUVECs and 1,333 HepG2 per microwell). After 5h of aggregation, spheroids could be placed in the centimeter square gel using a wide-bore pipette tip, and fused together to form a capillary bed. Concurrently, 1 x 10^6 HUVEC and 2 x 10^6 HepG2 were seeded into the centimeter square gel to form a quadrangle capillary bed. Mixed spheroids and capillary beds were maintained in EGM.

4.3.4 Evaluating Spheroid Fusion into a Tissue Bed

To better understand how spheroids fuse together to form a tissue bed, we developed the spheroid gap assay (SGA). The assay is based on the assumption, that when placed in contact with one another, spheroids have a void space between them (**Figure 4.3**). This void space, or gap, can be related to spheroid radius using the equation $r_v = \frac{2r_s}{\sqrt{3}} - r_s$ where r_v is the radius of the void space, and r_s is the radius of the spheroid. The radius of the void is directly proportional to the radius of the spheroid, with a larger spheroid resulting in a larger void radius. As spheroids fuse together, we hypothesize the void space and the total area will decrease over time.

Spheroids of HUVEC, HepG2 and mixtures of the two cells were self-assembled for 24 hours and then removed from the agarose gel by inverting the gel. Spheroids were then pipetted into the SGA chamber, filled with EGM, and imaged every 30 minutes for 24 hours using a Zeiss Axio Observer Z1 equipped with an AxioCam MRm camera with ZEN software (Carl Zeiss Microscopy, LLC, Thornwood, NY) and an X-Cite 120 fluorescence illumination system (EXFO Pho- tonic Solutions, Mississauga, Ontario, Canada). A positive replica of the SGA chamber was designed in SolidWorks (Dassault Systemes SolidWorks Corporation, Waltham, MA) and 3D printed on a Form1+ SLA 3D printer (FormLabs, Somerville, MA). The chamber was designed to fit in a 24-well tissue culture plate. There was a 2 mm diameter and 2 mm tall circular recess in the center of the mold topped by a 7 mm diameter and 5 mm tall funnel. 3D printed parts were replicated using OOMOO 30® Silicone Rubber (Smooth-On, East Texas, PA). Casts were vacuumed to remove air bubbles, and cured at room temperature overnight. Prior to use, the elastomer molds were autoclave sterilized. To create non-adhesive hydrogels, 2% (w/v) sterile, molten agarose was cast into silicone negatives, allowed to gel, and transferred to sterile 24-well tissue culture plates. Gels were equilibrated in serum free EGM at 5% CO_2 and 37ºC overnight prior to use.

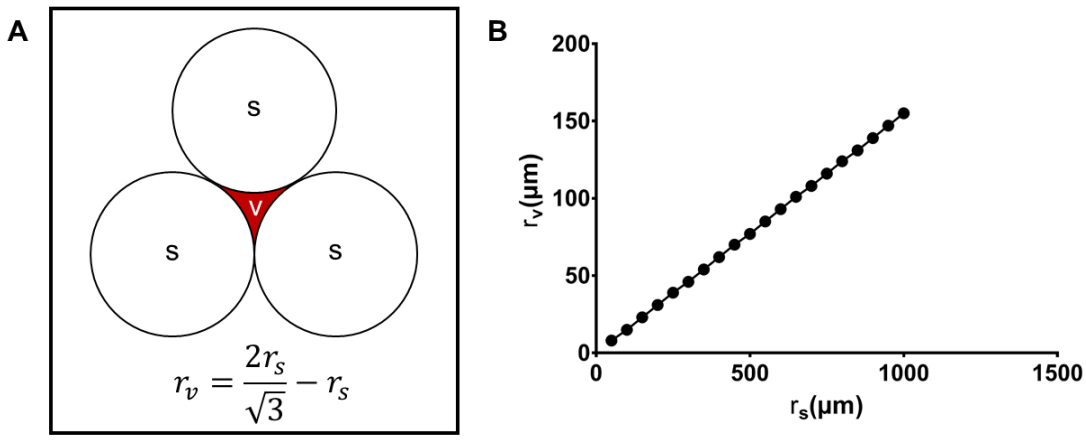

Figure 4.3. *Spheroid radius determines void radius.* Schematic of three adjacent spheroids and the resultant central void space (A). The radius of the void space can be determined using the equation shown where r_v is the radius of the void, and r_s is the radius of the spheroid. Graphical representation of the relationship between spheroid radius and void radius (B). As the spheroid radius increases, the void radius increases following a linear trend.

4.3.5 Testing the Gravity-Driven Flow Rate of Agarose

Agarose was evaluated as a potential porous substrate for use in the hypothesized perfusion platform. Non-adhesive agarose hydrogels will be fabricated by pipetting molten agarose (1% w/v) into molds containing a single hexagonal recess with 7 mm sides and 6 mm in height. The hexagonal molds were filled with water (MilliQ and deionized) and placed on various absorbent materials to evaluate the flow rate of capillary action via wicking. Absorbent materials tested included coffee filters, paper towel, and blotting paper. The 127 mm^2 hexagonal area held a volume of 700 µl. The flow rate was determined by timing how long it took for the 700 µl to be wicked onto the absorbent material. Trials were done in triplicate at 25 ºC and 37 ºC.

4.3.6 Perfusion Platform

A perfusion platform could be designed that houses the capillary bed and provides physiologically relevant flow rates. The platform could consist of a porous substrate such as agarose, a non-adherent membrane, such as nylon, or a sponge-like material such as GelFoam®, that the capillary bed will sit on. Fluid flow could be induced by gravity. Fluid pressure (P) is directly proportional to fluid height (h) ($P = \rho g h$). Thus to achieve a fluid pressure within the physiological range of capillaries, 10-30 mmHg, we could use a fluid column between 27-40 cm in height [74]. Thus it is feasible that a column of fluid over a porous substrate would be able to create a physiologically relevant flow rate. Flow rates could be based on the capillary mesh density of the liver, 3K capillaries/mm³ [75]. Assuming a capillary length of 1 mm, we can calculate the flow rate per surface area. Flow rates for a single capillary range from 0.0045-0.0342 µl/min, thus flow rates for 3K capillaries would range from 13.5-102.6 µl/min per mm² of capillary bed. Flow rates for various porous substrates and non-adherent membranes could be determined by timing the passage of a known volume of fluid, to determine which creates a gravity induced flow rate within this physiological range.

4.3.7 Capillary Network and Flow Evaluation

Capillary network formation in individual spheroids was evaluated via fluorescent microscopy of stained HUVECs using a Zeiss Axio Observer Z1 microscope equipped with an Axio MRm camera, and X-Cite 120 excitation light source at 24h, 48h and 72h. Capillary networks formed with exposure to flow in the perfusion platform could be evaluated using fluorescent dye and by monitoring perfusate volume. Total volume of perfusate could be compared at 24h, 48h and 72h across conditions; without cells, with

HepG2s only and with the capillary bed. This volume comparison could provide an indication of how permeable the capillary bed is. 70 kDa FITC dextran could be added to the perfusate and monitored using fluorescent microscopy. ImageJ/Fiji could be used to calculate vessel area within the capillary bed, and permeability via changes in fluorescent intensity overtime. Network formation in the center of the tissue could be evaluated via plastic sectioning and staining for CD31. Stained sections from the center of the tissue could then be visualized using microscopy to look for the presence of capillary networks.

4.3.8 Statistical Analysis

Statistical analysis was done on JMP software (SAS Institute Inc., Cary, NC). The area under the curve was calculated for each trial of the Spheroid Gap Assay, and these values were used for statistical analysis. Significance was determined using Welch's test with post-hoc Dunn's Method for Joint Ranking for multiple comparisons. Data were first examined using the Shapiro-Wilk test to determine that the data came from the normal distribution, and O'Brien's test to determine if the variances were equal.

4.4 Results

4.4.1 Capillary Networks Form in Spheroids

To determine if we could form capillary networks in spheroids, we tested various ratios of mixed HUVEC and HepG2 spheroids (**Figure 4.4**). Cells were mixed, because in scaffold-free systems, HUVECs alone will not form capillary networks. We mixed CellTracker™ Red stained HUVEC and unstained HepG2 cells in 1:1, 1:2, 1:3, and 1:4 ratios and self-assembled them into spheroids for 24h. Fluorescent microscopy was used to visualize network formation. Capillary networks were visible in spheroids seeded at 1:2

and 1:3 ratios. To determine how long capillary networks remain in the spheroid, we imaged a 1:2 ratio spheroid for 72h. Capillary networks were visible in the spheroid at 24h and 48h, but started to dissipate by 72h.

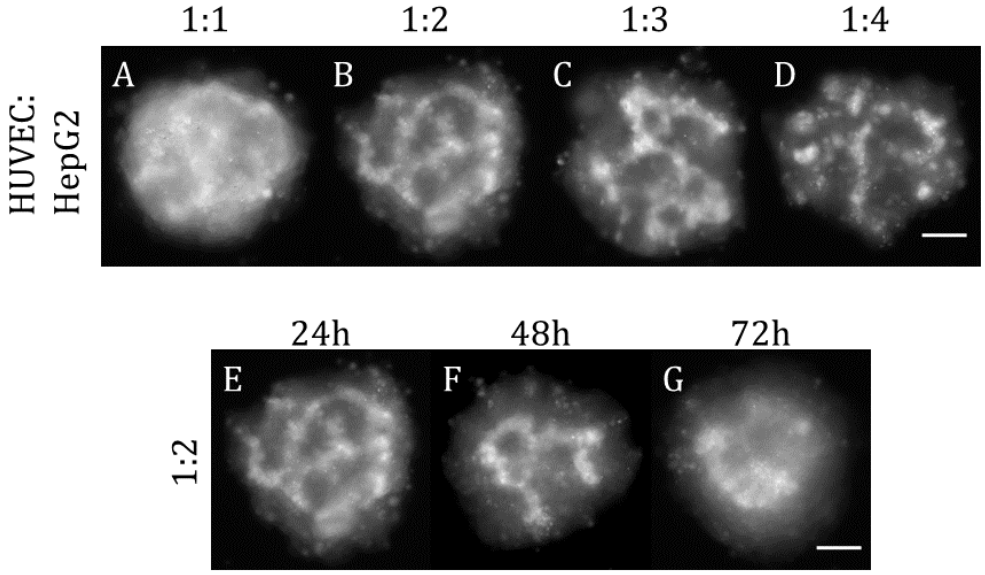

Figure 4.4. *Capillary networks form in spheroids*. Unstained HepG2 and CellTracker™ Red stained HUVEC were seeded in spheroid agarose gels in the following ratios of HUVEC to HepG2 cells, 1:1 (A), 1:2 (B), 1:3 (C), 1:4 (D) at a seeding density of 2K per spheroid. At 24h spheroids were imaged at 20X magnification to view capillary network formation. The capillary network formed in the 1:2 ratio spheroid was imaged for 3 days at 20X magnification at 24h (E), 48h (F), and 72h (G). Scale bars are 100 µm.

4.4.2 Spheroids Fuse to Form a Tissue Bed

To determine if spheroids composed of a mixture of HUVEC and HepG2 cells would fuse together to form a tissue bed, we developed the Spheroid Gap Assay (SGA). In this assay spheroids of HUVEC, HepG2 and a 1:2 mixture of the two cells were self-assembled for 24h before being removed from the agarose mold and transferred to a custom designed SGA chamber (**Figure 4.5**). The SGA chamber was circular in shape and had an agarose funnel to guide the spheroids into the chamber. Then, the groups of spheroids were imaged

every 30 minutes for 24 hours to visualize fusion. Fusion of the spheroids was quantified by measuring the total area of the tissue bed over time using ImageJ. As the spheroids fuse together, the total area decreases. To compare between groups, area measurements were normalized to the starting values and graphically displayed. All three groups decrease in area over 24 hours, but the HUVEC tissue bed decreases significantly more than the HepG2 only and the 1:2 mixture group.

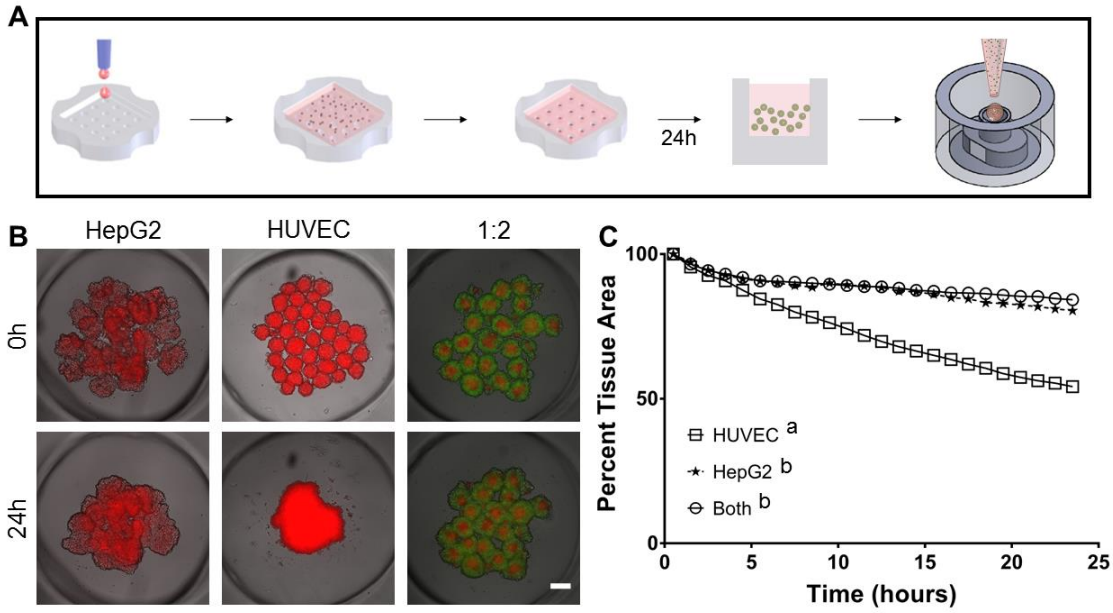

Figure 4.5. *Spheroids fuse and decrease in total area over time.* Schematic of the SGA (A). HepG2, HUVEC or a 1:2 mixture (HUVEC:HepG2) were seeded into agarose gels containing spheroid-shaped recesses, and allowed to self-assemble for 24 hours. Spheroids were then removed from the gel and transferred via pipette tip into the gap assay chamber, where they were timelapse imaged for 24 hours. Snapshot images of the gap assay chamber at 0h and 24h for HepG2, HUVEC and 1:2 mixture spheroids (B). Scale bar is 200 µm. Graphical representation of the normalized total spheroid area over time (C). All three groups decrease in total area over time, with HUVEC decreasing significantly more than HepG2 and the 1:2 mixture (Both), where groups with different letters are significantly different.

4.4.3 Slab Agarose Can be Perfused

To determine if agarose could be used as a porous substrate to perfuse a capillary tissue bed, we determined the flow rate of water wicking out of a hexagonal agarose recess using various absorbent materials; water would not perfuse out of agarose without an absorbent material placed underneath. The hypothetical experimental set-up is shown in **Figure 4.6**. An agarose gel was filled with 700 µl of water, placed on an absorbent material and monitored for wicking. We tested coffee filters, paper towel and blotting paper as potential absorbent materials that would wick water through the agarose. Coffee filters and paper towels took longer than 1 hour to wick the 700 µl of water, and were excluded. We tested thick and thin blotting paper at 25 ºC and 37 ºC. Thick blotting paper had an average flowrate of 15.5 µl/min at 25 ºC and an average flowrate of 14.3 µl/min at 37 ºC. The thin blotting paper had an average flow rate of 15.2 µl/min at 25 ºC and 22 µl/min at 37 ºC. When normalized to the cross-sectional area of 127 mm^2, the maximum flow rate achieved was 0.17 µl/min per mm^2 of area.

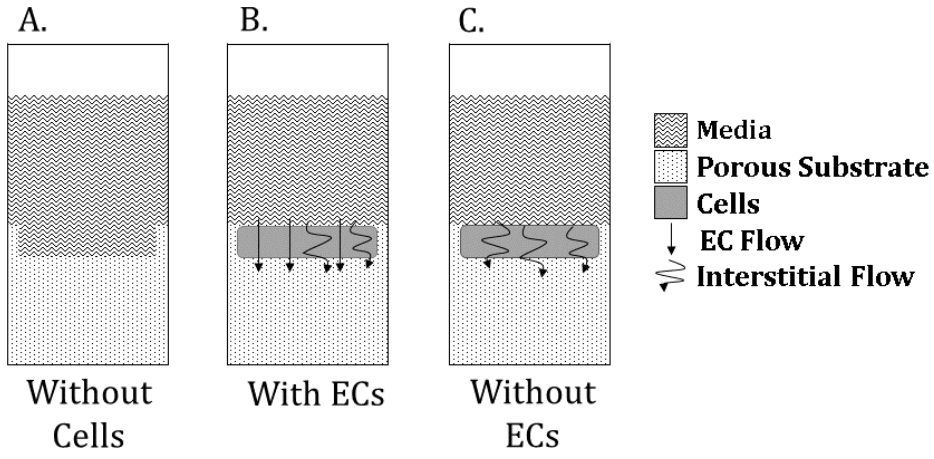

Figure 4.6. *Capillary network flow evaluation experimental set-up.* Perfusate volume could be compared between three conditions, no cells with just the porous substrate (A), a

capillary bed formed with ECs and parenchymal cells (B), and a tissue with only parenchymal cells (C). The differences in perfusate volume could provide an indication of the perfusivity of the capillary network compared to interstitial flow.

4.4.4 Gravity-Driven Perfusion System

A gravity driven perfusion system was developed for the funnel-guide as shown in **Figure 4.7**. A new molding technique and bottom cap was developed for the FG method to allow connection to flexible tubing. A peristaltic pump was used to cycle culture medium through the system, with an overflow return line maintaining a constant pressure head above the FG. To prevent excessive pressure build-up, an air vent was installed to normalize the system to atmospheric pressure. An air release valve on the lid acted as a bubble trap, allowing the user to release any air caught in the FG. A flow valve was placed after the FG to moderate the flow rate. To monitor the flow, drips could be sensed, and failures counted. A square piece of polyethylene terephthalate (PET) mesh (non-adhesive to cells) was placed in the bottom of the stacking chamber. The perfusion system ran for several days without tissues.

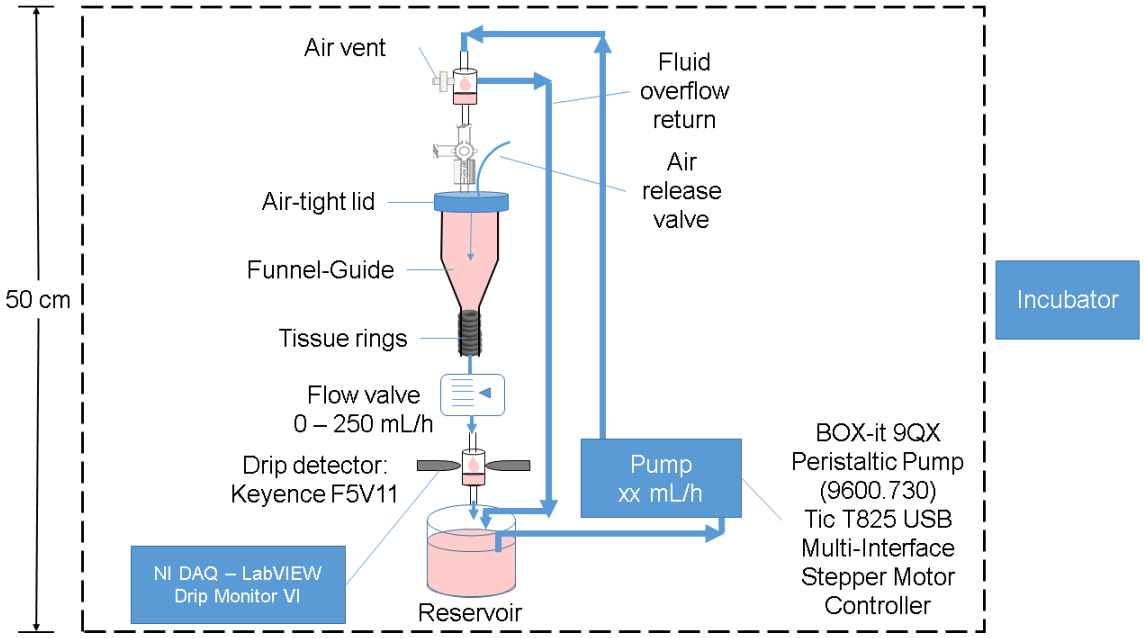

Figure 4.7. *Gravity driven perfusion system.* Schematic of the gravity driven perfusion system for the funnel-guide. A peristaltic pump is used to maintain a pressure head above the FG to drive perfusion of tissues in the stacking chamber. A flow valve is used to moderate the flow rate.

4.5 Discussion

Upon completion of the experiments outlined above, we could construct a portion of the vascular system, an arteriole that branches into a capillary bed. Capillaries are responsible for exchanging nutrients and oxygen for metabolic waste, this exchange is critical and replicated *in vitro* could contribute to overcoming the challenge of generating thick tissues with high cell density. To the best of our knowledge, a perfusable scaffold-free capillary bed has not been created; perfusion of scaffold-free structures containing capillaries has only occurred after implantation into a host such as a mouse or a chick chorioallantoic membrane [46], [51]. Thus fabrication of a perfusable tissue bed using

additive manufacturing techniques with prevascularized microtissue building blocks could create a novel structure that can be used for further evaluations.

First we investigated the fabrication of prevascularized spheroids to be used as microtissue building blocks. We mixed HepG2 cells with HUVECs in various ratios (1:1, 1:2, 1:3 and 1:4) to evaluate the ability of HUVECs to form networks within the spheroids. Initially, we saw success, with the most robust networks forming in the 1:2 mixture, and networks being visible through 72h of culture. However, we were unable to re-create the networks shown in **Figure 4.4** with newly ordered HepG2 cells. Instead of networks forming, the HUVECs clumped together amongst the HepG2 cells, either in the center of the spheroid for the 1:1 and 1:2 mixtures, or in distinct sporadic clumps in the 1:4 and 1:10 mixtures (**Supplemental Figure 4.1**). We do not know the origin of the initial HepG2 cells used, and they were in cryo-storage for years prior to use in this study. It is possible that the cells were contaminated by other cells, and thus acted differently than newly purchased HepG2 cells. Analysis on the cells could lend insight into any changes that may have occurred. With the newly purchased HepG2 cells, we were also unable to fabricate networks within a quadrangle shaped tissue at a 1:2 and a 1:4 mixture (**Supplemental Figure 4.1**). Future experiments can evaluate additional cell types to be mixed with HUVECs such as fibroblasts which have been shown to support the formation of networks in spheroids [41], [42].

Next, we developed the spheroid gap assay (SGA) to evaluate the fusion of spheroids into a tissue bed. The assay can be used to understand the overall morphological changes that occur as spheroids fuse into a macrostructure, and can be applied to understand the morphology of fusion at junctions (or void spaces) between adjacent

spheroids. As fusion occurs, the void spaces decrease in size, and the overall area of the tissue bed decreases in size. This change is cell type dependent and could be moderated via cell mixing. HUVEC's fused and decreased in area significantly more than HepG2s and a 1:2 mix of HUVEC to HepG2 cells, with the mixture behaving more like pure HepG2s than HUVECs. The 1:2 ratio allowed the HepG2 cells to attenuate the contractility of the HUVECs, but other ratio combinations may yield different results. Understanding these variations in fusion could allow us to predict void sizes and when the voids will fuse. This is valuable because void spaces remaining between spheroids could be beneficial; these gaps could be used as an alternative to capillary networks, with voids within the inner diameter range of capillaries being engaged with perfusion to nourish the tissue bed. This would provide vital nutrients while also providing mechanical stimulation to the endothelial cells, potentially encouraging them to grow towards the flowing media and fully vascularize the tissue bed. Future work could use image analysis to quantify void space area changes as a function of cell type and ratio to better understand the dynamics of tissue bed fusion. Additionally, experimentation could be done to evaluate the influence of dynamic flow rates and pressures on tissue bed fusion.

Finally, we considered porous substrate options for potential use in a tissue bed perfusion platform. The substrate porosity was intended to dictate gravity driven flow rate while also providing support for the tissue bed during fusion. We quickly determined liquid will not flow through agarose via gravity. As an alternative, we evaluated absorbent materials that would wick liquid through agarose. Flow rate measurements indicated the wicking ability of the material. We achieved a maximum flow rate of 0.17 μl/min per mm^2 using thin blotting paper. However, this is a hundred-fold less flow than our hypothetical

desired range of 13.5-102.6 µl/min per mm² for a hepatic tissue bed. Slab agarose is not porous enough to be a suitable perfusion substrate. Other materials that are more porous than agarose, but less porous than a mesh could be investigated in future studies. These materials could include sponge-like material such as GelFoam® or biocompatible polymer blends with tunable porosity.

Separate from the hypothesized tissue bed perfusion platform, we developed a perfusion system for the funnel-guide to circulate media through the bio-tube after fabrication, and to potentially be used as a platform to perfuse the hypothesized joint bio-tube tissue bed structure. To prevent placing excessive strain on the fusing tube, we designed the system to have low pressure by venting it to the atmosphere and being gravity driven by a small pressure head of 3.27 mmHg (~1/10 that of physiologic capillary pressure). Despite designing for a low pressure system, it was still too much force for the 4h 150K HUVEC toroids used to fabricate bio-tubes in Chapter 3. Upon initiating perfusion, the toroids were pushed through the mesh in the bottom of the stacking chamber and passed through the tubing into the media reservoir. We hypothesize the perfusion system could be used with more robust matured toroid building units. Future work could evaluate minor changes to the current system such as using small diameter rigid tubing, and a smaller pressure head, in addition to evaluating other perfusion methods such as tangential flow and flow akin to microfluidic systems as methods of reducing pressure experienced by the tissues.

The funnel-guide perfusion system could be used to perfuse other structures, such as the hypothetical tissue bed, by decreasing the mesh size in the bottom of the stacking chamber to prevent spheroids falling through prior to fusion. Additionally, the mesh

material could be modified to be adherent to cells, or an adherent material could be coated onto the bottom of the stacking chamber to secure the tissue bed in place. Securing the tissue bed to the bottom of the stacking chamber and the surrounding wall could encourage flow through the networks or through the void spaces. This could ensure the endothelial cells are being exposed to the mechanical stimulus of media flow, and would thus encourage network formation [65].

It is possible that capillary networks within individual spheroids will not join to create a single network. If this does not happen, it will be difficult to engage the capillaries with flow. If this is the case, an alternative strategy could be to place a monolayer of fibroblasts on one side of the perfusion platform, as capillary networks are known to grow towards fibroblasts [30]. Another technique to encourage joining of capillary networks, would be to add VEGF to the media, as it helps support angiogenesis [26], [76]. It is possible that a perfusion platform that directly engages the capillary bed with physiologically relevant flow cannot be built, or that there will not be interstitial flow within the tissue bed. If this is the case, then the single tissue perfusion system previously designed in our lab could be used. The capillary bed would sit on a mesh that is connected to a peristaltic pump, and be perfused. Another option would be to design a platform that uses flow tangential to the capillary bed, similar to a microfluidic set-up. PDMS could be used to create a chamber where the capillary bed will be placed, and media could be flowed through in a tangential direction using a pump. While this will not allow for the examination of the influence of direct flow on capillary networks, it could allow for investigation of the effects of interstitial flow.

The evaluation metrics outlined can be applied to any perfusable structure, with flow rate, pressure and capillary density modified to match the target organ system. The tissue bed could be formed via the fusion of prevascularized spheroids containing endothelial cells that could be perfused via void spaces maintained between adjacent spheroids and through the forming capillary networks. The described funnel-guide perfusion system could be modified to accommodate various meshes or adherent material in the bottom of the stacking chamber in order to encourage flow through a tissue bed. The construction of thick tissues with high cell density is a critical stepping stone in the development of tissues that more closely resemble organs *in vivo*. These tissues could be used for more accurate and efficient *in vitro* testing, as well as a starting point for the creation of organs *in vitro* for transplantation.

4.6 Acknowledgements

The author would like to thank Joshua Manning for developing the Spheroid Gap Assay image analysis pipeline, and Blanche Ip, Ph.D. for help with statistical analysis.

4.7 References

[1] S. Bersini, I. K. Yazdi, G. Talò, S. R. Shin, M. Moretti, and A. Khademhosseini, "Cell-microenvironment interactions and architectures in microvascular systems," *Biotechnol. Adv.*, vol. 34, no. 6, pp. 1113–1130, 2016.

[2] K. L. Manning, A. H. Thomson, and J. R. Morgan, "Funnel-Guided Positioning of Multicellular Microtissues to Build Macrotissues," *Tissue Eng. Part C Methods*, vol. 24, no. 10, pp. 557–565, Oct. 2018.

[3] E. Rabkin and F. J. Schoen, "Cardiovascular tissue engineering.," *Cardiovasc. Pathol.*, vol. 11, no. 6, pp. 305–17, 2002.

[4] G. E. Amiel *et al.*, "Engineering of blood vessels from acellular collagen matrices coated with human endothelial cells.," *Tissue Eng.*, vol. 12, no. 8, pp. 2355–65, Aug. 2006.

[5] P. A. Fleming, W. S. Argraves, C. Gentile, A. Neagu, G. Forgacs, and C. J. Drake, "Fusion of uniluminal vascular spheroids: a model for assembly of blood vessels.," *Dev. Dyn.*, vol. 239, no. 2, pp. 398–406, Feb. 2010.

[6] J. M. Kelm *et al.*, "Design of custom-shaped vascularized tissues using microtissue spheroids as minimal building units.," *Tissue Eng.*, vol. 12, no. 8, pp. 2151–60, Aug. 2006.

[7] J. D. Berglund, M. M. Mohseni, R. M. Nerem, and A. Sambanis, "A biological hybrid model for collagen-based tissue engineered vascular constructs.," *Biomaterials*, vol. 24, no. 7, pp. 1241–54, Mar. 2003.

[8] J. D. Berglund, R. M. Nerem, and A. Sambanis, "Incorporation of intact elastin scaffolds in tissue-engineered collagen-based vascular grafts," *Tissue Eng.*, vol. 10,

no. 9–10, pp. 1526–35, 2004.

[9] W. He *et al.*, "Pericyte-based human tissue engineered vascular grafts.," *Biomaterials*, vol. 31, no. 32, pp. 8235–44, Nov. 2010.

[10] M. B. Herring, R. Dilley, R. a Jersild, L. Boxer, a Gardner, and J. Glover, "Seeding arterial prostheses with vascular endothelium. The nature of the lining.," *Ann. Surg.*, vol. 190, no. 1, pp. 84–90, Jul. 1979.

[11] Y. Gafni *et al.*, "Design of a Filamentous Polymeric Scaffold for in Vivo Guided Angiogenesis," *Tissue Eng.*, vol. 12, no. 11, 2006.

[12] S. Kaushal *et al.*, "Functional small-diameter neovessels created using endothelial progenitor cells expanded ex vivo.," *Nat. Med.*, vol. 7, no. 9, pp. 1035–40, Sep. 2001.

[13] S. Koch *et al.*, "Fibrin-polylactide-based tissue-engineered vascular graft in the arterial circulation.," *Biomaterials*, vol. 31, no. 17, pp. 4731–9, Jun. 2010.

[14] M. D. Guillemette, R. Gauvin, C. Perron, R. Labbé, L. Germain, and F. a Auger, "Tissue-engineered vascular adventitia with vasa vasorum improves graft integration and vascularization through inosculation.," *Tissue Eng. Part A*, vol. 16, no. 8, pp. 2617–26, Aug. 2010.

[15] N. L'Heureux, T. N. McAllister, and L. M. de la Fuente, "Tissue-engineered blood vessel for adult arterial revascularization.," *N. Engl. J. Med.*, vol. 357, no. 14, pp. 1451–3, Oct. 2007.

[16] N. L'Heureux *et al.*, "Human Tissue Engineered Blood Vessel for Adult Arterial Revascularization," *Nat. Med.*, vol. 12, no. 3, pp. 361–365, 2006.

[17] T. Neumann, B. S. Nicholson, and J. E. Sanders, "Tissue engineering of perfused

microvessels," *Microvasc. Res.*, vol. 66, no. 1, pp. 59–67, 2003.

[18] S. F. Barreto-Ortiz *et al.*, "Fabrication of 3-dimensional multicellular microvascular structures," *FASEB J.*, vol. 29, no. 8, pp. 3302–3314, 2015.

[19] D. M. Cohen, E. Toro, A. A. Chen, P. A. Galie, and X. Yu, "Rapid casting of patterned vascular networks for perfusable engineered 3D tissues," *Nat Mater.*, vol. 11, no. 9, pp. 768–774, 2012.

[20] G. Y. Huang *et al.*, "Microfluidic hydrogels for tissue engineering.," *Biofabrication*, vol. 3, no. 1, p. 012001, Mar. 2011.

[21] D. B. Kolesky, K. A. Homan, M. A. Skylar-Scott, and J. A. Lewis, "Three-dimensional bioprinting of thick vascularized tissues," *Proc. Natl. Acad. Sci.*, p. 201521342, 2016.

[22] C. Norotte, F. S. Marga, L. E. Niklason, and G. Forgacs, "Scaffold-free vascular tissue engineering using bioprinting.," *Biomaterials*, vol. 30, no. 30, pp. 5910–7, Oct. 2009.

[23] N. I. Moldovan, N. Hibino, and K. Nakayama, "Principles of the Kenzan Method for Robotic Cell Spheroid-Based Three-Dimensional Bioprinting," *Tissue Eng. Part B. Rev.*, vol. 23, no. 3, pp. 237–244, 2017.

[24] "Cyfuse Biomedical K.K." [Online]. Available: http://www.cyfusebio.com/en/regenerative.html. [Accessed: 16-Sep-2014].

[25] R. Machino *et al.*, "Replacement of Rat Tracheas by Layered, Trachea-Like, Scaffold-Free Structures of Human Cells Using a Bio-3D Printing System," *Adv. Healthc. Mater.*, p. 1800983, Jan. 2019.

[26] J. T. Daub and R. M. H. Merks, "A cell-based model of extracellular-matrix-guided

endothelial cell migration during angiogenesis.," *Bull. Math. Biol.*, vol. 75, no. 8, pp. 1377–99, Aug. 2013.

[27] D. Ambrosi, F. Bussolino, and L. Preziosi, "A Review of Vasculogenesis Models," 2004.

[28] P. Carmeliet and M. Tessier-Lavigne, "Common mechanisms of nerve and blood vessel wiring.," *Nature*, vol. 436, pp. 193–200, Jul. 2005.

[29] D. Bouïs, G. a P. Hospers, C. Meijer, G. Molema, and N. H. Mulder, "Endothelium in vitro: a review of human vascular endothelial cell lines for blood vessel-related research.," *Angiogenesis*, vol. 4, no. 2, pp. 91–102, 2001.

[30] C. K. Griffith *et al.*, "Diffusion Limits of an in Vitro Thick Prevascularized Tissue," *Tissue Eng.*, vol. 11, no. 1/2, 2005.

[31] S. Levenberg *et al.*, "Engineering vascularized skeletal muscle tissue," *Nat. Biotechnol.*, vol. 23, no. 7, pp. 879–884, 2005.

[32] P. A. Galie, D.-H. T. Nguyen, C. K. Choi, D. M. Cohen, P. A. Janmey, and C. S. Chen, "Fluid shear stress threshold regulates angiogenic sprouting," *Proc. Natl. Acad. Sci.*, vol. 111, no. 22, pp. 7968–7973, 2014.

[33] I. Arnaoutova and H. K. Kleinman, "In vitro angiogenesis: endothelial cell tube formation on gelled basement membrane extract," *Nat. Protoc.*, vol. 5, no. 4, pp. 628–635, Apr. 2010.

[34] M. T. Pham *et al.*, "Generation of human vascularized brain organoids," *Neuroreport*, vol. 29, no. 7, pp. 588–593, May 2018.

[35] K. A. DiVito, M. A. Daniele, S. A. Roberts, F. S. Ligler, and A. A. Adams, "Microfabricated blood vessels undergo neoangiogenesis," *Biomaterials*, vol. 138,

pp. 142–152, Sep. 2017.

[36] D. M. Dean, A. P. Napolitano, J. Youssef, and J. R. Morgan, "Rods, tori, and honeycombs: the directed self-assembly of microtissues with prescribed microscale geometries.," *FASEB J.*, vol. 21, no. 14, pp. 4005–12, Dec. 2007.

[37] L. a Kunz-Schughart *et al.*, "Potential of fibroblasts to regulate the formation of three-dimensional vessel-like structures from endothelial cells in vitro.," *Am J Physiol Cell Physiol*, vol. 290, no. 5, pp. C1385-98, 2006.

[38] A. Alajati *et al.*, "Spheroid-based engineering of a human vasculature in mice," *Nat. Methods*, vol. 5, no. 5, pp. 439–445, 2008.

[39] L. De Moor *et al.*, "High-throughput fabrication of vascularized spheroids for bioprinting," *Biofabrication*, 2018.

[40] J. D. Baranski *et al.*, "Geometric control of vascular networks to enhance engineered tissue integration and function," *PNAS*, vol. 110, no. 19, pp. 7586–7591, 2013.

[41] C. a. Czajka, B. W. Calder, M. J. Yost, and C. J. Drake, "Implanted Scaffold-Free Prevascularized Constructs Promote Tissue Repair," *Ann. Plast. Surg.*, vol. 74, no. 3, pp. 371–375, 2015.

[42] C. A. Czajka and C. J. Drake, "Self-assembly of prevascular tissues from endothelial and fibroblast cells under scaffold-free, nonadherent conditions.," *Tissue Eng. Part A*, vol. 21, no. 1–2, pp. 277–87, 2015.

[43] C. W. Eckermann, K. Lehle, S. A. Schmid, D. N. Wheatley, and L. A. Kunz-Schughart, "Characterization and modulation of fibroblast/endothelial cell co-cultures for the in vitro preformation of three-dimensional tubular networks," *Cell Biol Int*, vol. 35, no. 11, pp. 1097–1110, 2011.

[44] S. Pattanaik, C. Arbra, H. Bainbridge, S. G. Dennis, S. A. Fann, and M. J. Yost, "Vascular Tissue Engineering Using Scaffold-Free Prevascular Endothelial-Fibroblast Constructs," *Biores. Open Access*, vol. 8.1, 2019.

[45] G. Giap, Y. Chiew, N. Wei, S. Sultania, S. Lim, and K. Q. Luo, "Bioengineered Three-Dimensional Co-Culture of Cancer Cells and Endothelial Cells: A Model System for Dual Analysis of Tumor Growth and Angiogenesis," *Biotechnol. Bioeng*, vol. 114, pp. 1865–1877, 2017.

[46] J. Rouwkema, J. de Boer, and C. a Van Blitterswijk, "Endothelial cells assemble into a 3-dimensional prevascular network in a bone tissue engineering construct.," *Tissue Eng.*, vol. 12, no. 9, pp. 2685–93, Sep. 2006.

[47] R. Noguchi *et al.*, "Development of a three-dimensional pre-vascularized scaffold-free contractile cardiac patch for treating heart disease," *J. Hear. Lung Transplant.*, vol. 35, no. 1, pp. 137–145, 2016.

[48] A. Citro *et al.*, "Biofabrication of a vascularized islet organ for type 1 diabetes," *Biomaterials*, vol. 199, pp. 40–51, Apr. 2019.

[49] T. Takebe *et al.*, "Massive and Reproducible Production of Liver Buds Entirely from Human Pluripotent Stem Cells," *Cell Rep.*, vol. 21, no. 10, pp. 2661–2670, 2017.

[50] M. Itoh, K. Nakayama, R. Noguchi, K. Kamohara, and K. Furukawa, "Scaffold-Free Tubular Tissues Created by a Bio-3D Printer Undergo Remodeling and Endothelialization when Implanted in Rat Aortae," *PLoS One*, vol. 10, no. 9, p. e0145971, 2015.

[51] J. M. Kelm *et al.*, "Tissue-transplant fusion and vascularization of myocardial microtissues and macrotissues implanted into chicken embryos and rats.," *Tissue*

Eng., vol. 12, no. 9, pp. 2541–53, Sep. 2006.

[52] Y. Pang, K. Montagne, M. Shinohara, K. Komori, and Y. Sakai, "Liver tissue engineering based on aggregate assembly: efficient formation of endothelialized rat hepatocyte aggregates and their immobilization with biodegradable fibres," *Biofabrication*, vol. 045004, 2012.

[53] A. M. Müller, M. I. Hermanns, C. Skrzynski, M. Nesslinger, K.-M. Müller, and C. J. Kirkpatrick, "Expression of the endothelial markers PECAM-1, vWf, and CD34 in vivo and in vitro.," *Exp. Mol. Pathol.*, vol. 72, no. 3, pp. 221–229, 2002.

[54] M. Inamori, M. Eng, H. Mizumoto, D. Ph, and T. Kajiwara, "An Approach for Formation of Vascularized Liver Tissue by Endothelial Cell-Covered Hepatocyte Spheroid Integration," *Tissue Eng. Part A*, vol. 15, no. 8, 2009.

[55] Y. K. Kurokawa, R. T. Yin, M. R. Shang, V. S. Shirure, M. L. Moya, and S. C. George, "Human Induced Pluripotent Stem Cell-Derived Endothelial Cells for Three-Dimensional Microphysiological Systems," *Tissue Eng. Part C Methods*, vol. 23, no. 8, 2017.

[56] A. M. Blakely, J. Y. Schell, A. P. Rago, P. R. Chai, A. P. Napolitano, and J. R. Morgan, "Formation of Multicellular Microtissues and Applications in Biofabrication," in *Biofabrication: Micro- and Nano-fabrication, Printing, Patterning and Assemblies*, F. Gabor and W. Sun, Eds. Elsevier, 2013, pp. 149–166.

[57] E. M. Kim *et al.*, "Fabrication of core-shell spheroids as building blocks for engineering 3D complex vascularized tissue," *Acta Biomater.*, Sep. 2019.

[58] A. Sobrino *et al.*, "3D microtumors in vitro supported by perfused vascular networks.," *Sci. Rep.*, vol. 6, no. July, p. 31589, 2016.

[59] M. L. Moya, Y.-H. Hsu, A. P. Lee, C. C. W. Hughes, and S. C. George, “In vitro perfused human capillary networks.,” *Tissue Eng. Part C. Methods*, vol. 19, no. 9, pp. 730–7, 2013.

[60] M. Moya, D. Tran, and S. C. George, “An integrated in vitro model of perfused tumor and cardiac tissue.,” *Stem Cell Res. Ther.*, vol. 4 Suppl 1, no. Suppl 1, p. S15, 2013.

[61] V. van Duinen, D. Zhu, C. Ramakers, A. J. van Zonneveld, P. Vulto, and T. Hankemeier, “Perfused 3D angiogenic sprouting in a high-throughput in vitro platform,” *Angiogenesis*, vol. 22, no. 1, pp. 157–165, Feb. 2019.

[62] J. T. Morgan, J. Shirazi, E. M. Comber, C. Eschenburg, and J. P. Gleghorn, “Fabrication of centimeter-scale and geometrically arbitrary vascular networks using in vitro self-assembly,” *Biomaterials*, vol. 189, pp. 37–47, Jan. 2019.

[63] S. Kim, H. Lee, M. Chung, and N. L. Jeon, “Engineering of functional, perfusable 3D microvascular networks on a chip.,” *Lab Chip*, vol. 13, no. 8, pp. 1489–500, 2013.

[64] V. K. Lee, A. M. Lanzi, H. Ngo, S. S. Yoo, P. A. Vincent, and G. Dai, “Generation of multi-scale vascular network system within 3D hydrogel using 3D bio-printing technology,” *Cell. Mol. Bioeng.*, vol. 7, no. 3, pp. 460–472, 2014.

[65] S. Kim, M. Chung, J. Ahn, S. Lee, and N. L. Jeon, “Interstitial flow regulates the angiogenic response and phenotype of endothelial cells in a 3D culture model,” *Lab Chip*, vol. 16, pp. 4189–4199, 2016.

[66] J. W. Song and L. L. Munn, “Fluid forces control endothelial sprouting.,” *Proc. Natl. Acad. Sci. U. S. A.*, vol. 108, no. 37, pp. 15342–15347, 2011.

[67] B. Zhang *et al.*, “Biodegradable scaffold with built-in vasculature for organ-on-a-chip engineering and direct surgical anastomosis,” *Nat. Mater.*, no. March, 2016.

[68] M. Heiss *et al.*, “Endothelial cell spheroids as a versatile tool to study angiogenesis in vitro.,” *FASEB J.*, vol. 29, no. 7, pp. 3076–84, 2015.

[69] K. A. Homan *et al.*, “Flow-enhanced vascularization and maturation of kidney organoids in vitro,” *Nat. Methods*, vol. 16, no. 3, pp. 255–262, Mar. 2019.

[70] E. Sano, C. Mori, Y. Nashimoto, R. Yokokawa, H. Kotera, and Y. Torisawa, “Engineering of vascularized 3D cell constructs to model cellular interactions through a vascular network,” *Biomicrofluidics*, vol. 12, 2018.

[71] Y. Nashimoto *et al.*, “Integrating perfusable vascular networks with a three-dimensional tissue in a microfluidic device,” *Integr. Biol.*, vol. 9, no. 6, pp. 506–518, 2017.

[72] J. D. Bronzino, *Biomedical Engineering Handbook*, Second. CRC Press LLC, 2000.

[73] J. W. Prothero, *The Design of Mammals A Scaling Approach*. Cambridge University Press, 2015.

[74] M. Kutz, *Standard Handbook of Biomedical Engineering & Design*. McGraw-Hil, 2003.

[75] A. Freitas Jr., Robert, *Nanomedicine*. Landes Bioscience, 1999.

[76] Z. K. Otrock, R. a R. Mahfouz, J. a Makarem, and A. I. Shamseddine, “Understanding the biology of angiogenesis: review of the most important molecular mechanisms.,” *Blood Cells. Mol. Dis.*, vol. 39, no. 2, pp. 212–20, 2007.

4.8 Supplemental Information

4.8.1 Supplemental Figures

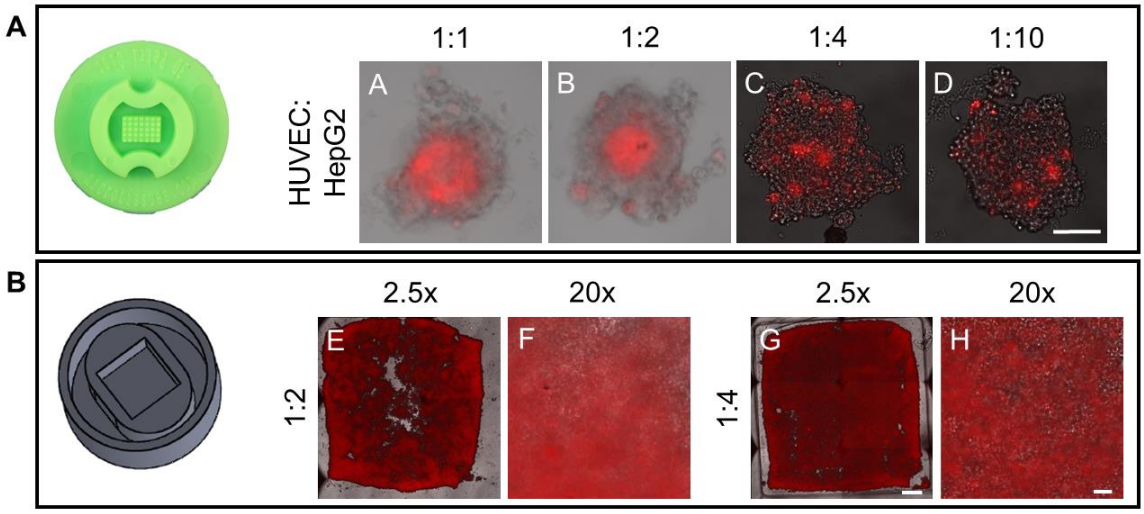

Supplemental Figure 4.1. *Mixed spheroids and quadrangle tissues using newly purchased HepG2.* Spheroids were formed using a mixture of CellTracker™ Red stained HUVEC and HepG2 cells in various ratios (A). This is a repeat of previous experiments using a newly purchased HepG2 cell vial, and the same HUVEC from all previous experiments. Image of a 3d Petri Dish® mold used to fabricate agarose gels with spheroid-shaped recesses. Snapshots of individual spheroids at 24 hours after seeding, composed of various ratios of HUVEC and HepG2 cells. In the 1:1 and 1:2 mix, HUVEC self-sort to the center of the spheroids. In the 1:4 and 1:10 mix, clumps of HUVEC are seen throughout the spheroids. Images taken at 20X magnification. Mixtures were also seeded into a quadrangle shaped mold (B). Schematic of the quadrangle shaped mold. Snapshot images of the square-shaped tissue formed from a mix of 1:2 and 1:4 HUVEC and HepG2 cells. HUVEC are evenly distributed amongst the HepG2 cells at both ratios. Scale bars are 100 µm, 1 mm and 50 µm respectively.

Chapter 5

Conclusion and Future Work

The work in this thesis developed a new microtissue manipulation method for the fabrication of bio-tubes. The first part of this thesis described a novel additive manufacturing method, the funnel-guide. The funnel-guide is a quick, simple, self-aligning microtissue manipulation technique that guides microtissue rings into a stacking chamber, where they settle, stack and fuse together to form a bio-tube. The second portion described how the funnel-guide method was automated to decrease human error and increase throughput. The integrity of the fabricated bio-tubes was also increased through the addition of real-time evaluation of ring quality using vision recognition. Lastly, this thesis discussed the theory behind the fabrication of a capillary tissue bed and the construction of a perfusion system for bio-tubes and tissue beds.

5.1 Chapter 2

Chapter 2 discussed the development and evaluation of a new microtissue manipulation technique for the fabrication of bio-tubes, the funnel-guide. Given the physiological relevance of tubular structures, and the need for a simple, quick, self-aligning method to fabricate bio-tubes, we harnessed the self-righting capability of ring-shaped microtissue building parts and guided them with a funnel into a chamber where they stacked and fused, requiring only a single pipetting step to transfer the rings [1]–[3]. The use of toroid building blocks decreased the total number of parts needed to build compared

to other methods such as the Kenzan method, which uses upwards of 500 spheroid building parts to construct bio-tubes [4]. We showed how the funnel-guide method can be used with toroids of different sizes and of various cell-types, making the system modular and applicable to any organ system containing a tubular structure. This simple method occurs while submerged under cell culture medium, and does not involve contacting the tissue structures, unlike the Kenzan method which punctures the spheroids onto a microneedle array [5]. Using the funnel-guide method we constructed a bio-tube containing 45 tissue rings in about 1 hour, making each build cycle approximately 1.3 minutes. In comparison, the Bio-Pick, Place and Perfuse (Bio-P3) can construct a stack of 16 rings in 60 minutes, making each build cycle about 4 minutes [2]. The funnel-guide resulted in a 68% reduction in build cycle length compared to the Bio-P3. Additional experiments could be conducted to ascertain the impact of the funnel angle on guiding tissue rings to the stacking chamber, and computational modelling could be performed to understand the mechanics of tissue free-fall.

5.2 Chapter 3

Chapter 3 discussed the evaluation of tissue ring building part morphology, automation of the funnel-guide method and the development of real-time quality control of ring building parts during biofabrication. The formation of the Advanced Regenerative Manufacturing Institute (ARMI), reinforced the need to consider manufacturing techniques for human tissue products as one facet to progress the field of tissue engineering [6]. One thrust area of ARMI is tissue process automation and monitoring; and the ease of funnel-guided fabrication made it amenable to automation. Automation is an essential component of manufacturing in order to increase throughput, decrease human error, and increase part

quantity and quality. With any manufacturing scheme you need to understand the raw materials so that it can be properly employed to create a quality product. Since we are working with dynamic living materials, we needed to develop metrics to understand and employ them. Using our metrics, we were able to build with dynamic endothelial cells. This is a step towards the fabrication of tissue engineered blood vessels, given the presence of endothelial cells on the lumen of every blood vessel in the body [7].

Given the simplicity of the funnel-guide method, it was amenable to automation using a liquid handling robot and 96-well plates, standardly available components. Liquid handling robots are ubiquitous in the field, and can load, move and incubate 96-well plates. This enables the automated funnel-guided biofabrication method to be easily incorporated with existing automated schemes. Using the automated system, we were able to reduce the build cycle time to 43 seconds, a 45% reduction from the manual funnel-guide method, and an 82% reduction in time from the Bio-P3. The recently developed automated Kenzan method, which punctures an array of spheroid simultaneously takes 1.3 hours to move 500 spheroids, which is a build cycle length of 2.5 minutes. The automated funnel-guide system is a 71% reduction in build cycle time compared to the automated Kenzan system, and uses 1/5 the number of building parts. Using the automated system, we could construct a stack of 96 rings, equivalent to a bio-tube 2.64 cm in height in 45 minutes, a length in excess of physiological values of blood vessels with a similar lumen diameter [8]. Not only does the automated funnel-guide system reduce the build cycle time, but it is a self-aligning method that requires a single pipetting step and doesn't involve additional post-processing steps that occur outside culture medium such as puncturing through a needle, or stringing around a mandrel like other methods available [4], [9].

Manufacturing methods increase the quality of the final product by ensuring the use of quality materials during fabrication. Since the funnel-guide method is susceptible to total failure from the placement of a faulty building part (once a ring is placed in the funnel-guide, it cannot be removed), we wanted to incorporate a quality control step during the build cycle. We were able to do this because just like in the funnel-guide, the ring rights itself and settles into the center of the meniscus while inside the pipette tip. Once centered in the meniscus we imaged the ring using an upward facing camera and performed a custom QC algorithm to evaluate it in real-time. While it may not be overtly noticeable, when comparing the bio-tube of endothelial cell rings fabricated with the manual method and automated method, there is an increase in the uniformity and alignment of the endothelial cell bio-tube fabricated using the automated method. Our QC step increased the quality of our bio-tubes. To the best of our knowledge, no other QC evaluation exists in other biofabrication methods, making the funnel-guide method advantageous and unique.

Future experiments could evaluate additional building part parameters to inform usability in biofabrication. Assessments of additional cell types, and combinations of cell types would allow for the user to predict tissue ring part dimensions. These predictions would allow for the creation of designer building parts, specific to user needs. The desired outcome dimensions would dictate the initial seeding specifications including peg angle, dimensions and cell density. Additionally, tissue rings of a variety of cell types could be constructed with to make more physiologically relevant tubular structures. For example, rings fabricated with smooth muscles cells on the exterior and endothelial cells on the interior could be used to fabricate a blood vessel like bio-tube.

5.3 Chapter 4

Chapter 4 discussed the theory behind fabricating a perfusable capillary bed, a primary challenge of tissue engineering. Biofabrication methods can construct large, high cell density tissue constructs, however without access to nutrients and removal of waste via a perfusion network, the tissue will rapidly develop a necrotic core [10]. The human body overcomes this via the cardiovascular system, which has a capillary within an average of 200 μm of every cell in the body [11]. Thus vascularization of fabricated tissue constructs with a capillary network that can be perfused is essential to viability. In order for a vascularized tissue bed to be translatable to clinical settings, it must be attached to a vessel so that it can connect to either a perfusion system, or to the host vasculature with ease. A tissue engineered blood vessel fabricated using the funnel-guide method could be fused to a capillary tissue bed and perfused. To the best of our knowledge, a vessel connected to a capillary bed is a novel structure, that if fabricated could take a step towards overcoming the vascularization challenge of tissue engineering and be used as an *in vitro* model or as a starting point for the creation of organs for *in vivo* transplant.

5.4 Closing Remarks

The goal of this thesis was to work towards the development of an automated platform for the fabrication of bio-tubes using ring-shaped microtissue building parts. This is evident in the studies depicted here from developing a new biofabrication technique for production of bio-tubes, to defining parameters to evaluate the living building parts and inform their usability, and finally automating the funnel-guide method using a

commercially available liquid handling robot while incorporating real-time quality control using visual inspection in order to increase fidelity of the manufactured bio-tubes. The funnel-guide method is a simple, quick, self-aligning additive manufacturing method that uses living building parts to fabricate tubes of any cell type [3]. With any manufacturing technique, it is imperative to understand the raw materials so they can be properly employed to construct the finished product. This also applies to manufacturing living tissue constructs. However, fabrication with dynamic living building parts presents a unique set of challenges, and requires the development of metrics and techniques to understand and inform how they can be properly built with. We developed a set of parameters to inform when our dynamic tissue rings are used, and successfully formed bio-tubes with luminal alignment. Automated workflows with quality control steps increase production quality and quantity, a necessity for any manufactured parts, including human tissue products. Our developed automated workflow incorporates standard components ubiquitous in the field including a commercially available liquid handling robot and ANSI/SLAS 96-well plates. These components and QC regimen would easily fit into existing automated workflows, making the funnel-guide method translatable, and amenable to incorporation into a completely automated tissue fabrication workflow from thawing the vial of cells, performing cell culture and microtissue formation, to microtissue manipulation and macrotissue fusion [12], [13].

This thesis also discussed hypotheses and preliminary data surrounding the unmet need of fabrication of a perfusable capillary tissue bed. From the physiological metrics of a hepatic tissue bed containing a capillary network, to a funnel-guide perfusion platform that could be used to perfuse a bio-tube, tissue bed, or bio-tube joined with a tissue bed.

Fabrication of a bio-tube using endothelial cells (as discussed in Chapter 3) is a step towards constructing a tissue engineered blood vessel, which could be fused to a capillary network and perfused as a single vascular-like unit. The vascular-like unit of a tissue engineered blood vessel joined to a tissue bed is, to the best of our knowledge, a novel structure that would overcome the primary challenge still faced by tissue engineering, construction of a perfusable vascularized tissue bed [14]. If this can be accomplished, we will be a step closer to creating physiologically relevant tissue structures that can be used as *in vitro* models and eventually organs for replacement *in vivo*.

5.5 References

[1] N. I. Moldovan, N. Hibino, and K. Nakayama, "Principles of the Kenzan Method for Robotic Cell Spheroid-Based Three-Dimensional Bioprinting," *Tissue Eng. Part B. Rev.*, vol. 23, no. 3, pp. 237–244, 2017.

[2] A. M. Blakely, K. L. Manning, A. Tripathi, and J. R. Morgan, "Bio-Pick, Place, and Perfuse: A New Instrument for 3D Tissue Engineering," *Tissue Eng. Part C Methods*, vol. 21, no. 7, pp. 737–746, 2015.

[3] K. L. Manning, A. H. Thomson, and J. R. Morgan, "Funnel-Guided Positioning of Multicellular Microtissues to Build Macrotissues," *Tissue Eng. Part C Methods*, vol. 24, no. 10, pp. 557–565, Oct. 2018.

[4] W. LaBarge, A. Morales, D. Pretorius, A. Kahn-Krell, R. Kannappan, and J. Zhang, "Scaffold-Free Bioprinter Utilizing Layer-By-Layer Printing of Cellular Spheroids," *Micromachines*, vol. 10, no. 9, p. 570, Aug. 2019.

[5] R. Machino *et al.*, "Replacement of Rat Tracheas by Layered, Trachea-Like, Scaffold-Free Structures of Human Cells Using a Bio-3D Printing System," *Adv. Healthc. Mater.*, p. 1800983, Jan. 2019.

[6] "Advanced Regenerative Manufacturing Institute." [Online]. Available: https://www.armiusa.org/. [Accessed: 26-Nov-2019].

[7] A. A. Poot, D. W. Grijpma, J. Feijen, and I. Vermes, "Vascular tissue engineering," vol. 37, no. 1, pp. 44–46, 2012.

[8] W. Huang, R. T. Yen, M. McLaurine, and G. Bledsoe, "Morphometry of the human pulmonary vasculature.," *J. Appl. Physiol.*, vol. 81, no. 5, pp. 2123–2133, 1996.

[9] C. J. Nycz, H. A. Strobel, K. Suqui, J. Grosha, G. S. Fischer, and M. W. Rolle, "A

Method for High-Throughput Robotic Assembly of Three-Dimensional Vascular Tissue," *Tissue Eng. Part A*, vol. 25, no. 17 and 18, pp. 1251–60, 2019.

[10] S. Bersini, I. K. Yazdi, G. Talò, S. R. Shin, M. Moretti, and A. Khademhosseini, "Cell-microenvironment interactions and architectures in microvascular systems," *Biotechnol. Adv.*, 2016.

[11] M. Kutz, *Standard Handbook of Biomedical Engineering & Design*. McGraw-Hil, 2003.

[12] R. J. Thomas, A. Chandra, Y. Liu, P. C. Hourd, P. P. Conway, and D. J. Williams, "Manufacture of a human mesenchymal stem cell population using an automated cell culture platform," *Cytotechnology*, vol. 55, no. 1, pp. 31–39, Sep. 2007.

[13] R. Kato *et al.*, "A Compact, Automated Cell Culture System for Clinical Scale Cell Expansion from Primary Tissues," *Tissue Eng. Part C Methods*, vol. 16, no. 5, pp. 947–956, Oct. 2010.

[14] K. R. Adhikari, B. S. Tucker, and V. Thomas, "Tissue engineering of small-diameter vascular grafts," in *Biointegration of Medical Implant Materials*, Elsevier, 2020, pp. 79–100.